INVESTIGATION OF THE DECAY SCHEMES OF CERTAIN ELECTRON CAPTURE ISOTOPES

Thesis submitted by

JOHN CAMERON McGEORGE

for the degree of

Doctor of Philosophy

University of Edinburgh

December, 1968.

CONTENTS

C O N T E N T S (Contd.)

CHAPTER I

PREVIOUS WORK ON ARSENIC-73

1.1. Introduction

The phenomenon of radioactivity has been the object of considerable investigation since its discovery by Becquerel in 1896. It is the process by which unstable nuclei release energy to give a more stable product. The rate at which the decay process proceeds depends on the nature of the process and nuclei involved, and the energy difference between initial and final states of the atoms (decay energy Q).

Apart from a few neutron emitters all the active nuclei known decay by one or more of four processes, each characterised by the way in which the 'excess' energy is radiated.

1. α-decay. Radiation of heavy, positively charged particles, which have been identified as helium nuclei, and are successfully understood as fragments of nuclear matter which are thrown off when this results in a stabler structure.

2. β-decay. Radiation of positively or negatively charged electrons.

a) β^- decay. Emission of a negative electron and an antineutrino. This process may occur provided the decay energy is greater than zero and is described by the equation $X^A_Z \longrightarrow Y^A_{Z+1} + \beta^- + \bar{\nu}$ with A, Z in the usual notation.

b) β^+ decay. Emission of a positron and a neutrino. This process can only occur if the available decay energy is greater than the rest mass of an electron-positron pair ($2m_oc^2 \simeq 1$ Mev, m_o = electron rest mass). The equation

describing this case is

$$X^{A}_{Z} \rightarrow Y^{A}_{Z-1} + \beta^{+} + \nu .$$

Since (a) and (b) are three-body processes the β particle can be emitted with any energy from zero up to the available decay energy (end-point) or decay energy - $2m_{o}c^{2}$ (for β^{+} decay).

In the latter case when the decay energy is $< 2m_{o}c^{2}$ the decay may still occur by means of:

c) Electron capture. In this process an atomic electron is captured by the nucleus which emits a neutrino of energy = Q - atomic electron binding energy. Since the neutrino is very difficult to detect, only X-rays characteristic of the daughter atom (and/or Auger electrons) are observed. These are the X-rays emitted when the vacancy left by the captured electron is filled by an electron from a higher atomic shell.

If Q is small then capture may only occur from the outer shells, but provided Q > K shell binding energy electron capture is possible from any shell.

Arsenic-73, which decays by electron capture is the subject of this investigation.

3. γ-decay. The chargeless γ radiations have been identified as electromagnetic. Emissions of radiation during motions within systems of charges are well known, and so γ-rays are to be expected whenever another decay process leaves the daughter nucleus in an excited state requiring internal charge redistribution before the ground state can be reached.

For example Ge^{73}, the decay product of As^{73}, is formed in an excited state which decays to the ground state by means of two γ decays.

4. Fission, in which the nucleus splits into roughly equal fragments, possibly with the emission of neutrons.

Since β and γ decay are relevant to the study of As^{73} a brief outline of the theory of these processes will now be given.

1.2. β-decay.

The problem of the theory of β-decay is to calculate the probability of the processes 2(a), (b) or (c). To make the calculations it is necessary to introduce an interaction which can produce the changes involved, i.e. convert a neutron into a proton or vice versa, and at the same time produce an electron or positron and a neutrino.

In the Fermi theory the operation of such an interaction is treated by methods analogous to those used in the quantum mechanical treatment of electromagnetic radiation (see, for example, "β-decay", Konopinski[1]). The electron and antineutrino (leptons) are pictured as being created when a neutron transforms into a proton. Since the total number of leptons is not constant, the appropriate mathematical formalism is that of second quantization, where the probability amplitudes ψ, ϕ for electrons and neutrinos are viewed as operators.

The theory yields a formula for the energy distribution of the emitted β particles, i.e. for the probability per unit time $P(T)dT$ for the emission of a β particle in the kinetic energy

range T to T + dT. This is given by

$$P(T)dT = G^2|M|^2 F(S, T)(T + m_o c^2)(T^2 + 2m_o c^2 T)^{\frac{1}{2}}(T_o - T)^2 \, dT,$$

where G is a constant expressing the strength of the β-decay interaction, F(Z, T) is a function describing the effect of the Coulomb field on the emitted β particle.

M is a matrix element of the form

$$M = \int \Psi_f^* H_\beta \Psi_i \, d\tau \qquad (1)$$

where Ψ_i, Ψ_f refer to the initial and final nuclear states, H_β is the Hamiltonian appropriate to the β-decay interaction. The other quantities form the statistical factor which describes how the available energy T_o is shared among the electron (kinetic energy T), the neutrino and the product nucleus. This factor is responsible for the general properties of the continuous β spectrum.

The disintegration constant $\lambda = \int_o^{T_o} P(T)dT$ or, assuming M independent of energy

$$\lambda = G^2|M|^2 \, f(Z, T_o)$$

where

$$f(Z, T_o) = \int_o^{T_o} F(Z, T)(T + m_o c^2)(T^2 + 2m_o c^2 T)^{\frac{1}{2}} (T_o - T)dT \; .$$

This may be written $ft = \frac{1}{k|M|^2}$ where t is the half-life and k is a constant.

The product ft depends only on Z, T_o and t. Measurement of the last two quantities can therefore give an experimental estimate of the matrix element M.

To evaluate M from the theory it is necessary to formulate H_β. Conservation of momentum and angular momentum and Lorentz invariance are not sufficient to specify completely the form of H_β and it can be shown that the most general interaction consistent with the relativistic requirements is a sum of five terms:

$$H_\beta = C_S H_S + C_V H_V + C_T H_T + C_A H_A + C_P H_P$$

where the C_i's are constants.

The suffixes S, V, T, A, P, indicate that the terms are scalar contractions of two scalars, vectors, tensors of second rank, axial vectors or pseudo-scalars.

Analysis of the experimental results in the light of the discovery of parity non-conservation (Wu et al.[2]) has led to the conclusion (see, for example, the review article by Konopinski[3]) that of the five possible interactions, only the V and A terms need be incorporated in the H_β - referred to as the V - A interaction.

H_V and H_A are of the form

$$H_V = (\mathcal{F}_f^* \mathcal{F}_i)(\psi^* \phi) - (\mathcal{F}_f^* \underline{\alpha} \mathcal{F}_i)(\psi^* \underline{\alpha} \phi)$$

$$H_A = (\mathcal{F}_f^* \underline{\sigma} \mathcal{F}_i)(\psi^* \underline{\sigma} \phi) - (\mathcal{F}_f^* \gamma_5 \mathcal{F}_i)(\psi^* \gamma_5 \phi)$$

where $\underline{\alpha}$ and β are the Dirac matrices (defined, for example, by Konopinski and Uhlenbeck[4]), and where ψ and ϕ refer to the electron and neutrino states.

$\gamma_5 = \gamma_1 \gamma_2 \gamma_3 \gamma_4$ where $\gamma_k = -i\,\alpha_k\,\beta$ for $k = 1,2,3$ and $\gamma_4 = \beta$.

Also $\underline{\sigma} = \gamma_5 \underline{\alpha}$.

Experimental evidence (e.g. electron polarization) shows that fermions appear to participate in the β interaction only through the left handed components of their states (and through right-handed components of antiparticle states) which is described formally by means of the operator γ_5. The left-handed projection of a state Ψ is Φ, say, given by

$$\Phi = \tfrac{1}{2}(1 + \gamma_5)\Psi \ .$$

Allowed Transitions. The expressions H_V and H_A contain terms of order v/c, where v is the nucleon speed, namely the terms containing $\underline{\alpha}$ and γ_5. Ignoring these gives

$$H_V = (\Psi_f^* \Psi_i)(\psi^* \phi)$$
$$H_A = (\Psi_f^* \underline{\sigma} \Psi_i)(\psi^* \underline{\sigma} \phi)$$

which have to be used in the evaluation of M in equation (1).

Assuming that the lepton wave functions do not vary appreciably over the nuclear volume, they may be taken outside the integration sign. If it is further assumed that the lepton wave functions are plane waves of the form $\exp i\,\underline{p}.\underline{r}$, $\exp i\,\underline{q}.\underline{r}$ for the electron and neutrino respectively, then the function $\exp i\,(\underline{p} + \underline{q})\underline{r}$ may be expanded as a power series in r/λ where λ is the de Broglie wavelength given by

$$\lambda = h/|\underline{p} + \underline{q}| \ .$$

Retaining only the first term of the series constitutes the allowed approximation. The remaining nuclear matrix elements are $\int \Psi_f^* \Psi_i \, d\tau$ and $\int \Psi_f^* \boldsymbol{\sigma} \Psi_i \, d\tau$, conventionally abbreviated to $\int \underline{1}$ and $\int \boldsymbol{\sigma}$ respectively.

Nuclear states have definite spin and parity values and therefore the matrix elements $\int \underline{1}$ and $\int \boldsymbol{\sigma}$ determine the allowed selection rules, namely

$$\Delta J = 0 \qquad \Delta\pi = \text{no from } \int \underline{1}$$

$$\Delta J = 0, \pm 1 \quad (\text{no } 0 \rightarrow 0) \qquad \Delta\pi = \text{no from } \int \boldsymbol{\sigma}.$$

These are known as Fermi and Gamow-Teller selection rules. The Fermi rule arises from the V interaction and the Gamow-Teller from the A interaction.

Forbidden Transitions. If the initial and final nuclear states are such that the selection rules listed above cannot be complied with the approximations used must be reconsidered.

Retaining the relativistic term of order v/c in the V interaction gives a nuclear matrix element $\int \underline{\alpha}$ in the previous notation. Retaining the first power of r/λ in the series expansion gives $\int \underline{r}$, which is expected to be of the same magnitude.

The selection rules are:

$$\int \underline{\alpha} : \quad \Delta J = 0, \pm 1 \quad (\text{no } 0 \rightarrow 0) \qquad \Delta\pi = \text{yes}$$

$$\int \underline{r} : \quad \Delta J = 0, \pm 1 \quad (\text{no } 0 \rightarrow 0) \qquad \Delta\pi = \text{yes}.$$

Similarly the A interaction yields terms

$$\int \gamma_5 : \quad \Delta J = 0, \qquad \Delta\pi = \text{yes}$$

$$\int \boldsymbol{\sigma}.\underline{r} : \quad \Delta J = 0, \qquad \Delta\pi = \text{yes}$$

$\int \underline{\sigma} \wedge \underline{r}$: $\Delta J = 0, \pm 1$ (no $0 \rightarrow 0$), $\Delta \pi$ = yes

$\int \beta_{ij} = \int \sigma_i x_j + \sigma_j x_i - \frac{2}{3} \delta_{ij} (\underline{\sigma}.\underline{r})$:

$\Delta J = 0, \pm 1, \pm 2$ (no $0 \rightarrow 0$, $\frac{1}{2} \rightarrow \frac{1}{2}$, $1 \rightarrow 0$), $\Delta \pi$ = yes.

The above are the selection rules for first forbidden decay, and those for still higher degrees of forbiddenness may be derived by consideration of further terms in the expansion of $\exp i(\underline{p} + \underline{q}).\underline{r}$.

$\beta^{\pm}$ decay and Electron Capture. The assumption of plane wave eigenfunctions is justified for the neutrino, but the appropriate wave functions for the electron are the solutions of the Dirac equation for a free β particle in a Coulomb potential (β^{-} decay) or a bound atomic electron (capture).

At first sight this would appear to lead to different selection rules. However the radial part of the electron wave functions can be expanded as a power series in r/λ in both cases (just as for plane waves).

The lowest order term in the capture case is $(r/\lambda)^{\ell} C_{\ell}$ for bound states with $j = \ell + \frac{1}{2}$ or $(r/\lambda) C_{\ell-1}^{\ell-1}$ for bound states with $j = \ell - \frac{1}{2}$, where the c's are coefficients of the expansion. Thus capture from the K, L_I L_{II} shells (and outer sub-shells with $\ell = 0$ or $\ell = 1$ (if $j = \ell - \frac{1}{2}$)) follows the selection rules listed above, but capture from the L_{III} shell ($\ell = 1$, $j = \ell + \frac{1}{2}$) is at best first forbidden.

Physically this corresponds to the fact that to conserve angular momentum the neutrino must carry off orbital angular momentum in capture from a shell with $\ell = 1$, $j = \ell + \frac{1}{2}$, whilst it can be emitted 'radially' from a shell with $\ell = 0$, or $\ell = 1$,

$j = \ell - \frac{1}{2}$.

Capture probabilities from the K, L_I and L_{II} shells are not all equal because the coefficients C_ℓ, $C_{\ell-1}$ of the terms of the series expansion are functions of the principal quantum number n. In fact $C^2_\ell(n) \propto \frac{1}{n^3}$. Thus the fraction $L_I/K \simeq \frac{1}{8}$. Rose and Jackson[5], using more accurate wave functions, have calculated that the L capture fraction in the arsenic case is 11%.

As implied by the above theory the measured ft values have been found to cluster. For normal allowed decays, the quantity log ft has a value between 4 and 5.8, whilst the range 6-9 is characteristic of first forbidden transitions. A few second forbidden decays are known with log ft in the range 12.2 - 13.5.

In the special case of decays between 'mirror' nuclei, where the numbers of neutrons and protons interchange, the log ft value lies between 2.7 and 3.7. Such transitions are called 'super' allowed.

By evaluating the quantity log ft it is therefore possible to deduce some information about the spin and parity of the parent or daughter nucleus provided the spin and parity of one of them is known.

1.3. Υ-Decay.

In decay from an excited nuclear state to a lower state the energy may be removed by Υ-radiation, or conversion electrons or (if energetically possible) by internal pair production.

The electromagnetic radiations are classified into 2^L multipole types, corresponding to the amount of angular momentum L

carried away by the γ photon. For each L value there are two radiation types called Electric (EL) and Magnetic (ML) which differ in parity.

Conservation of angular momentum and parity applied to the system of nucleus plus γ photon lead to the selection rules:

$$J_i - J_f \leqslant L \leqslant J_i + J_f$$

$$(\pi_i \times \pi_f) = (-1)^L \text{ for EL radiation}$$

$$(\pi_i \times \pi_f) = (-1)^{L+1} \text{ for ML radiation.}$$

Transitions from $J_i = 0$ to $J_f = 0$ are forbidden.
$J_i\ \pi_i$ are the spin and parity of the initial state and
$J_f\ \pi_f$ " " " " " final " .

Time dependent perturbation theory yields the result that the transition probability per second $\lambda = |M|^2 \frac{2\pi}{h} \frac{dN}{dE}$ (where $\frac{dN}{dE}$ denotes the number of possible final states per unit energy and the matrix element M responsible for the transition is given by $M = \int \psi_f H_\gamma \psi_i \, d\tau$ where H_γ is the Hamiltonian describing the interaction between the electromagnetic field and the nucleus. ψ_f and ψ_i refer to initial and final nuclear states.)

Weisskopf[6] and Moszkowski[7] have independently estimated the transition probability on the assumption that the radiation is caused by a transition of one single proton which moves independently in a central potential.

The formulae derived are:

$$\lambda = \lambda_o \frac{4.4\,(\ell+1)}{\ell(1,3,5..(2\ell+1))^2} \left(\frac{3}{\ell+3}\right)^2 \left(\frac{E}{E_o}\right)^{2\ell+1} \left(\frac{k}{k_o}\right)^{2\ell}$$

for electric 2^ℓ pole transitions and

$$\lambda = \lambda_o \frac{1.9(\ell+1)}{\ell(1,3,5..(2\ell+1))^2} \left(\frac{3}{\ell+3}\right)^2 \left(\frac{E}{E_o}\right)^{2\ell+1} \left(\frac{k}{k_o}\right)^{2\ell-2}$$

for magnetic 2^ℓ pole transitions,

where $\lambda_o = 10^{21}\ \text{sec}^{-1}$

$k_o = 10^{-13}$ cm.

$E_o = 197$ Mev, E = decay energy.

$k = 1.2\ A^{1/3} \times 10^{-13}$ cm = nuclear radius.

As the gamma transition probability decreases rapidly with increasing multipole order **L,** the transition will usually proceed with the lowest value of L permitted by the selection rules, or by a mixture of the two lowest multipole orders of the type E2 + M1.

Internal Conversion. Since the probability of finding an atomic electron in the vicinity of the nucleus is non-zero, it is possible for the energy of an excited nucleus to be transferred to an atomic electron which is emitted with the decay energy minus the atomic shell binding energy.

The process is exactly analogous to the Auger effect in atomic transitions and may be described in terms of the emission and absorption of a virtual photon.

The magnitude of the effect is implied by the total internal conversion coefficient α defined by

$$\alpha = \frac{\text{Probability of decay by emission of a conversion electron}}{\text{Probability of decay by } \gamma \text{ ray emission.}}$$

The internal conversion coefficients for the individual shells α_K, α_L, α_M etc. are defined in an analogous way.

Theoretical calculations of conversion coefficients show α is a function of the multipolarity of the transition and the decay energy. The result may be summarized by

$$\alpha = \sum_K \left| R_K + \sum_i \Delta R_{K_i} \lambda_i \right|^2 \qquad \text{where}$$

R_K the 'electron radial integral' depends on initial and final state (designated by K) of the electron. This is the only term which applies if the nucleus can be taken as a point. Finite nuclear size not only brings in static effects which merely modify the interaction by smearing the nuclear charge distribution, but also a dynamic effect which depends on features of nuclear dynamics and requires a nuclear model. The latter effect is described by the remaining ('penetration') terms which are contributions arising from inside the nucleus. The ΔR_{K_i} are proportional to the amplitude for the electron to be inside the nucleus and are therefore small. The experimental data indicate that dynamic effects are only appreciable for M1 and E1 transitions in some heavy nuclei.

Values quoted later (Tables 1.3, 1.5, 1.6) are due to calculations by Rose (1958) using the Thomas-Fermi-Dirac potential to compute the electron wave functions with exchange effects ignored. Finite nuclear size was taken into account. Values due to Band and Sliv[9] also include some exchange effects and a dimensional estimate of the penetration contribution.

The most recently calculated values are by Hager and Seltzer

(1968). Electron wavefunctions used in this case were based on a relativistic self-consistent field calculation - (the Hartree-Fock-Slater method) - and nuclear size effects are taken into account using a realistic charge distribution. Allowance was made for the hole of the emitted electron in both direct and exchange potentials.

1.4. Previous Work on As^{73}

Sagane et al.[10] (1939) isolated an arsenic beta activity of about 100 day half-life after bombardment of germanium with deuterons. They assigned the activity to As^{77}. Assignment to As^{73} was made by Elliot and Deutsch[11] (1943). Using a magnetic spectrometer these workers showed the electrons to be due to internal conversion of a 52 ± 3 keV gamma transition, with conversion in the K-shell about five times stronger than that in the L-shell. K-X rays were also observed.

Coincidence experiments between K-X rays and electrons showed that L-shell conversion electrons were accompanied by about half as many X rays as those from the K-shell. This result suggested decay by orbital electron capture followed within 1 μsec. by a highly converted 52 keV gamma ray (Fig. 1.1).

An upper limit of 2% was set on positron emission.

McCowan et al.[12] (1948) measured the As activity as a function of time after bombardment of Ge by deuterons. The decay curves indicated the presence of an activity of 17.5 day half-life assigned to As^{74}, and that of a 76 day activity assigned to As^{73}.

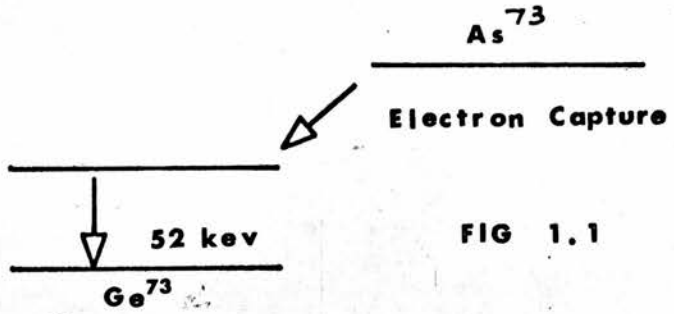

FIG 1.1

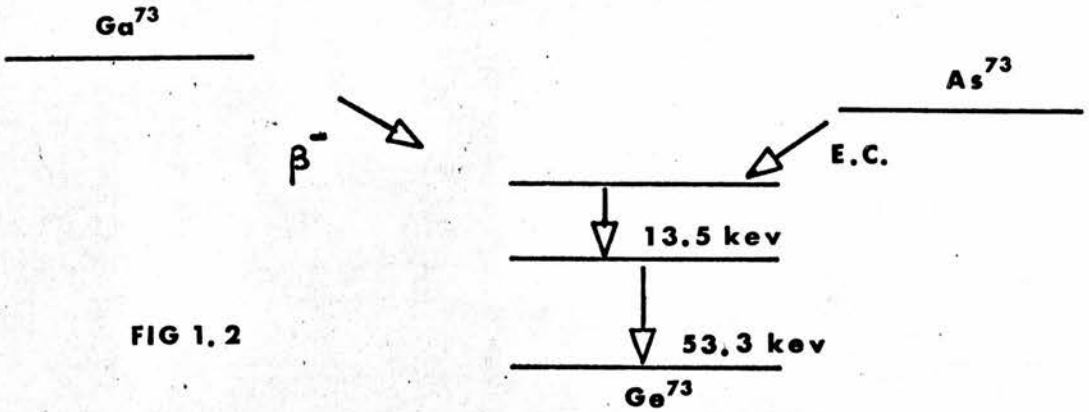

FIG 1.2

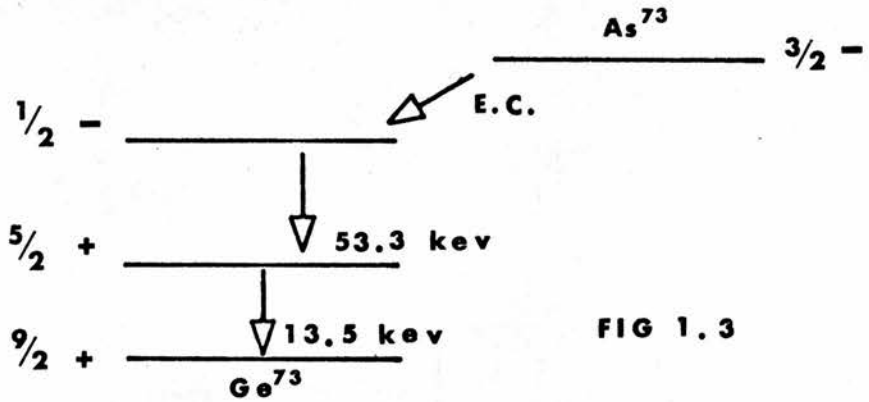

FIG 1.3

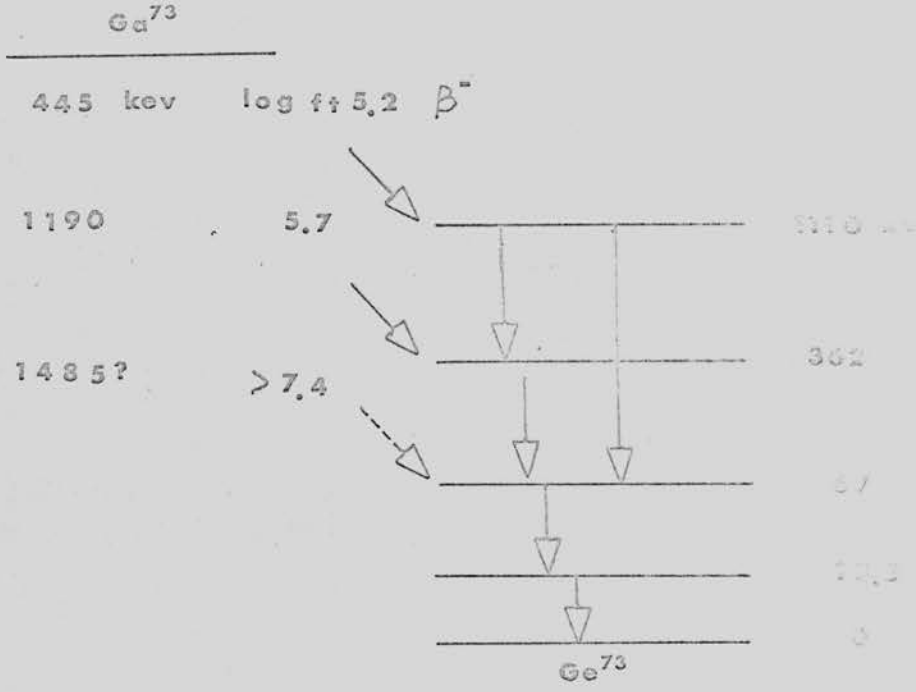

FIG 1.4

The 76 day activity was also produced by bombarding Ge with 20 Mev α particles. The half-life of 76 ± 3 days measured over four half-lives of the decay curve is the most accurate to date.

The assignment to As^{73} was confirmed by bombarding a Ge target enriched in the stable isotope Ge^{70} by about four times the abundance in ordinary Ge. The amount of 76 day activity appearing in the enriched sample was about four times that of the ordinary sample, suggesting the reaction $Ge^{70}(\alpha,p)As^{73}$. These authors found no evidence of beta activity from cloud chamber and ionization chamber observations, but an X ray wavelength of 1.27 Å (cf. Ge K-X ray 1.25 Å) derived from a curve of absorption in aluminium gave evidence of a K capture process in the activity.

Townes et al.[14] (1949) measured the ground state spin of Ge^{73} from an examination of the hyperfine structure of the microwave spectrum of the molecule GeH_3Cl. They obtained the value $^9/_2$. The nuclear quadrupole moment was found to be - 0.21 barns. The magnetic moment of Ge^{73} is listed[14a] as - 0.8792 n.m. based on a nuclear magnetic resonance experiment. (Aksenov and Vladimirski[14b]. Trail and Johnsson[13] (1953) found the threshold of the reaction $Ge^{73}(p, n)As^{73}$ to be 1.17 ± 0.03 Mev, leading to the value 390 ± 30 keV as the decay energy of As^{73}.

Johansson[15] (1952) produced As^{73} by bombarding Ge with deuterons. After chemical separation of the Arsenic electromagnetically separated samples were made on thin supports which confirmed the mass assignment made by McCowan et al. The electron spectrum, observed by means of a magnetic lens spectrometer of 3.5% resolution, showed the K and L conversion electrons of a

53.3 ± 0.5 keV gamma ray previously seen by Elliot and Deutsch, Auger lines at 8.4 and 9.6 keV, and two other lines at 12.1 and 13.3 keV, which could only be due to L and M shell conversion of a 13.5 keV γ-ray. A very weak line at about 75 keV was also reported.

From the intensity ratios of the various lines (Table 1.1) Johansson deduced that the gamma transitions must both be strongly converted (lower limit about 70%), and in cascade, and that K capture to the lower excited state must be of low intensity.

The same conversion lines were also found in the decay of Ga^{73} showing that the 53.3 keV and 13.5 keV transitions are common to both decays. (Fig. 2). The lines decayed with the 5-hour half-life of the Ga^{73} parent setting an upper limit on the lifetimes of these levels.

Stoker and Hok[17] (1953) have also observed the conversion electrons, using a beta spectrometer. Their results for energies and the intensity ratio K/L + M for the 53.3 keV transition agree well with those of Johansson.

More recently an investigation of the As^{73} conversion electron spectrum has been made by Grigor'ev et al.[18] (1958), using a $\pi\sqrt{2}$ double focussing magnetic spectrometer with resolution 0.4%. Their values of energies agree well with those of Johansson and the intensity ratios are only slightly different. (Table 1.1). The spectrometer resolution was good enough to enable the L and M + N conversion lines to be separated.

The Arsenic decay scheme now adopted (Fig. 1.3) was first put forward by Welker et al.[19] (1953). These workers studied the

TABLE 1.1

Intensity Ratio	Experimental Values		
	Johansson (1952)	Grigor'ev et al. (1958)	Others
K_2/L_2+M_2	5.6 ± 0.3	6.2 ± 0.2	7.6 ± 2.1[23], 5[11], 5.2[17]
$K_2+L_2+M_2/L_1+M_1$	1.2	1.4 ± 0.6	1.25[19]
$L_2/M_2 + N_2$		6.3 ± 0.2	
K_1/L_1	< 0.5		0.63 ± 0.22[19]
L_1/M_1	5.4 ± 0.5	6.6 ± 1.6	-
$K_1/L_1 + M_1$			0.37 ± 0.06[23]
L_1+M_1/Auger	0.77	-	-
K_3+L_3/K_2	0.001	0.0001	-
K-X rays/γ_2	-	-	6.2 ± 0.6[19]
K-X rays/γ_1	-	-	$\geqslant 1400$[19]
α_2 (Total conversion coefficient)	-	-	$8 (6 \leqslant \alpha_2 \leqslant 12)$[20,21]
	-	-	4.7 ± 0.6[19]
α_1 (Total conversion coefficient)	-	-	$\geqslant 1300$
K captures/53.3 keV transitions	-	-	$\leqslant 1.5$[19]
K-X rays/K_2+L_2	-	-	1.08 ± 0.08[20,21]
K-X rays/X - X coincidences	-	-	37 ± 1.5[20,21]
K-X rays/K_2	-	-	0.77 ± 0.15[23]

N.B. The subscript 1 refers to the 13.5 keV transition and subscript 2 to the 53.3 keV transition. Subscript 3 refers to the weak line reported by Johansson (see text).

γ-rays and X-rays using a sodium iodide scintillation counter with both an external and internal source. With the external source only the 53.3 keV gamma and 9.9 keV K-X rays could be observed, implying that the 13.5 keV transition is highly converted. Pulses at 13.5 keV energy were, however, seen following within a few μsecs. of the 53.3 keV pulses using the internal source, i.e. in the reverse order to that suggested by Johansson. No pulses were observed following the 9.9 keV pulses, confirming that none of the As^{73} decays feed the 13.5 keV level in Ge^{73}.

An upper limit of 1.5 was set on the ratio of K captures to 53.3 keV transitions by measuring the areas under the 9.9 keV and 53.3 keV peaks in spectra of the internal source.

The half-life of the 13.5 keV level (Table 1.2) was measured by the delayed coincidence method, also using the internal source.

TABLE 1.2

Observed Half-Lives

	As^{73}	66.8 keV Ge^{73} level	13.5 keV Ge^{73} level
Sagane et al.[10]	100d	-	-
Elliot & Deutsch[11]	~90d	-	-
McCowan et al.[12]	76 ± 3d	-	-
Welker et al.[19]	-	900μS < $T_{\frac{1}{2}}$ < 10secs.	4.6 ± 0.5 μS
Shaikh[23]			3.04 ± 0.07 μS
Campbell & Nelson[22]		0.53 ± 0.03secs.	

Using a source external to a NaI crystal with an aluminium window 0.001" thick the intensity ratio of 9.9 keV X rays and 53.3 keV gamma rays $^{X}/_{\gamma}$ was found (Table 1.1).

Welker also used an Argon-Methane gas proportional counter to look for unconverted 13.5 keV γ-rays. No evidence for 13.5 keV photons was found, the upper limit on the ratio of unconverted photons to K X rays being $^{1}/_{1400}$.

Barloutand et al.[20,21] used a double proportional counter to investigate the As^{73} decay scheme. The results of the first paper do not take account of the 13.5 keV level and are corrected in the second. A direct measurement of the 53.3 keV conversion coefficient using a scintillator detector to observe the γ-rays gave $6 \leqslant \alpha \leqslant 12$.

These workers also measured the intensity ratio of K-X rays to 53.3 keV conversion electrons, and the ratio R = no. of K-X rays/ no. of K-X ray - K-X ray coincidences (Table 1.1).

The lifetime of the second excited state of Ge^{73} has been measured by Campbell & Nelson[22] (1957). High purity Germanium was irradiated in a reactor for a few seconds producing Ge^{73} in the second excited state by capture of a thermal neutron by Ge^{72}. The sample was then propelled in about one tenth of a second to a shielded NaI scintillation spectrometer. Analysis of the decay curve with the spectrometer set on 53.3 keV gave the result $T_{\frac{1}{2}} = 0.53 \pm 0.03$ secs.

The short lived Ge^{73} isomer was also produced by chemical separation from an As^{73} source. With the As in concentrated hydrochloric acid solution at 100°C the volatile Ge $C\ell_4$ was formed and swept out by nitrogen gas to a lusteroid tube in a shielded well type NaI scintillation counter. By following the decay after stopping the gas flow the result $T_{\frac{1}{2}} = 0.52 \pm 0.03$ sec. was obtained. These values are well within the limits set primarily by Welker et al.

The most recent work on As^{73} is that of F. Shaikh (1968) of this department. Using a proportional counter he has measured the ratio of K-X rays to K conversion electrons (Table 1.1). The ratio $^{K}/_{L+M}$ for the 53.3 keV transition was measured directly from the proportional counter spectra, and the same ratio for the 13.5 keV transition was obtained from a delayed coincidence experiment, between 53.3 keV conversion electrons and K-X rays. The half-life of the 13.5 keV level was deduced from this delayed coincidence curve and that of 53.3 keV γ rays with the K-X rays (Table 1.2).

Multipolarity of the Transitions

53.3 keV. The experimental values of the ^{K} conversion coefficient α_K ($\alpha_K = {}^{\alpha}/(1 + \frac{L+M}{K})$ where α is the total conversion coefficient) and of $^{K}/_{L}$ ratio are compared with the theoretical values of Rose[44] (Table 1.3). The values of $^{K}/_{L}$ derived from the empirical curves of $^{K}/_{L}$ versus Z^2/E (where E is the transition energy) given by Goldhaber and Sunyar[16] are also listed. The measured K/L ratio favours an E1, M1, M2 or E2 transition for the 53.3 keV γ rays. The most accurately measured value suggests M2.

The observed half-life when compared to Weiskopf's[6] single particle estimates, (Table 1.4), excludes E1 or M1. The observed values of α_K all suggest M2 also although the two that agree are rather low (see later).

13.5 keV. Theoretical K conversion coefficients for such low energies have only very recently[8] become available and extrapolation gives only a rough value because the transition energy is

close to the threshold for conversion in the K shell. Comparison with Spinard's[47] threshold values and Rose's values (extrapolated) eliminate pure E1 and M1 type transitions (Table 1.6).

Comparison of the experimental values of K/L for the 13.5 keV transition with the theoretical values of Rose[44] (extrapolated by Shaikh[23] (1968)) and Spinard[47] (1955) and of Hebb[48] (also extrapolated by Shaikh) and the empirical values of Goldhaber[16] (1951) (Table 1.5) definitely excludes E1, E3 and M2 transitions. The experimental value agrees fairly well with the theoretical values for an E2 transition which suggests that the 13.5 keV γ ray is most probably a pure E2 type. Shaikh[23] (1968) states that the slightly higher experimental value may be attributed to uncertainty in the experimental measurements or to an admixture of about one percent M1 type in a mixed E2 + M1 transition.

From the measured half-life (and conversion coefficient) and comparison with the single particle estimates (Table 1.4), the 13.5 keV transition is either an E2 type accelerated by about 18 or an M1 retarded by 1.8×10^5. Most E2 transitions are enhanced by factors less than 10^3 (Gove[45] (1966)), and on the average by a factor of about 12 (Way[46] et al. (1956)). As pointed out by Shaikh[23] (1968), strongly retarded M1 transitions are not known, the average retardation being about 100 (Gove[45] (1966)).

TABLE 13

Theoretical and Experimental Values of the Ratios $^{K}/_{L}$ and α_K for 53.3 keV γ-rays

Multipole order	Theoretical $^{K}/_{L}$			Experimental $^{K}/_{L}$	Theoretical α_K		Experimental α_K
	Rose (1958)	Goldhaber (1951)	Hager (1968)		Rose (1958)	Hager (1968)	
E1	9.7	-	10	8 ± 2[23]	0.37	0.44	4.5 ± 0.6[23]
E2	6.1	~1.9	5.5	6.6 ± 0.4[15]	6.2	6.5	4.0 ± 0.6[19]
E3	2.4	~1.4	2.2	7.2 ± 0.3[18]	82	91	
M1	10.2	7.9	9.8	~5.9[11]	0.39	.48	
M2	7.6	6.9	6.9		7.1	8.2	
M3	4.6	4.1	4.4		105	130	~ 7[11]

(a) Shaikh(1968)[13]

(b) Johansson (1952)[6]

(c) Grigor'ev et al. (1958)[8]

(d) Elliot et al. (1943)[2]

(f) Welker et al. (1953)[9]

(g) Barloutaud et al. (1953)[11]

TABLE 1.4

Theoretical (Single particle) Estimates of $T_{\frac{1}{2}}$ (secs.)

					Experimental Results
13.5 keV	E1	$.12 \times 10^{-12}$	M1	7×10^{-12}	
	E2	5.3×10^{-5}	M2	3.1×10^{-3}	4.6 ± 0.5 μS (Welker et al.)[19]
	E3	1.1×10^{-2}	M3	.67	3.04 ± 0.7 μS (Shaikh)[13]
53.3 keV	E1	2.7×10^{-9}	M1	1.6×10^{-7}	
	E2	$.74 \times 10^{-4}$	M2	$.43 \times 10^{-3}$	0.53 ± 0.03 sec. (Campbell & Nelson)[12]
	E3	$.24 \times 10^{3}$	M3	$.16 \times 10^{5}$	

TABLE 1.5

K to L Conversion Electron Ratios for Z = 32 and E = 13.5 keV

Authors	Theoretical K/L						Experimental K/L
	E1	E2	E3	M1	M2	M3	
Rose (1958) (L-extrapolation)	7.2	0.43	0.01	9.5	4	0.45	0.44 ± 0.08[a]
Spinard (1955) (K-conv. electrons)						<0.5[b]	
Hebb (1940) (conv. electron table)	6.2	0.4	0.01	-	-	-	0.63 ± 0.22[c]
Hebb (1940) (K/L curve extrap'n)	8.0	~0.25	<0.1				
Goldhaber (1951) (K/L Curve extrap'n)	3.5	~0.17	<0.1	7.3	3.0	0.8	
Hager (1968)	6.7	.38	.01	9.8	4.8	0.6	

(a) Shaikh (1968)[23]

(b) Johansson (1952)[15]

(c) Welker et al. (1953)[19]

TABLE 1.6

Theoretical Values of α_K and α_L for Z = 32, E = 13.5 keV.

Conversion coefficient	Author	Multipolarity					
		E1	E2	E3	M1	M2	M3
α_K	Rose (extrapolated)	20	700	16000	25	1300	50000
	Spinard	18	260	1500	21	1300	21000
	Experiment	$\alpha_K \geq 500$[(a)]					
α_L	Rose (extrapolated)	2.5	600	150000	2.2	330	47000
	Experiment	$\alpha_L \geq 800$[(a)]					

(a) Derived from $\alpha \geq 1300$ and $K/L = 0.63$ (Welker et al.)

Spins and Parities of the Levels in the As^{73} Decay

The spin of the Ge^{73} ground state is known from direct measurement (see above) to be $^9/_2$ and the parity is even from the sign of the magnetic moment. This agrees with the shell model prediction that the 41^{st} neutron should be in a $g_{9/2}$ shell. (The isotopes $_{48}Nb^{89}_{41}$, $_{56}Nb^{97}_{41}$, $_{50}Nb^{9}_{41}$, also have 9/2 + ground states.)

Direct measurement of the ground state spin of As^{73} has not yet been made. The spin 3/2 with odd parity (Nuclear Data B1-6-48, Grigor'ev[24], 1963) is inferred from the shell model (33^{rd} proton in a $p_{3/2}$ shell) and from analogy with other nuclei with 33 odd nucleons, viz. $_{42}As^{75}_{33}$ $_{44}As^{77}_{33}$ $_{33}Zn^{63}_{30}$ $_{33}Ni^{61}_{28}$ $_{33}Fe^{59}_{26}$.

From the half-life, the log ft value is found to be 5.2 indicating an allowed decay so that the second excited state should have odd parity and spin $\frac{1}{2}$, $\frac{3}{2}$ or $\frac{5}{2}$. The absence of an M2 transition direct to the ground state excludes $\frac{5}{2}$ - .

The forbidden nature of the As^{73} decay to the ground and first excited states of Ge^{73} is pointed out by Grigor'ev (1963). Based on Welker's results, using the internal source (see Sec. 1.4), he states that less than 5% of the decays take place to these levels. This suggests a spin assignment of $\frac{5}{2}(+)$ or greater for the 13.5 keV level.

The E2 multipolarity of the 13.5 keV transition means that spin values $\frac{5}{2}$ + to $\frac{13}{2}$ + are possible. $\frac{9}{2}$, $\frac{11}{2}$, $\frac{13}{2}$ are all ruled out because the level is filled by means of the M2 transition with energy 53.3 keV (from the level with spin $\frac{1}{2}$ or $\frac{3}{2}$ -) and the value $\frac{7}{2}$ is highly improbable, because in that case the

multipolarity of the 13.5 keV transition would be mainly M1.

Since there is an M2 transition from the 66.8 keV level to the $\frac{5}{2}$ + 13.5 keV level, the spin of the 66.8 keV level is $\frac{1}{2}$ -. Grigor'ev[24] (1963) points out that any other choice of spins and parities for the first two levels would lead to difficulty in the interpretation of transitions in the decay of Ga^{73}. The decay of As^{73} adopted by Nuclear Data (1966)[43] is therefore as shown in Fig. 1.3.

1.5. Decay of Ga^{73}

Siegel and Glendenin[25] first reported the 5-hour nuclide Ga^{73} as a fission product of uranium and it has since been obtained by:

Irradiation of natural Ge with neutrons[25]	$^{73}Ge(n,p)Ga^{73}$
Irradiation of natural Ge with 100 Mev betatron X rays[26,27]	$^{74}Ge(\gamma,p)Ga^{73}$
Irradiation of Arsenic with 50 Mev X-rays[28]	$^{75}As(\gamma,2p)Ga^{73}$
and the reactions	$^{75}As(\alpha,\alpha 2p)Ga^{73}$ (29)
	$^{76}Ge(d,\alpha n)Ga^{73}$ (30)
	$^{74}Ge(n,pn)Ga^{73}$ (30)

Ga^{73} was also found in the products of 190 Mev deuteron fission of bismuth[31].

The half life of Ga^{73} has been measured by many authors (Table 1.7), the most accurate value of 4.85 ± 0.10 hours being due to Ythier et al.[30] (1959). These workers also observed the

TABLE 1.7

Ga^{73} Half-Life Measurements

Investigator	$T_{\frac{1}{2}}$ hours
Siegel & Glendenin[25] (1946)	5.0 ± .5
Perlman[26] (1949)	5
Goeckermann & Perlman[31] (1949)	4.94
	5
Rudstam[32] (1956)	4.77
Lenkoiskii[33] (1958)	4.5 ± 0.5
Ythier et al.[30] (1959)	4.85 ± 0.10
Marquez et al.[27] (1959)	5

TABLE 1.8

Ga^{73} β and γ energies

(β End point energy (Mev) and intensity; γ energy (keV) and intensity)

		1	2	3	
β	Siegel & Glendenin (1946)			1.4 ± 0.2 (100%)	
	Ythier et al.(1959)	0.40 ± 0.15 4.5 ± 2%	1.19 ± 0.04 95.5 ± 7%	<5%	
	Marquez et al.(1959)	0.55 (7%)	1.3 (83%)	1.6 ? (10%)	
γ	Ythier et al.	54 ± 1 (9 ± 1%)	295 ± 3 (97 ± 7%)	745 ± 10 6 ± 1%	1040 ± 15 1%
	Marquez et al.	53 ± 2 (13.5± 2%)	310 ± 5 (90 ± 15%)	740 ± 10 7%	

53.3 keV γ-ray (also found in the Arsenic-73 decay), using a scintillation counter. The presence of this line and the 13.5 keV transition had previously been confirmed (from the conversion electron spectrum) by Johansson[15].

The β^- spectrum has been studied using the absorption method[25,27,30] and with a scintillation spectrometer. As pointed out by Grigor'ev (1963) the results of Ythier et al.[30] are probably the most reliable as they used sources obtained by different reactions ((d, αn) and (n,pn)) from both natural Ge and Ge enriched in mass number 76. The β^- spectrum was observed using an end window G-M counter and a 4 cm. x 1 cm. stilbene scintillator. γ rays were found at the energies given in Table 1.8 by means of a 2.5 cm. x 2.5 cm. NaI crystal.

From a Kurie plot of the β^- spectrum these workers inferred a decay with limiting energy 1.19 Mev. A softer component (limiting energy 0.40 Mev) was responsible for a slight non-linearity towards the lower end of the plot.

The measured intensities (Table 1.8) and β-γ coincidence results showed that the 1.19 Mev endpoint β decay branch was followed by a 295 ± 3 keV γ ray, which populates the 66.7 keV level. Hence the total Ga^{73} decay energy was given as 1.55 ± 0.04 Mev.

Two other γ rays at 745 and 1040 keV were observed by Ythier et al.[30] and listed as coming from a single level at 1.11 ± 0.01 Mev fed by the lower energy β branch. Coincidences were also observed between the gammas at 295 and 745 keV.

No β branch to the 66.8 keV, 13.5 keV or ground levels of Ge^{73} could be found by absorption or coincidence measurements. The decay scheme proposed by Ythier et al. is shown in Fig. 1.4.

A more recent investigation by Schweizer et al.[34], using semiconductor counters, has confirmed that the main features of the decay are as given in Fig. 1.4. More gammas of low intensity were found and all the gamma energies measured more accurately. They are listed in Table 1.9. These workers found no gamma at 1040 keV (listed by Ythier et al.) and its observation in the Ga^{73} decay has been ascribed to summing of the 396 and 740 keV gammas[27]. It was listed by Ythier as a crossover transition which was in fact observed at 1066 keV by Schweizer. (A level at 1040 keV decaying direct to the ground state has, however, been found by Coulomb excitation (see later)).

The 296 keV γ ray was shown to be coincident with the 770 and 284 keV gammas, and that at 742 keV coincident with that at 325 keV.

The presently adopted Ga^{73} decay scheme[43] (Fig. 1.5) is basically that of Fig. 1.4, augmented by the levels suggested by the work of Schweizer et al. The other levels have all been found to result from Coulomb excitation or a (d,p) reaction on Ge^{72}.

Temmer and Heidenburgh[35] (1956) obtained the level at 67.03 keV by exciting Ge^{73} with 3.5 Mev α-particles and observing γ-rays with a scintillation spectrometer. Because of the long lifetime of the 66.8 keV level and consequent narrow energy width the probability of exciting it in this way is very small. Observation of a level implies a half-life $<10^{-7}$ sec. That this level has different properties to the 66.8 keV level was further confirmed by the absence of the 53.3 keV γ and presence of a 67keV gamma.

TABLE 1.9

List of γ Rays found in Ga^{73} Decay

	Energy Mev.	Relative Photon intensity normalised to 100 for γ_{4+5}	
γ_1	.054	9% [a]	
	.053	15% [b]	
	.053	2% [c]	
γ_2		0.5% [a]	(γ_{12} 1.066 [c])
	0.067	0.13% [c]	
γ_3	0.284	weak [c]	
γ_4	0.296	87% [c]	
γ_5	0.325	13% [c]	
γ_{4+5}	0.295	100% [a]	
(unresolved)	0.310	100% [b]	
γ_6	0.377	0.1% [c]	
γ_7	0.487	0.1% [c]	
γ_8	0.541	0.1% [c]	
γ_9	0.745	6% [a]	
	0.740	7% [b]	
	0.742	7% [c]	
γ_{10}	0.770	1.7% [c]	
γ_{11}	1.040	1% [a]	
		0.3% [c]	

a - Ythier et al.[25]

b - Marquez et al.[22]

c - Schweizer et al.[29]

Decay of As^{73} and Ga^{73}

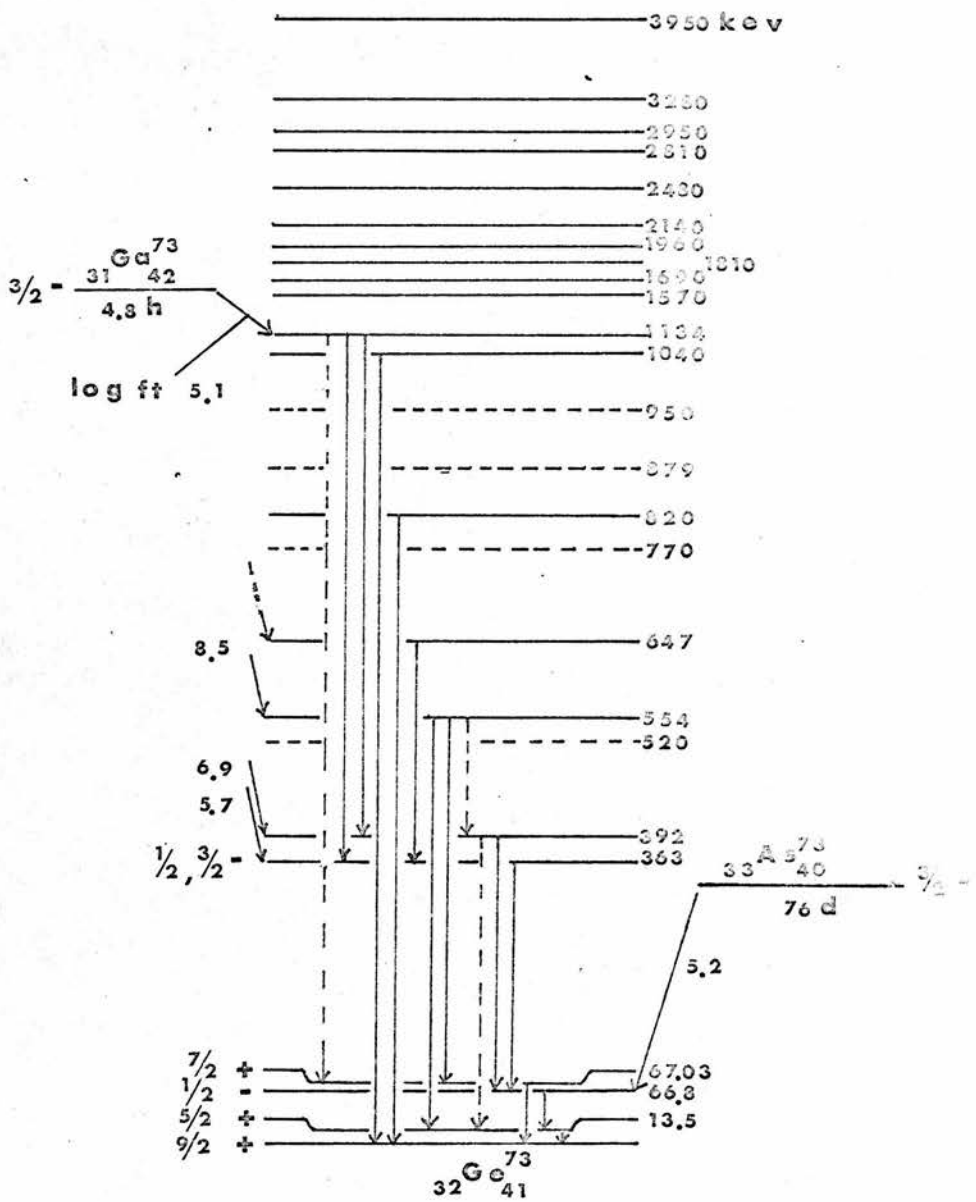

FIG 1.5

gamma. The relative yield of γ rays plotted against α particle energy fitted well to the theoretical curve for an E2 transition.

The half-life of the 67.03 keV level (1.54 nsec.) has been measured by Holland and Lynch[37]. They used a pulsed beam of α particles to excite the level and measured the time delay for the emission of the γ ray.

Du Mond[36] (1958) obtained the most accurate energy value of 67.03 $\pm$ 0.01 keV determined by a crystal spectrometer. The source in this case was made by inelastic scattering of protons by Ge.

The 67.03 keV level has also been obtained by Coulomb excitation using the heavier ions N^{14} (5.6 Mev)[38] and Ne^{20} (8-15 Mev)[39]. An angular correlation experiment performed in the Ne^{20} case gave results consistent with a spin assignment of $\frac{7}{2}$ or $\frac{11}{2}$.

A level at 820 keV has been established from Coulomb excitation using 1-3 Mev α particles (Temmer and Heidenburgh (1956))[35] and using N^{14} (Vasilev et al.[40] (1962)). Vasilev also observed the level at 1.04 Mev in the same experiment.

The other levels shown result from (d,p) reaction work by Silva and Eichler[41] and Bochin et al.[42].

Assignment of levels found in Ga^{73} decay and reactions.

The Ga^{73} ground state spin has not been measured directly, but from analogy with other nuclei with 31 nucleons, e.g. $^{71}_{40}Ga_{31}$ $^{69}_{38}Ga_{31}$ $^{67}_{36}Ga_{31}$ $^{57}_{31}Fe_{26}$ the spin and parity are taken to be $\frac{3}{2}^-$[43]. On the shell model the 31st proton should be in a

$2p_{3/2}$ orbit.

The half life of the 67.03 keV level shows the transition to the ground state to be of the type M1, with a hindrance factor $\gtrsim 0.1$. Thus the possible spin values are $\frac{7}{2}$, $\frac{9}{2}$ or $\frac{11}{2}$ the value $\frac{9}{2}$ being discarded from the Ne^{20} - γ angular correlation experiment(39).

The creation of this level by Coulomb excitation implies that the parity is even. It is listed in Nuclear Data(43) as $\frac{7}{2}+$, but $\frac{11}{2}+$ cannot be definitely ruled out.

Grigor'ev (1963) has attempted to explain the missing β^- decay feed to the 66.8 keV level ($Ga_{3/2}^- \rightarrow \frac{1}{2}$ - Ge^{73M}) (which should be allowed) by a $\frac{5}{2}$ - assignment to the Ga^{73} ground state. (In the shell model the $2p_{3/2}$ level lies just below the $1f_{5/2}$ level).

He does not, however, show the 67.03 keV level, which, if it has spin $\frac{7}{2}+$, would be fed (1st forbidden decay) by a β^- decay of a $\frac{5}{2}$ - Ga^{73} ground state.

The log ft = 5.7 for the 1.19 Mev β^- decay to the 363 keV level indicates an allowed transition, and gives $\frac{1}{2}$ -, $\frac{3}{2}$ -, $\frac{5}{2}$ - as possible spin values. Absence of a γ transition to the 13.5 keV ($\frac{5}{2}$ -) level rules out the spin $\frac{5}{2}$ - . The γ transition to the 66.8 keV ($\frac{1}{2}$ -) level supports an assignment of $\frac{1}{2}$ - or $\frac{3}{2}$ - .

1.6. "Anomalies" not explained by the accepted Decay Scheme

Conversion coefficient and X/γ ratio.

As pointed out above two of the values quoted for α_K are rather low compared to the theoretical value. Welker et al. obtained

$\alpha_K = 4.0 \pm 0.6$, using their own value of $^X/\gamma = 6.2 \pm 0.6$ and the values of electron intensity ratios measured by Johansson (Table 1.1), on the assumption that all captures proceed to the 66.7 keV level. Also assumed in the calculation were the K-shell fluorescence yield ($\beta_K = 0.56$) taken from Broyles et al.[49] and the fraction of L capture in As^{73} ($L_{Cap.frac.} = 0.11$) computed according to Rose and Jackson[5].

The other result in agreement with Welker's was obtained by Shaikh using the ratio K electrons/X rays measured in a proportional counter, and also the Welker $^X/\gamma$ ratio.

The earlier result $\alpha_K \simeq 7$ obtained by direct measurement using a proportional counter to detect conversion electrons and a scintillator to detect the 53.3 keV γ rays has a rather large error, probably due to uncertainty in the efficiency and solid angle for the two counters.

Grigor'ev[24] (1963) assuming the decay scheme of Fig. 1.3 and the electron intensity ratios measured by Johansson (and others) are correct, shows that results of a calculation to find the intensity of the K capture branch to the 13.5 keV level are reasonable only if the Welker result underestimates the $^X/\gamma$ ratio.

The correct value of this ratio is fairly important because a low value might suggest the presence of a K capture branch to a short-lived level 40-60 keV above the 66.8 keV level. If this level decayed to the 66.8 keV level without appreciable conversion it could explain the source of 'extra' γ rays. This would account for the low values of $^X/\gamma$ and α_K.

In the present work experimental reasons for a low $^X/\gamma$ value have been considered. Experiments have been performed in the light

of these considerations in an attempt to obtain a more accurate value of $^{X}/_{Y}$ (Chapter 2).

Direct measurement of the conversion coefficient has been repeated, paying particular attention to the estimation of solid angles and counter efficiencies. (Chapter 5).

The ratio K electrons/K-X rays has also been measured, using a proportional counter to detect the electrons and a scintillator to observe the K-X rays (Chapter 5).

Half-Lives

The 53.3 keV transition has been labelled M2 and comparison with the theoretical single particle estimate of Weiskopf shows it to be retarded by between 1.2×10^{3} and 8×10^{2} (depending on the value of α_K). As pointed out by Grigor'ev[24] (1963) this is about 100 times greater than usual.

On the other hand, the E2 gamma decay of the 13.5 keV level is accelerated by a factor of about 18[23].

The lifetime of the 66.8 keV level has been measured by a method different to that used by Campbell and Nelson[22] - the delayed coincidence method using a time to amplitude converter (Chapter 4).

A time to amplitude converter has also been used in a new measurement of the 13.5 keV level half-life, the results also giving the ratio K/L + M for this level and the K fluorescence yield (β_K) for Ge (Chapter 5).

Alternative suggestions to those of Shaikh (1968) for the acceleration and retardation of these decays are considered in the last chapter.

CHAPTER 2

EXAMINATION OF POSSIBLE EXPERIMENTAL REASONS FOR A LOW $^{X}/_{\gamma}$ RATIO

As pointed out in Chapter 1 the ratio of the intensities of 9.9 keV K-X rays and 53.3 keV γ rays emitted from As^{73} should be higher than the value 6.2 measured by Welker et al. In this chapter several suggestions which could at least partly account for a low experimental value are put forward. These come under the headings: summing (Section 2.2), dead time effects (Section 2.3) and window absorption (Section 2.4). From these considerations it becomes clear that a measurement of $^{X}/_{\gamma}$ as a function of solid angle might be of interest. The experiment performed to achieve this is described in Section 2.5 and the results and their analysis discussed in Section 2.6.

2.1. Notation

It is convenient to introduce a notation for the probability per As^{73} decay for the emission of the various possible radiations.

With the decay scheme of Fig. 1.3 K-X rays may arise in three ways:

1) From the electron capture process. The fraction of decays which produce a vacancy in the K shell is that fraction which occurs by K capture, i.e. $(1 - L_{\text{cap. frac.}} - M_{\text{cap. frac.}} - N_{\text{cap. frac.}})$ where $L_{\text{cap. frac.}}$ is the fraction proceeding by capture of an L shell electron, etc.

The probability that a K vacancy fills with the emission of

a K-X ray is the fluorescence yield β_K.

Thus the probability of a K X ray arising from the capture process is $p_1 = \beta_K(1 - L_{\text{cap. frac.}} - M_{\text{cap. frac.}} - N_{\text{cap. frac.}})$.

2) From the 53.3 keV transition. The number of conversion electrons produced per 53.3 keV transition is

$$\frac{\text{No. of conversion electrons}}{\text{No. of } \gamma\text{'s + No. of conversion electrons}} = \frac{K+L+M}{\gamma+K+L+M} = \frac{\alpha}{1+\alpha}$$

where $\alpha = \frac{K+L+M}{\gamma}$ = conversion coefficient for the 53.3 keV transition. Of these only the fraction $\frac{K}{K+L+M}$ will be K electrons, i.e. will give rise to K vacancies. Thus the no. of K vacancies per 53.3 keV transition is

$$\frac{1}{(1+\frac{L+M}{K})} \quad x \quad \frac{\alpha}{1+\alpha}$$

and the no. of K X rays per decay produced by this transition is

$$p_1' = \frac{\beta_K}{(1+\frac{L+M}{K})} \quad x \quad \frac{\alpha}{1+\alpha} \quad .$$

3) From the 13.5 keV transition. Similarly the no. of K X rays per 13.5 keV transition is

$$p_1'' = \frac{\beta_K}{1+(\frac{L+M}{K})_{13}} \quad x \quad \frac{\alpha'}{1+\alpha'}$$

where $(\frac{L+M}{K})_{13}$ is the $\frac{L+M}{K}$ ratio for the 13.5 keV conversion electrons and α' is the total 13.5 keV conversion coefficient.

Hence the probability per decay for a K X ray to be emitted is $p_X = p_1 + p_1' + p_1''$.

The probability per decay for emission of a 53.3 keV γ ray

will be called p_2.

The total internal conversion coefficient for the 53.3 keV transition (α) is defined by

$$\alpha = \frac{\text{No. of 53.3 keV conversion electrons}}{\text{No. of } \gamma \text{ rays}} .$$

Also, no. of conversion electrons per decay + No. of γ rays per decay = 1 (2.1)

From these two equations it follows that $p_2 = \frac{1}{1+\alpha}$.

The probability per decay that a 53.3 keV conversion electron is emitted will be called p_e.

From equation (2.1), $p_e = 1 - p_2 = \frac{\alpha}{1+\alpha}$.

The probability of a K conversion electron is

$$p_{Ke} = \frac{1}{(1 + \frac{L+M}{K})} \left(\frac{\alpha}{1+\alpha}\right) ;$$

The probability of a L,M,N conversion electron is

$$p_{Le} = \frac{1}{(1 + \frac{K}{L+M})} \left(\frac{\alpha}{1+\alpha}\right) .$$

Clearly $p_{Ke} + p_{Le} + p_2 = 1$, $\alpha_K = \frac{p_{Ke}}{p_2}$, $\alpha_L = \frac{p_{Le}}{p_2}$.

Using the values of electron intensity ratios listed in Table 1.1 and assuming

$$L_{cap.\ frac.} \simeq 0.1 \gg M_{cap.frac.}, N_{cap.frac.}$$

and $\beta_K = 0.56$, the p values are found to be those listed in Table 2.1a.

TABLE 2.1a

p Values, Calculated using Experimental Data in Table 1.1

	p_1	p_1'	p_1''	p_X	p_2	p_{Ke}	p_{Le}	p_e
$\alpha = 4.7$	0.50	0.39	0.19	1.08	0.175	0.71	0.13	0.84
$\alpha = 8.0$	0.50	0.42	0.19	1.11	0.111	0.76	0.14	0.90

2.2. Effects of and Search for Summing

For a source with two (or more) γ rays (γ_1 and γ_2) in cascade, a sodium iodide detector with high overall efficiency will exhibit a 'sum' peak at energy $\gamma_1 + \gamma_2$. This is because the light output of a scintillator is proportional to the energy deposited in the crystal, so that, provided γ_1 and γ_2 both deposit their energy in the crystal within the decay time of the phosphor, the light output will be proportional to the sum of their energies.

In the present case the overall detection efficiency must be kept high to ensure a good signal to noise ratio. Even a thin NaI crystal has an intrinsic efficiency of nearly 100% (for γ energy $<$60 keV), so that, with an external source, an overall efficiency of almost 50% is possible.

Since the 53.3 keV conversion coefficient is ~ 8 and the 13.5 keV coefficient is very high, the most likely 'summation', if any, is between two 9.9 keV K X rays - viz. the one marking the 'birth' of the 13.5 keV level and that marking its 'death'.

Less likely, but possible, is 53.3 - 9.9 keV summation.

The result of the second case would be to remove one count per 'summation' from the K X ray peak. In the first case the sum pulse, of energy 20 keV, would probably be included in the 53.3 keV escape peak (25 keV). Thus both 'sums' would reduce the numerator and the first would also increase the denominator in the $^{X}/_{\gamma}$ ratio, in both cases reducing its value.

For summing to occur in the crystal the lifetime of the intermediate level must be less than, or of the same order as, the scintillator decay time, which for NaI is $\sim 0.25\mu$sec. The accepted value of the half life of the 13.5 keV level is $\sim 3\mu$sec, so summing in the crystal can be expected to be comparatively rare. Summation at the photomultiplier anode cannot be ruled out so easily since the output pulses are $\sim 2\mu$sec long.

The output pulse length is controlled by $\tau = R_A C_A$ where R_A = anode load resistance and C_A = anode capacitance. Unless $\tau > 0.2\mu$sec (the NaI decay time), the output pulse height is reduced because the charge 'leaks' appreciably from the anode during its collection there.

With the notation of Section 2.1:

$$N_X = N_o(p_1+p_1'+p_1'')\varepsilon_K\omega_K$$

$$N_\gamma = N_o\, p_2\varepsilon_\gamma\omega_\gamma$$

where N_X, N_γ are the numbers of K X rays and γ rays detected, when N_o As^{73} atoms decay. ε is the detection efficiency and ω is the fractional solid angle subtended by the source at the counter, the subscripts X and γ referring to K X rays and 53.3 keV γ rays respectively.

Therefore in the absence of summing the observed $^{X}/_{\gamma}$ ratio is

$$(X/\gamma)_{n.s.} = \frac{(p_1+p_1'+p_1'')}{p_2} \times \left(\frac{\varepsilon_X \omega_X}{\varepsilon_\gamma \omega_\gamma}\right) .$$

Of the N_X KX rays $N_o\, p_1'\, p_1'' (\varepsilon_X\, \omega_X)^2$ are followed by a second K X ray within a few μsec. This is the number lost by the K X ray peak and (possibly) gained by the 53.3 keV escape peak. Hence the number of counts recorded when summing occurs is

$$N_{X\ obs.} = N_o(p_1 + p_1' + p_1'' - p_1'\, p_1''\, \varepsilon_X\, \omega_X)\varepsilon_X\, \omega_X$$

$$N_{\gamma\ obs.} = N_o(p_2\, \varepsilon_\gamma \omega_\gamma + p_1'\, p_1'' (\varepsilon_X \omega_X)^2)$$

$$\therefore (X/\gamma)_{obs.} = \frac{p_1 + p_1' + p_1'' - p_1'\, p_1''\, \omega}{p_2 + p_1'\, p_1''\, \omega} \simeq \left(\frac{X}{\gamma}\right)_{n.s} \left(1 - \frac{p_1' p_1'' \omega}{p_2}\right)$$

assuming $\varepsilon_X = \varepsilon_\gamma = 1$ and $\omega_X = \omega_\gamma = \omega$.

(Fraction of 53.3 keV rays absorbed at normal incidence $= 1 - e^{-\frac{\mu}{\rho}\rho x}$

> 0.999 using $\frac{\mu}{\rho} = 8$ (Siegbahn[50]), $\rho = 3.5$ gm./cc., and

$t = 0.5 \times 2.54$ cm.).

Adopting the p values in Table 2.1a and taking $\omega = 0.5$ yields $(X/\gamma)_{obs.} \simeq (X/\gamma)_{n.s.}\ (1 - 0.3)$.

Thus, if summing occurs, the observed value of X/γ could be too low by up to about 30%. However, summing should also produce a change in the shape of the spectrum. This change can be made apparent by subtracting the spectrum due to the 53.3 keV γ rays alone from that due to the 53.3. keV γ rays and 9.9 keV K X rays. Any peaks left above 9.9 keV would indicate the presence of summing. These peaks are to be expected at about 20 keV and 63 keV.

The spectrum due to the 53.3 keV γ rays alone was obtained by placing a Zn absorber (10 thou thick) between the source and the detector. This absorber is thick enough to absorb the 9.9 keV K X rays (almost totally), and allow no characteristic Zn K X rays (~8.6 keV) to reach the detector, while thin enough to transmit about 70% of the 53.3 keV γ rays at normal incidence (see Section 2.6).

Counter, Electronics and Source. A sodium-iodide detector was chosen for this work because of its high constant efficiency, fairly good resolution, and low background ndse at low energies. Solid state detectors are to be preferred for strong sources owing to their superior resolution but the relatively high background noise (at 10 keV) makes them useless for low activity work. Proportional counters show good resolution and fairly low background, but their efficiency varies rapidly with energy (and gas pressure) so that although almost 100% efficiency is possible for 10 keV photons, say, the efficiency at 53.3 keV is then very low.

The present set-up consisted of a 1" dia. NaI crystal, $\frac{1}{2}$" deep and fitted with a 36 mgm/cm^2 Be window. This was mounted using silicon optical grease on a 56 AVP photomultiplier tube. The P.M. tube supply chain is shown in Fig. 2.1. The focus and deflection electrode potentials were adjusted to give maximum count rate with a fairly strong Am^{241} source.

It is assumed above that the 13.5 keV level always decays in a time < the length of the output pulse. To make this more reasonable, and any effect therefore more noticeable, the output pulse length was increased to ~ 20μsec. by using an anode load $R_L \simeq 500$ kΩ.

Photomultiplier Supply Chain

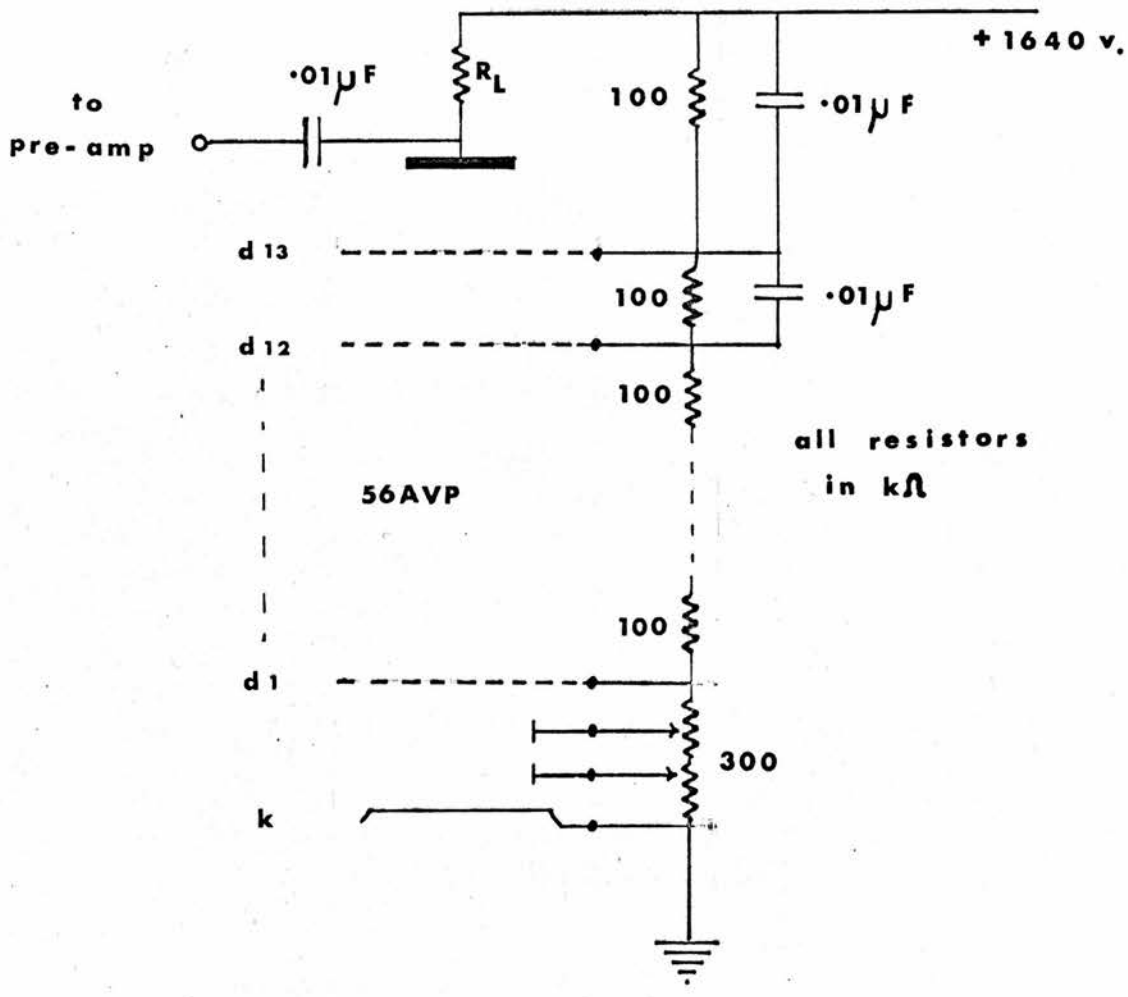

FIG 2.1

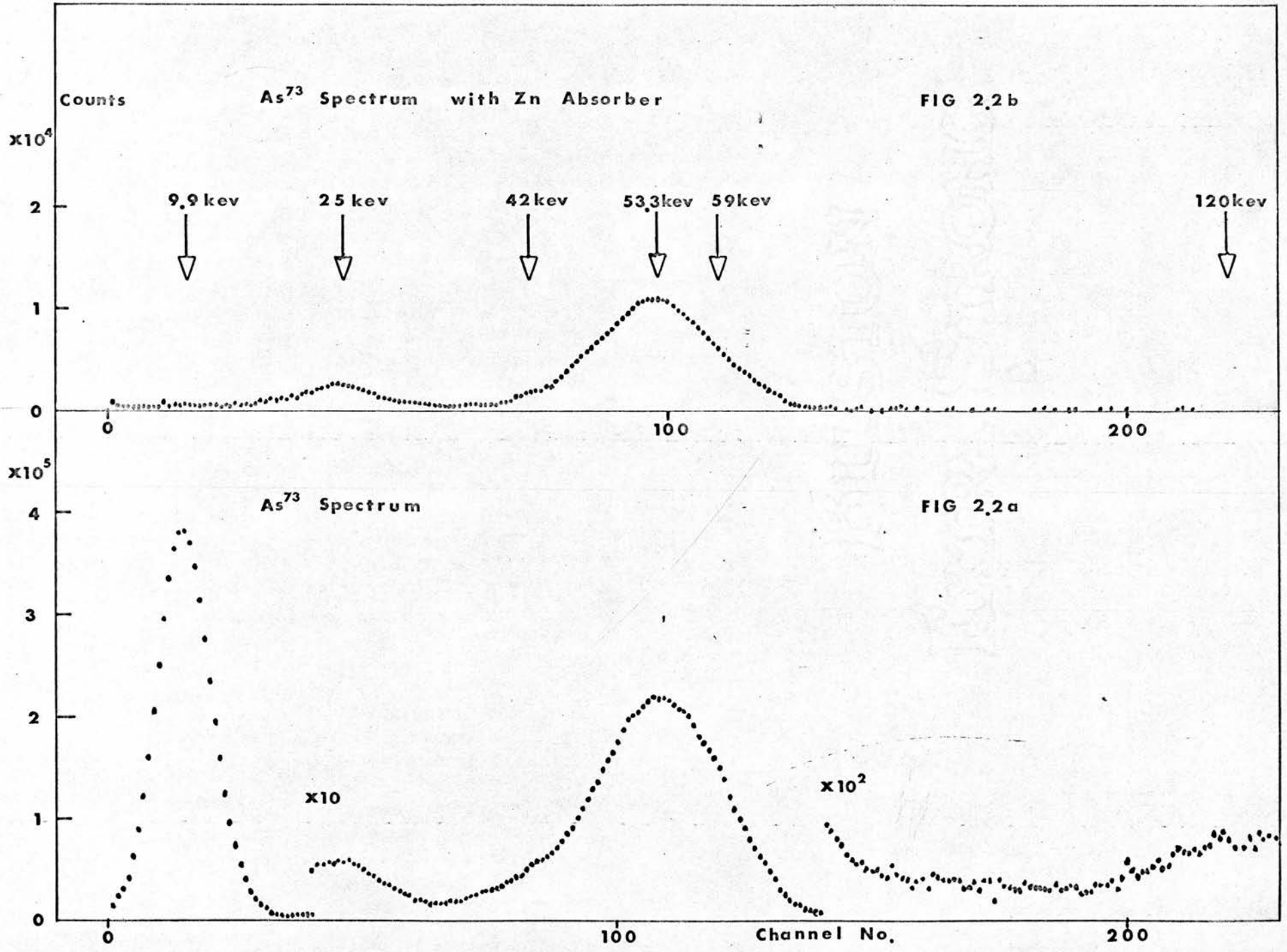
Counts
As73 Spectrum with Zn Absorber
FIG 2.2b
x10⁴
2
1
0
9.9 kev
25 kev
42 kev
53.3kev
59kev
120kev
0
100
200
x10⁵
As73 Spectrum
FIG 2.2a
4
3
2
1
0
x10
x10²
0
100
Channel No.
200

FIG 2.2c Background Spectrum

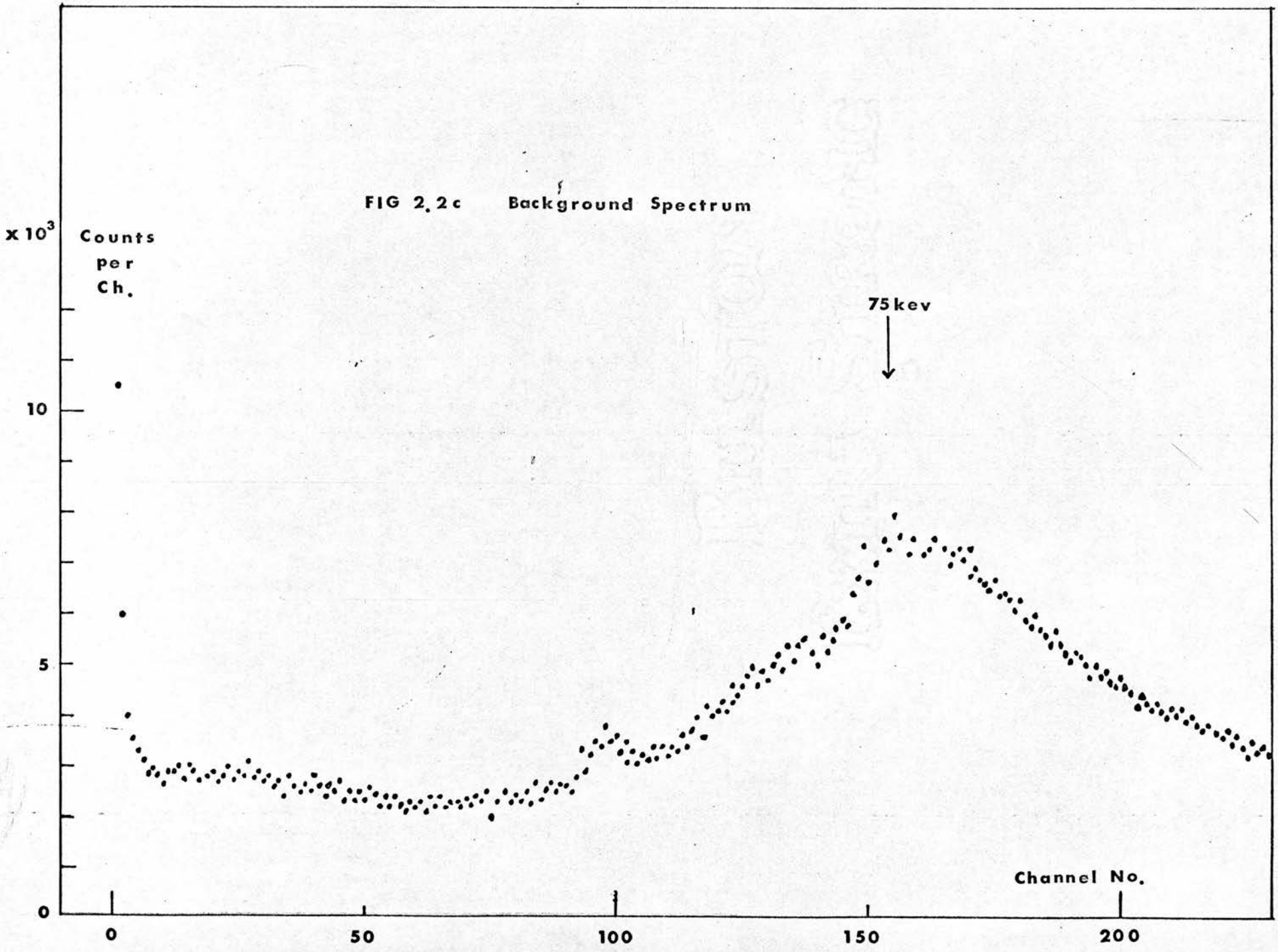

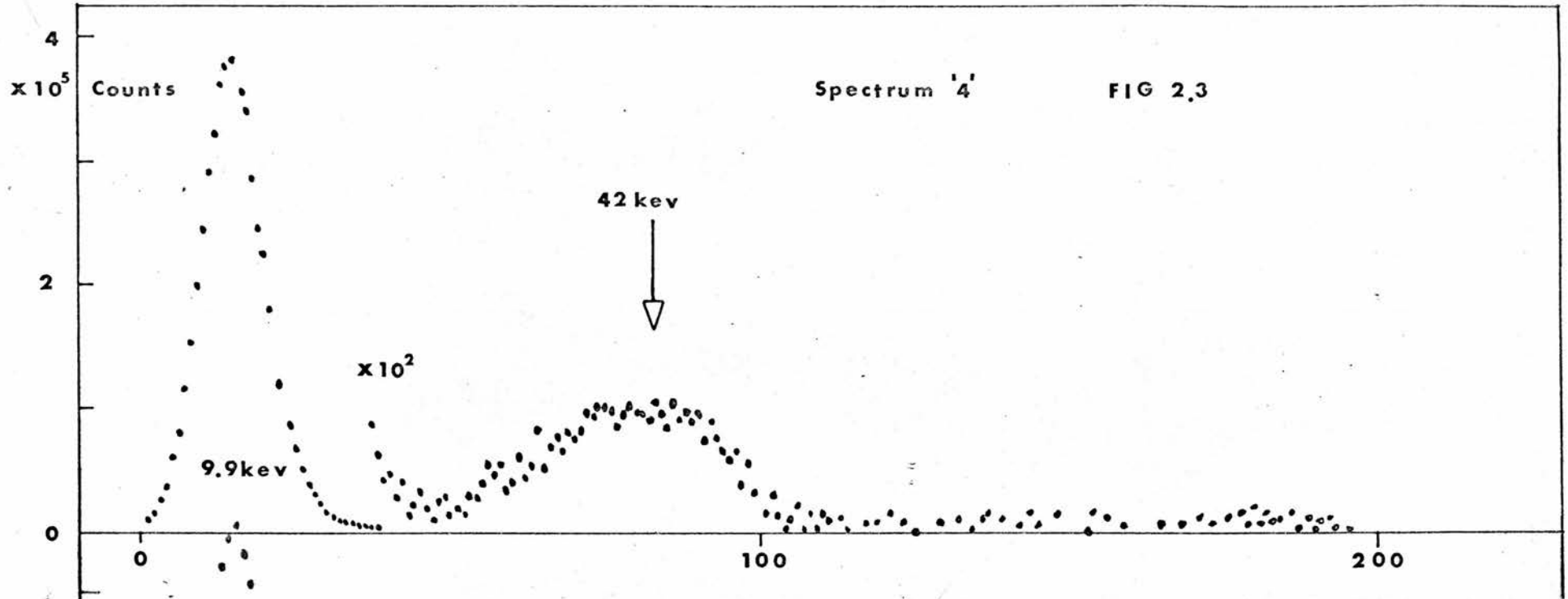
4
x10^5 Counts
Spectrum '4'
FIG 2.3
42 kev
2
x10^2
9.9kev
0
0
100
200

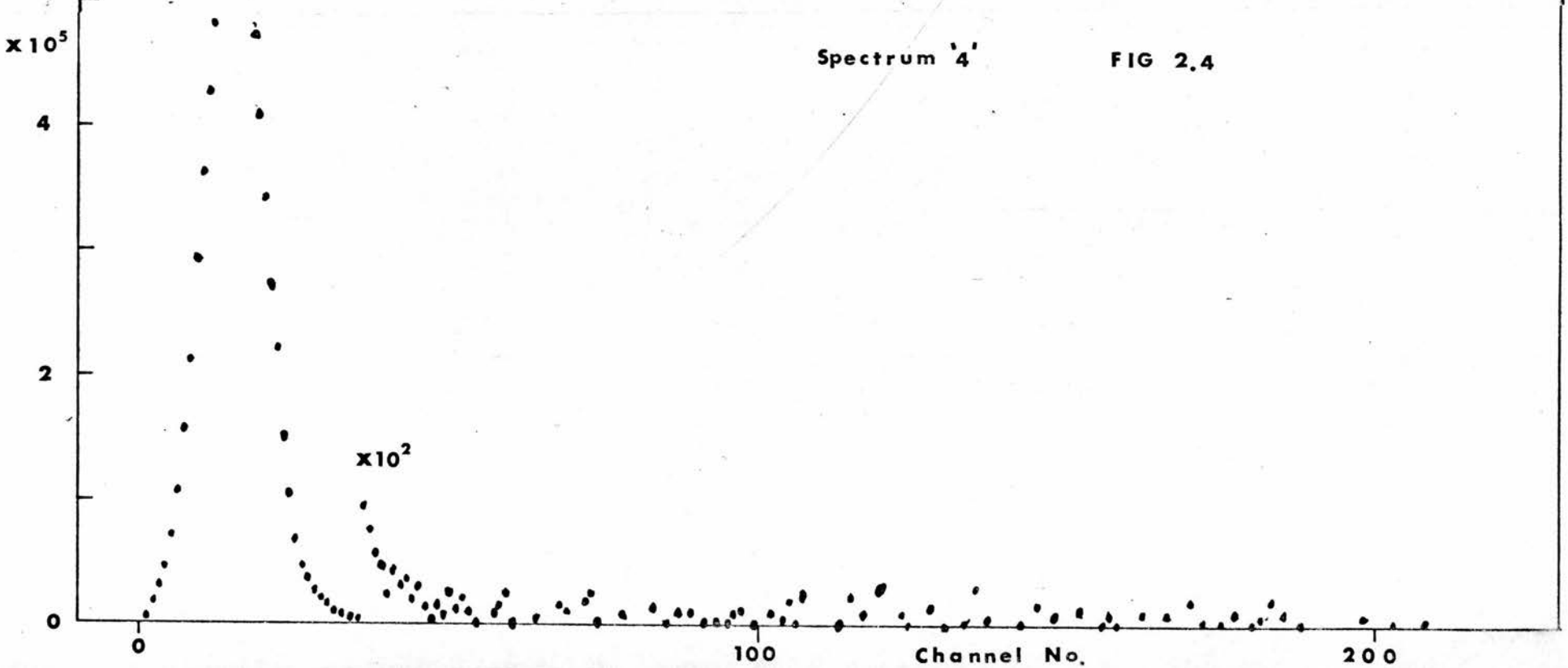
x10^5
Spectrum '4'
FIG 2.4
4
2
x10^2
0
0
100
Channel No.
200

Scintillation Counter Assembley

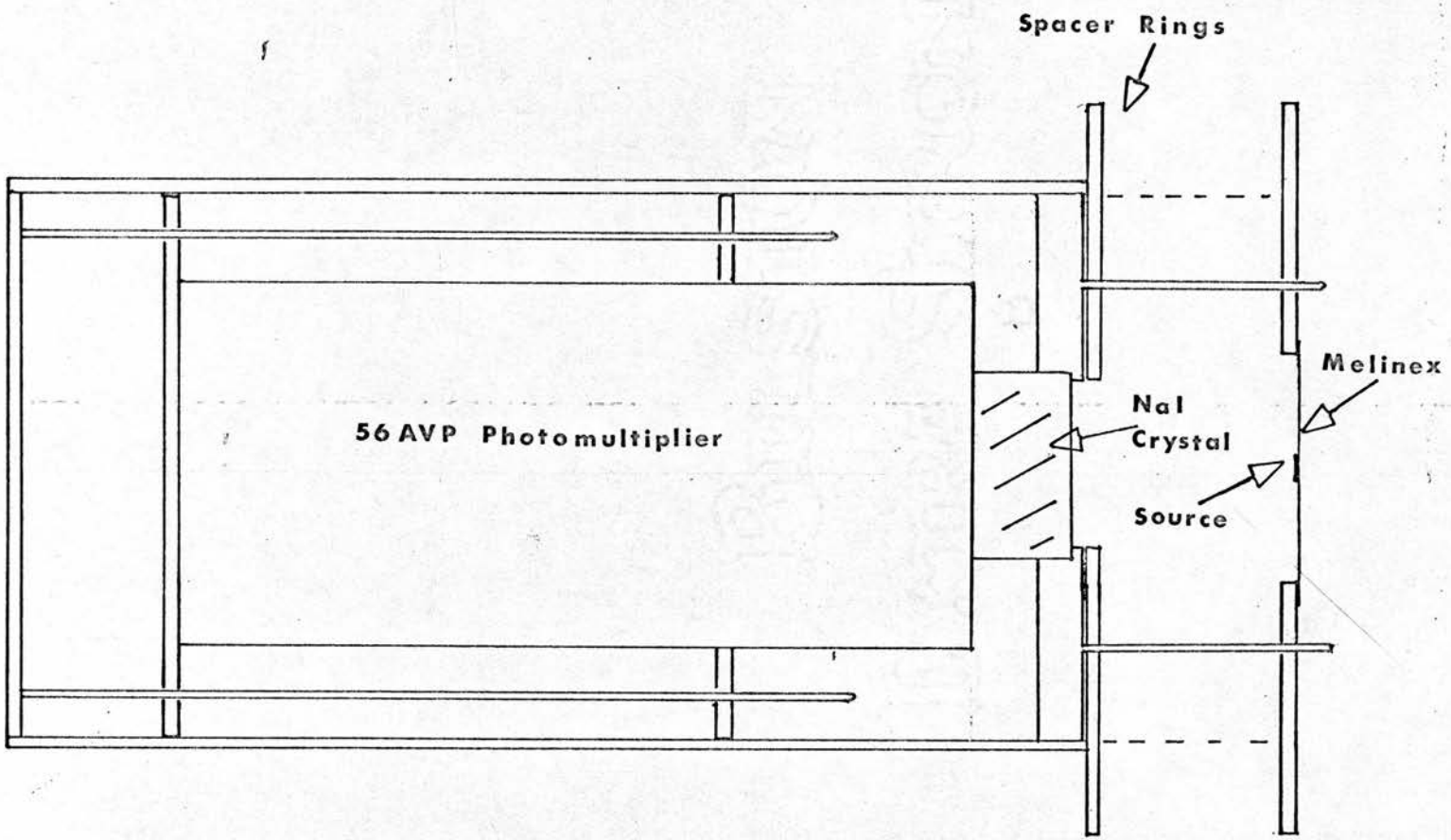

FIG 2.5

The P.M.-tube-crystal assembly was mounted in a paxolin tube closed at one end by a brass plate which carried the E.H.T. supply and signal output plugs. Three screwed rods mounted on this plate carried the P.M. tube base (fixed to a paxolin ring) and paxolin rings to keep the P.M. tube in position. Three 1" long springs on these rods kept the P.M. tube crystal assembly pressed firmly against the front of the tube - a $\frac{1}{8}$" thick paxolin ring screwed to a brass collar.

Spacer rings and one carrying the source could be bolted to the front of the counter. (Fig. 2.5).

The main amplifier was type NE 5259 and the pre-amp. type NE 5281. Amplifier output pulses were fed to a Laben 512 channel analyser of which about 300 channels (40 mV. wide) were used. The power supplies were Solartron type AS 1410 delivering + and - 24 v. for the amplifier and pre-amp., and the E.H.T. supply for the P.M. tube was obtained from an Isotope Developments type 532D unit. This was set to supply 1640 v.

The source was made by allowing several drops of active sodium arsenate solution, supplied by the Radiochemical Centre, Amersham, to evaporate on a 1" square melinex sheet 2 mgm/cm.^{2} thick, and then covering it with a second sheet of the same thickness.

The experiment involved recording three spectra.

1. Background.
2. Source (open).
3. Source covered by Zn absorber.

After background (Fig. 2.2c) subtraction the spectra obtained are shown in Figs. 2.2a and 2.2b. The factor r by which the 53.3 keV intensity was reduced by the Zn absorber was found by taking the ratio of the number of counts under the 53.3 keV photo-peaks of spectra '3' and '2' respectively. Spectrum '2' was then

multiplied by r and spectrum '3' subtracted from the result yielding spectrum 4 shown in Fig. 2.3. In the absence of summing this should contain only the 9.9 keV photopeak. The actual result exhibits a small peak at about 40 keV. This was at first thought to be due to some kind of non-linear summation but is more readily explained as due to Eu^{152} contamination present in the source.

During this work a small peak was noticed at about 120 keV - apparently a new line in the As^{73} spectrum. To see if it decayed at the same rate as As^{73} several spectra were taken over a period of ~1 month, when it became clear that the 120 keV activity was much longer lived than As^{73}. It was then discovered that the fume cupboard used to evaporate the As^{73} source had previously been used to make a strong Eu^{152} source ($T_{\frac{1}{2}} \simeq 12$ years). A spectrum recorded with a strong Eu^{152} source showed that the spurious 'As^{73}' peak coincided well with the 122 keV line in the Eu^{152} spectrum. The apparent sum peak at 40 keV is almost certainly due to the small contamination of Eu^{152} which has a strong K X ray line at 42 keV. (Eventually, as the As^{73} 53.3 keV activity decreased the 42 keV activity became evident as a distortion of the low energy half of the 53.3 keV photopeak.) Since considerable data had been acquired on the decay of the As^{73} 53.3 keV activity, the measurements were continued and used to determine the half-life of As^{73} (see Chapter 3).

Another source was made (in a 'clean' fume cupboard) and the above measurements repeated. As can be seen from the spectrum '4' (Fig. 2.4), no appreciable ($< 1\%$) summing apparently takes place in the counter, at least with the kicksorter system used.

The arithmetic was done on the spectra stored in a 20 x 300 array in a KDF9 computer. Routines were written in Atlas Autocode

to enable spectra to be read in and subtracted from each other. Other routines enabled spectra with and without absorber to be matched (the ratio of counts under their photopeaks giving the value of r), the number of counts over any particular channel range to be calculated, spectra to be plotted and to be shifted up or down to allow for small zero channel drifts.

2.3. Effects of Counter Dead Time on $^{X}/_{\gamma}$ Ratio.

Although no summing effects have been found it is still possible that a 9.9 keV X ray pulse following within a few microseconds of a 53.3 keV γ ray pulse or another 9.9 keV pulse could be lost due to the counter still being 'dead', i.e. in the act of recording the first pulse. The half life of the 13.5 keV level is $\sim 3\mu s$. so that pulse pairs separated by a time of this order are to be expected. The 'kick sorter' was always used on the variable dead time setting, when recording As^{73} spectra. This means that the instrument is dead for a time which depends on the amplitude of the recorded pulse in a way given by: $(22 + 0.25 \times N)\mu s$ (N = ch. no.), i.e. a minimum possible dead time of $\sim 22\mu s$. Hence it might be expected that some X ray pulses could be lost and the observed $^{X}/_{\gamma}$ ratio therefore be too low.

Consider the simplified decay scheme with a short lived intermediate state. If the detector dead time is taken to be $22\mu s$ for all pulses, then when γ_1 is detected γ_2 is nearly always lost. The number of times this happens depends on the counter efficiency ($\simeq 100\%$ for γ_1 and γ_2 in the As^{73} case)

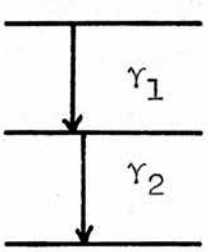

and on the effective solid angle Ω subtended by the counter at the source:

e.g. for $\Omega = 4\pi$ γ_2 is always suppressed.

for $\Omega = 2\pi$ of the γ_2 counts are suppressed

$$\therefore \quad N_{\gamma_2} = 2N_{\gamma_2 \text{ obs.}}$$

for $\Omega = \Omega \quad \frac{\Omega}{4\pi}$ of the γ_2 counts are suppressed

$$\therefore \quad N_{\gamma_2} = \frac{1}{(1 - \frac{\Omega}{4\pi})} \; N_{\gamma_2 \text{ obs.}}$$

where N_{γ_2} is the 'true' γ_2 count rate and $N_{\gamma_2 \text{ obs}}$ is the observed γ_2 count rate, and where γ_1 is always detected.

However in the As^{73} case the decay scheme (introduced in Chapter I) is more complicated:-

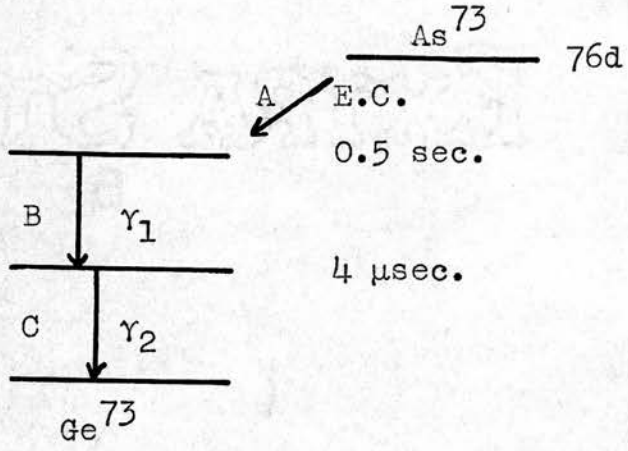

There are three contributions to the K X ray count rate, namely those originating from transitions (A), (B) and (C). The K X rays from the K capture (transition (A)) should always be detected if they enter the counter. With the notation of Chapter I this occurs with probability $p_1 \varepsilon_X \omega_X$ per decay where ε_X is the intrinsic X ray detection efficiency and ω_X is the effective fractional solid angle subtended by the counter at the source for K X rays.

The 53.3 keV gamma pulses (γ_1) probability $p_2\varepsilon_\gamma\omega_\gamma$ per decay, and the K X rays which arise from the transition (B) probability $p_1'\varepsilon_X\omega_X$ will not be suppressed because of the long half-life ($\sim\frac{1}{2}$ sec. >> 22μs.) of the present level. (The probability of the level decaying within time t is $1 - e^{-\lambda t} \simeq 25 \times 10^{-6}$ for $T_{\frac{1}{2}} = \frac{0.6931}{\lambda} = 0.5$ sec. and $t = 22\ \mu$sec.) However, the K X rays from transition (C) will be suppressed if they follow either a 53.3 keV γ or a K X ray from the transition (B) detected in the counter. These K X rays will be detected if they follow an undetected 53.3 keV γ, an undetected KX ray from transition (B) or an Auger transition (B). Hence the probability per decay of recording a K X ray from transition (C) is $p_1''(1 - p_1'\varepsilon_X\omega_X - p_2\varepsilon_\gamma\omega_\gamma)\varepsilon_1\omega_1$ rather than $p_1''\varepsilon_X\omega_X$.

Hence the actual number of K X rays counted per decay is $[p_1 + p_1' + p_1''(1 - p_1'\varepsilon_X\omega_X^{-p_2\omega_\gamma\varepsilon_\gamma})]\varepsilon_X\omega_X$ instead of $(p_1 + p_1' + p_1'')\varepsilon_X\omega_X$.

Thus the observed ratio $^X/_\gamma = \dfrac{[p_1+p_1'+p_1''(1 - p_1'\varepsilon_X\omega_X - p_2\varepsilon_\gamma\omega_\gamma)]\ \varepsilon_X\omega_X}{p_2\ \varepsilon_\gamma\ \omega_\gamma}$

The true $^X/_\gamma$ ratio is $\dfrac{p_1 + p_1' + p_1''}{p_2}$ and

$$C_N \times (\text{obs } {}^X/_\gamma) = \frac{p_1+p_1'+p_1''}{p_2} - \frac{p_1''p_1'\varepsilon_X\omega_X}{p_2} - p_1''\ \varepsilon_\gamma\ \omega_\gamma$$

$$= (\text{true } {}^X/_\gamma) - \frac{p_1''p_1'\varepsilon_X\omega_X}{p_2} - p_1''\ \varepsilon_\gamma\ \omega_\gamma\ ,$$

where C_N = normal efficiency and solid angle correction factor

$$\frac{\varepsilon_\gamma\ \omega_\gamma}{\varepsilon_X\ \omega_X}\ .$$

$$\therefore \quad (\text{true } {}^{X}/_{\gamma}) = C_N(\text{obs. } {}^{X}/_{\gamma}) + \frac{p_1'' p_1' \varepsilon_X \omega_X}{p_2} + p_1'' \varepsilon_\gamma \omega_\gamma \ .$$

Taking $\varepsilon_X = \varepsilon_\gamma = 1$ and $p_1 = 0.5$, $p_2 = 0.11$, $p_1'' = 0.19$, $p_1' = 0.42$ from Table 2.1a gives

$$\text{true } {}^{X}/_{\gamma} = C_N(\text{obs. } {}^{X}/_{\gamma}) + 0.25 + 0.06 \quad \text{for } \omega_X = \omega_\gamma = 0.5$$

i.e. $$\text{true } {}^{X}/_{\gamma} = C_N(\text{obs. } {}^{X}/_{\gamma}) + 0.31$$

and $$\text{true } {}^{X}/_{\gamma} = C_N(\text{obs. } {}^{X}/_{\gamma}) + 0 \quad \text{for } \omega_X = \omega_\gamma = 0 \ .$$

Thus it is to be expected that the ${}^{X}/_{\gamma}$ ratio measured using large solid angles will be underestimated by up to about 0.3 because of counter dead time. The necessary correction factor can be made small by performing the experiment with small solid angles, but for a given source strength statistical accuracy suffers due to reduction in the signal/noise ratio.

The above result suggests that the observed ${}^{X}/_{\gamma}$ ratio should increase as solid angle decreases. Another effect concerning the disparity in absorption of 53.3 keV and 9.9 keV in the counter window, discussed in the next section, suggests a similar variation with solid angle. To find out if this variation could at least partly explain the low ${}^{X}/_{\gamma}$ value discussed in Chapter 1 the experimental work described in Section 2.5 was undertaken.

2.4. Effect of Counter Window on ${}^{X}/_{\gamma}$ ratio.

The relatively high light output of sodium iodide, supplied by Nuclear Enterprises (G.B.) Ltd., makes it an attractive material for use as a scintillation detector of low energy radiation. However, being highly deliquescent it cannot be conveniently used

unless encapsulated in an air tight container, usually made of aluminium. Some of the incident photons to be detected may be absorbed in passage through the container, and this effect increases as the incident photon energy decreases. In fact, the fraction of the incident intensity transmitted on the assumption that the photons are incident normal to the container walls is $\frac{I}{I_o} = e^{-\mu t}$ where μ is the absorption coefficient of the wall material in $cm.^{-1}$ and t its thickness in cm. This can be written $\frac{I}{I_o} = e^{-\mu/\rho \cdot \rho t}$ where ρ is the density of the absorber material in gm./cc. For a parallel beam of radiation incident at angle θ, this becomes $e^{-\mu t/\cos\theta}$. If (as in the present case) an intensity comparison is made between photons of different energy the lower energy component will be underestimated by an amount which depends on the absorption coefficient and thickness of the container material and also on the source-crystal geometry.

In order to keep this effect small the crystal used in the X/γ ratio experiments was 1" dia. × ½" deep NaI (supplied by Nuclear Enterprises (G.B.) Ltd.) encapsulated in aluminium but fitted with a Be window of thickness 36 $mgm/cm.^2$. To gain some idea of the advantage of using Be, consider the transmitted fraction of a normally incident parallel beam. Taking the theoretical value for μ/ρ = 0.554 $cm.^2/gm.$ (given by Sighbahn[50]) leads to I/I_o = 0.98. For the thinnest usable $A\ell \sim 0.001"$ (i.e. 7 $mgm/cm.^2$), however, this ratio is 0.84, again using Sighbahn's[50] theoretical value for μ/ρ = 22.3 $cm.^2/gm.$

If the above case were relevant, then neglecting the very small absorption of the 53.3 keV (I/I_o = 0.994), a correction factor of $\sim +2^o/o$ should be applied to the X/γ ratio. However,

this correction was calculated on the assumption of a parallel beam of radiation normally incident on the counter window and is therefore only justified in the limit of small solid angle, i.e. when the source is distant from the window.

To find the magnitude of the effect of non-normal incidence consider a point source S placed at the centre of the counter window and just outside it:-

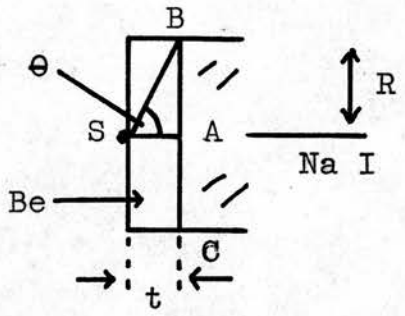

Due to the window thickness (t cm.), the distance a photon must travel in the Be before reaching the sensitive detector is t cm. The maximum distance is SB = $t/\cos\theta$ where θ is the half angle subtended by the sensitive counter at the source, given by

$$\tan\theta = \frac{AB}{SA} = \frac{R}{t} .$$

Taking t = 0.008", R = 0.4", yields θ 89° so that SB 1 cm.

The transmission of photons passing through 1 cm. of Be is $e^{-\frac{\mu}{\rho}\rho.1} = 0.14$, where $\rho = 1.8$ gm./cc. and $\frac{\mu}{\rho} = 0.95$ cm.^{2}/gm.

Thus the transmitted fraction of 9.9 keV K X rays must lie somewhere between 0.14 and 0.98. In the next paragraph an exact expression is derived for this factor.

In the general case of a point source placed centrally in front of the window at a distance 'd' from the sensitive detector face (i.e. from the back of the window) the figure given below

applies:

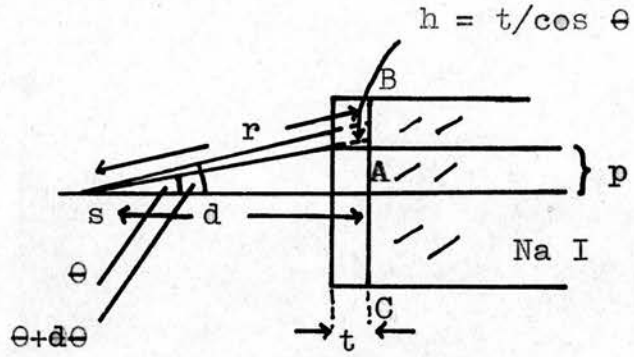

If the source emits $4\pi N_o$ K X rays/sec then this number pass through the surface (area $4\pi r^2$) of a sphere, (radius r) centered at S, per second. Therefore the intensity r cm from the source $I(r) = N_o/r^2$/unit area/sec. The area of the annulus on the window subtending the cones of half angles θ and $\theta + d\theta$ is $2\pi p.rd\theta$. Hence the number of photons incident on this annulus = area x intensity = $\frac{N_o}{r} .2\pi\ p\ d\theta$ per sec.

After passing through the window this number is reduced to

$$\frac{N_o}{r} .\ 2\pi\ p\ e^{-\mu h}\ d\theta\ ,\ \text{where}\ \sin\theta = \frac{AB}{SB}\ .$$

$\therefore$ The total no. of photons entering the counter

$$= \int_o^{\theta} 2\pi p \frac{N_o}{r} e^{-\mu h}\ d\theta$$

$$= \int_o^{\theta} 2\pi\ N_o .d \tan\theta\ .\ \frac{\cos\theta}{d}\ e^{-\mu t/\cos\theta}\ d\theta$$

$$= \int_o^{\theta} 2\pi\ N_o \sin\theta\ e^{-\mu t/\cos\theta}\ d\theta$$

$$= -2\pi\ N_o \int_1^{\cos\theta} e^{-\mu t/x}\ dx\ .$$

where $x = \cos\theta$.

On the assumption that every photon reaching the NaI is detected, the fraction of the emitted X rays recorded is

$$\varepsilon_1 \omega_1 = \frac{-2\pi}{4\pi} \int_1^{\cos\Theta} e^{-\mu t/x}\, dx.$$

In the case when d is large compared to R, i.e. $\cos\Theta \simeq 1$ the integrand does not change appreciably between the limits and

$$\varepsilon_1 \omega_1 = + \tfrac{1}{2} e^{-\mu t/x} (1 - \cos\Theta).$$

This is the normal efficiency factor since the fractional solid angle is given by $\frac{1}{2}(1 - \cos\Theta)$ and $e^{-\mu t/x} \simeq e^{-\mu t}$, the attenuation factor for normal incidence.

Unless approximations are made, the integral in the expression for $\varepsilon_1 \omega_1$ can only be evaluated numerically.

<u>Approximation for $\cos\Theta \simeq 1$</u> : $\varepsilon_1\omega_1 = \frac{1}{2}\int_{\cos\Theta}^{1} e^{-\mu t/x} dx$

$$= \tfrac{1}{2}\int_{\cos\Theta}^{1} e^{-a'/x}\, dx.$$

where $a' = \mu t$.

Provided $a'/x < 1$ the exponential can be expanded as:

$$e^{-a'/x} = 1 - a'/x + \tfrac{1}{2}\left(\frac{a'}{x}\right)^2 - \frac{1}{6}\left(\frac{a'}{x}\right)^3 + \ldots\ldots$$

Neglecting higher terms in this expansion will involve an error of only about 1% provided $\frac{1}{6}\left(\frac{a'}{x}\right)^3 < 10^{-2}$ for all x. This condition is satisfied if $\frac{1}{6}\left(\frac{a'}{\cos\Theta}\right)^3 < 10^{-2}$ <u>or</u> $\cos\Theta > a'\sqrt[3]{\frac{10^2}{6}} \simeq 2.5a'$.

i.e. $\Theta < \cos^{-1}(2.5a')$ (2.3.1)

In this case

$$\varepsilon_1 \omega_1 \simeq \tfrac{1}{2}\int_{\cos\Theta}^{1} \left[1 - a'/x + \tfrac{1}{2}(a'/x)^2 - \tfrac{1}{6}(a'/x)^3\right] dx$$

$$= \tfrac{1}{2}\left[x - a' \log x - \tfrac{1}{2}(a'^2/x) + \tfrac{1}{12}\left(\frac{a'^3}{x^2}\right)\right]_{\cos\Theta}^{1}$$

$$\therefore \quad \varepsilon_1 \omega_1 \simeq \tfrac{1}{2}(1 - \cos\Theta) + \frac{a'}{2}\log(\cos\Theta) - \frac{1}{4}a'^2\left(1 - \frac{1}{\cos\Theta}\right)$$

$$+ \frac{a'^3}{24}\left(1 - \frac{1}{\cos^2\Theta}\right) .$$

The first term is the fractional solid angle and the others may be regarded as a correction for the effect of window absorption. Calculation for several Θ values yields the results shown in Table (2.1), using $\mu = 0.694$ cm.^{2}/gm. (see Appendix II).

For Θ values greater than $\cos^{-1}(2.5a')$ it is preferable to integrate numerically. This may be done by breaking the region of integration up into an even number (2m) of panels by means of 2m + 1 parallel lines drawn at constant distance h apart and applying the well known Simpson's Rule:

$$A = \tfrac{1}{3}h\left[(y_o + y_{2m}) + 4(y_1 + y_3 + \cdots y_{2m-1}) + 2(y_2 + y_4 + \cdots y_{2m-2})\right]$$

where $y_o\ y_1 \cdots y_{2m}$ denote lengths of the intercepted segments. The accuracy of this method improves with the number of panels. A computer program has been written (Appendix I) which, starting with 10 panels, calculates the integral for 2m increasing in steps of 10 up to 200. In all cases the value calculated changed by less than 0.1°/o as m increased above 30. The results obtained by this method are also listed in Table (2.1).

TABLE 2.1 : Effective Values of $\varepsilon\omega$

d (inches)	Geometrical Solid Angle $\frac{1}{2}(1-\cos\Theta)$	$\varepsilon\omega$ for Be			$\varepsilon\omega$ for Aℓ		
		$\omega e^{-a'}$ (normal incidence)	by series expansion	by numerical integration	$\omega e^{-a'}$ (normal incidence)	by series expansion	by numerical integration
9.9 keV							
0.001	0.499				0.416	-	0.2992
0.008	0.490	0.478	0.4472	0.4474			
0.125	0.351	0.342	0.3361	0.3361	0.293	0.2582	0.2582
0.25	0.235	0.229	0.2272	0.2272	0.176	0.1842	0.1843
0.375	0.158	0.154	0.1534	0.1534	0.131	0.1272	0.1272
0.50	0.110	0.107	0.1065	0.1065	0.091	0.0893	0.0894
0.625	0.079	0.077	0.0767	0.0767	0.066	0.0648	0.0648
53.3 keV							
0.001	0.499				0.498	0.4941	0.4941
0.008	0.490	0.489	0.4845	0.4845			
0.125	0.351	0.350	0.3491	0.3491	0.350	0.3499	0.3499
0.25	0.235	0.234	0.2341	0.2341	0.235	0.2345	0.2345
0.375	0.158	0.158	0.1575	0.1575	0.158	0.1577	0.1577
0.50	0.110	0.109	0.1092	0.1092	0.109	0.1094	0.1094
0.625	0.079	0.079	0.0786	0.0786	0.079	0.0787	0.0787

The values of $\varepsilon_1\omega_1$ have also been tabulated for the case of a .001" Aℓ window, and show that the $^X/_\gamma$ value calculated using normal absorption should be multiplied by up to 1.4 depending on the source position.

2.5. Experimental Method

The experimental arrangement used to measure the $^X/_\gamma$ ratio was basically the same as described in Section 2.2 of this chapter. However, the source was mounted on a $\frac{1}{8}$" thick paxolin ring, which could be bolted to the face of the counter. The source was then $\frac{1}{4}$" from the detector. This distance could be easily changed to $\frac{3}{8}$", $\frac{1}{2}$" or $\frac{5}{8}$" by inserting 1, 2 or 3 other $\frac{1}{8}$" thick paxolin ring spacers as shown in Fig. (2.5). The value $d = \frac{1}{8}$" was achieved by mounting the source on the counter face as in Section 2.2, and the maximum solid angle measurement was carried out with the source mounted directly on to the Be window. Preliminary readings for this last case were made with the source covered by a thin (2 mgm/cm.^{2}) sheet of melinex to avoid contamination of the crystal. To discover the absorption effect of the melinex two sets of spectra were recorded with the source covered for the $d = \frac{1}{8}$" case. Finally, after all the other spectra had been recorded two sets for the $d = 0$ case were taken with the uncovered source mounted in contact with the Be window.

The only details of the counter which differed from the description given in Section 2 were amplifier gain and the value of the anode load. The latter was reduced to 47 kΩ giving output pulses ~ 2μs long, and was found to be about optimum for best resolution. (Good resolution enables the distinction between

9.9 keV X ray photo peak and 53.3 keV escape peak to be more readily drawn.)

For each d value a group of three spectra were recorded:

a) Open source.

b) Background.

c) Source covered by Zn absorber.

The Zn absorber was the 10 thou thick material used in Section 2 and in each case it was placed in contact with the As source. Each spectrum was counted for a 9 hour overnight period, and the counter gain and resolution checked for stability before and after each run using the 120 keV and 42 keV lines of a strong Eu^{152} source. The observed 120 keV peak position drifted by less than $\pm$ 10 channels in 200 during the total period of observation ($\sim$ 60 days). The As^{73} spectra were very similar to those of Fig. (2.2) except for a slight improvement in resolution.

The first group of readings was taken with $d = \frac{5}{8}"$ and the source brought nearer in steps of $\frac{1}{8}"$ (the azimuthal position of the source being kept fixed) until $d = \frac{1}{8}"$. The source was then covered by melinex and the $d = \frac{1}{8}"$ readings repeated. Two $d = 0$ and another $d = \frac{1}{8}"$ reading were then made. The melinex was then removed before taking second readings at $d = \frac{1}{8}", \frac{1}{4}", \frac{3}{8}", \frac{1}{2}", \frac{5}{8}"$. Finally two groups of spectra for $d = 0$ (source uncovered by melinex) were recorded. Thus two sets of data were obtained for every d value.

The background spectra (for example, Fig. 2.2c) showed the high energy tail of the PM tube noise confined to the first few channels, and the broad peak at $\sim$ 75 keV reported by Hanson[52a]. The position of this peak remained fairly constant throughout the period but the overall noise intensity showed considerable

variations, suggesting that a simple subtraction of the previous (or subsequent) noise spectrum for the As or As + Zn spectrum might give an erroneous 'noiseless' spectrum, particularly for the 2nd set of large d value readings where the source is weak and the solid angle small. For this reason the noise subtraction was preceded by a matching process described in the next section.

2.6. Treatment of Results

The background intensity during a source run was estimated in the following way. First of all the number of counts (N_W) in the source spectrum above the high energy tail of the 53.3 keV photopeak was calculated. This number was then divided by the total number of counts N_B recorded in the same channel range during a background run (i.e. with source removed). All channels of the background spectrum were then multiplied by this ratio ($\varepsilon = \frac{N_W}{N_B}$), the result being a background spectrum appropriate to the source run. The multiplying factors were usually fairly close to unity, an extreme case being $\varepsilon = 1.10$.

This modified background was then subtracted from the source spectrum. The intensity of the K X ray and γ ray lines was determined by summing the counts under the respective peaks in the 'noiseless' spectra, the limits of the peaks being determined by inspection. The escape peak was included in the 53.3 keV summation.

The mean values obtained from the two runs are shown in Table 2.2, the errors being estimated from the statistics and also from the effect of the possible range of ' limits' of the peaks.

One difficulty of this method lies in deciding the division between the high energy tail of the 9.9 keV K X ray peak and the low energy tail of the 53.3 keV escape peak. Due to relatively poor resolution of the former these overlap slightly. In an attempt to overcome this problem the technique described in the next paragraph was used.

An example of spectra obtained with the As^{73} source covered by 10 thou thick Zn sheet is shown in Fig. 2.2b. As may be expected the 9.9 keV X rays are completely absorbed, leaving only the 53.3 keV γ ray reduced in intensity by the factor $r \simeq 0.5$.

TABLE 2.2

d (inches)	Mean $^{X}/_{\gamma}$	Mean ($^{X}/_{\gamma}$) (Absorber Method)
0.625	7.3 ± 0.9	7.1 ± 1.5
0.50	7.3 ± 0.7	7.5 ± 1.5
0.375	7.1 ± 0.7	7.0 ± 0.7
0.25	7.4 ± 0.5	7.0 ± 0.6
0.125	7.5 ± 0.4	7.6 ± 0.7
0.008	7.3 ± 0.4	7.8 ± 0.6

Making the assumption that the Zn absorber has no effect on the response of the detector (i.e. no effect on line shape), such spectra can be used to determine how much of the open As^{73} spectrum is due to the 53.3 keV γ ray.

Using the notation N_{open} = total counts under 9.9 and 53.3 keV in 'no absorber' case

N_{Zn} = total counts in 'with absorber' case

$$^{X}/_{\gamma} = r \times N_{open}/N_{Zn} - 1 \ .$$

The factor r may also be calculated using the known absorption coefficient for zinc (see Appendix II) and the results of Section 4. In this case the deviation from the normal absorption factor $e^{-\mu x}$ is quite large but agreement with the calculated values is good (Fig. 2.6). Almost total absorption of the 9.9 keV K X rays is obtained with this absorber, which also reabsorbs any characteristic Zn K X rays (K edge 9.66 keV) emitted after 9.9 keV or 53.3 keV absorption. That the absorber was thick enough for this purpose is verified by the absence of any peak at about 8.5 keV in the 'with absorber' spectra.

The $^{X}/_{\gamma}$ values calculated in this way are also included in Table 2.2.

Discussion of the Results

The $^{X}/_{\gamma}$ values obtained in the present experiment were significantly larger than the result ($^{X}/_{\gamma} = 6.2 \pm 0.6$) found by Welker et al. However, the results show no variation with solid angle outside the estimated errors. This is not surprising as the errors are comparable with the estimated size of solid angle effects. A further complication was that the $^{X}/_{\gamma}$ value appeared to increase slowly with time.

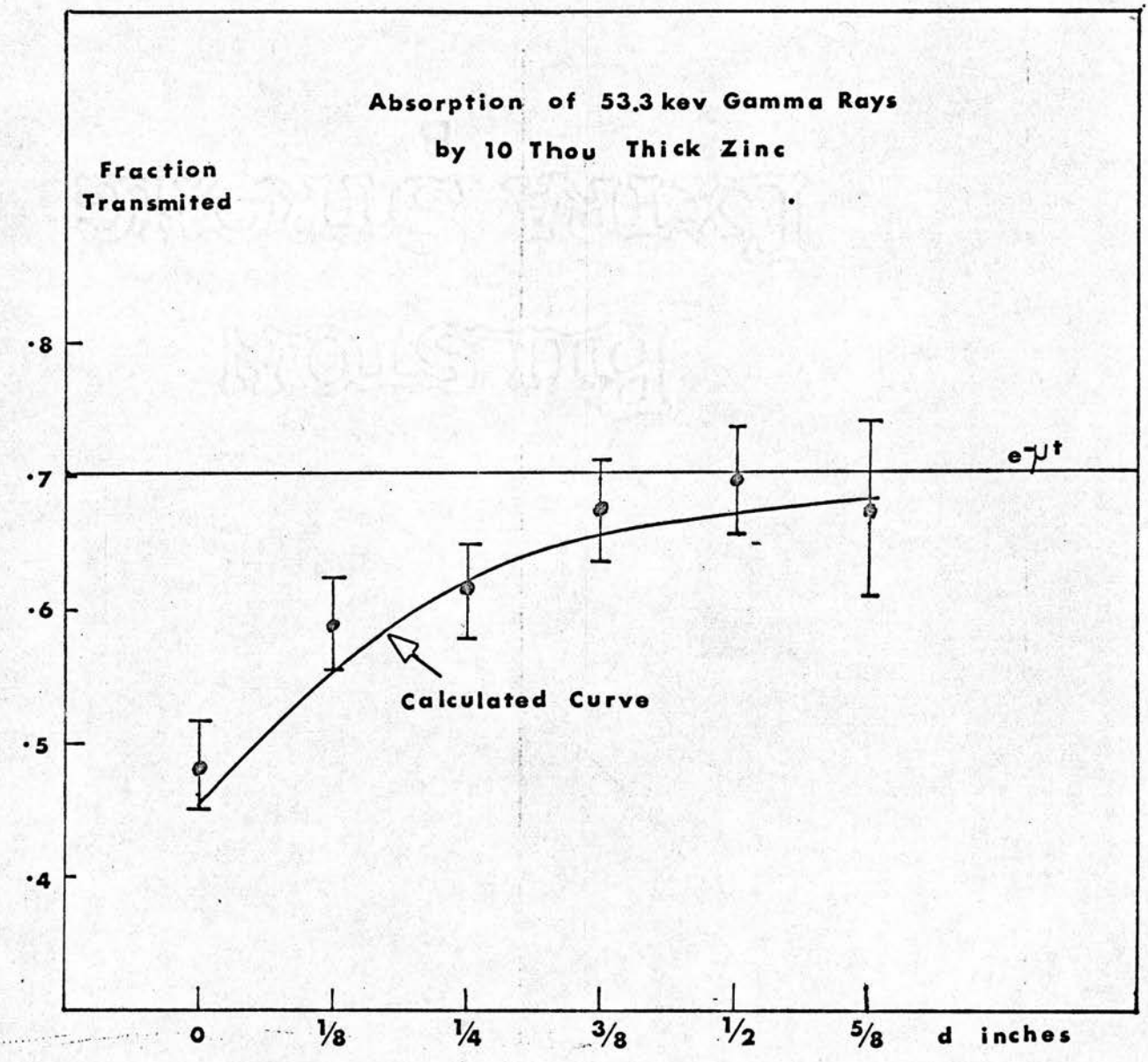
Absorption of 53.3 kev Gamma Rays
by 10 Thou Thick Zinc
Fraction
Transmited
·8
·7
·6
·5
·4
e-μt
Calculated Curve
0
1/8
1/4
3/8
1/2
5/8
d inches

FIG 2.6

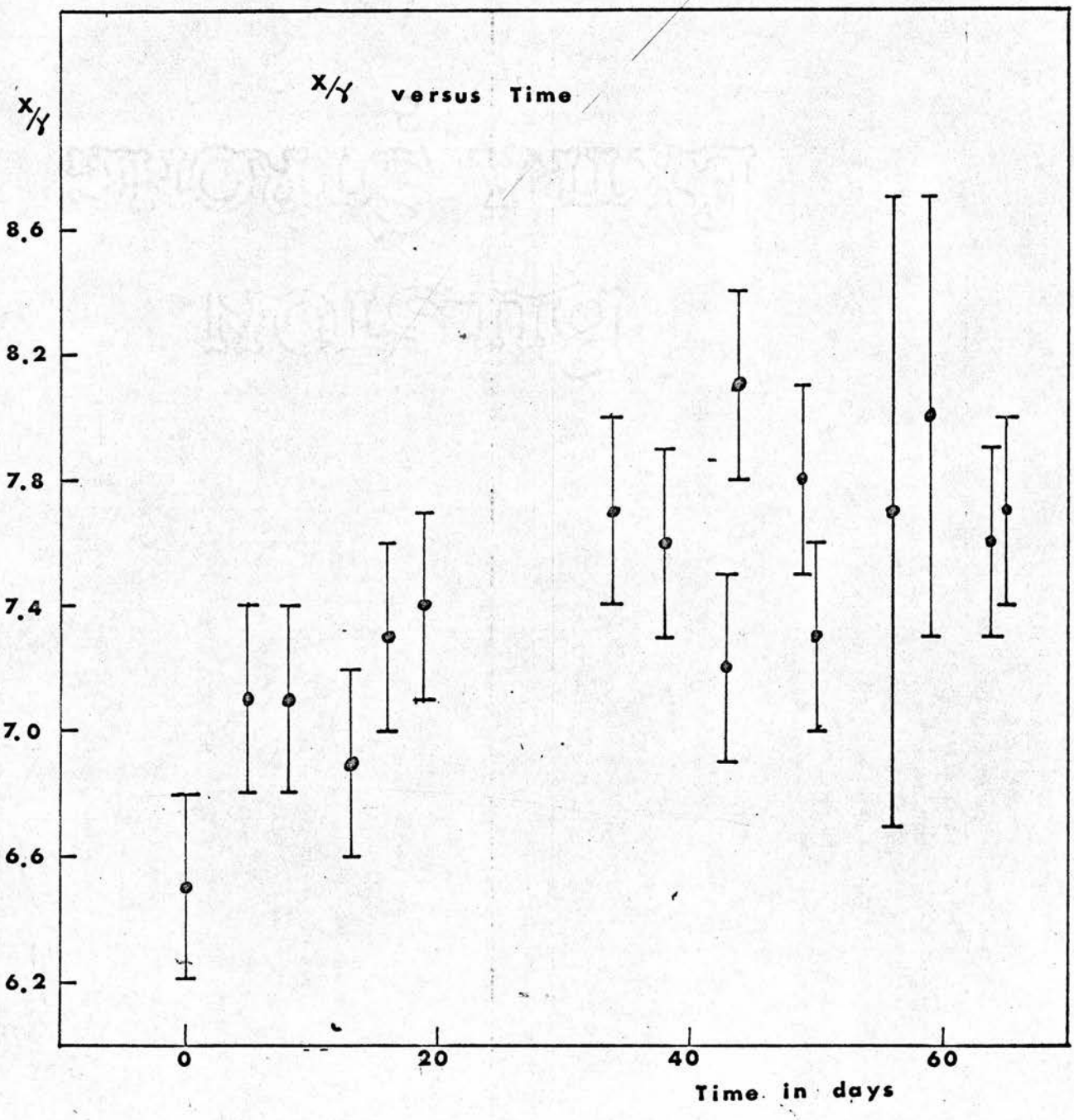

FIG 2.7

Source Holder

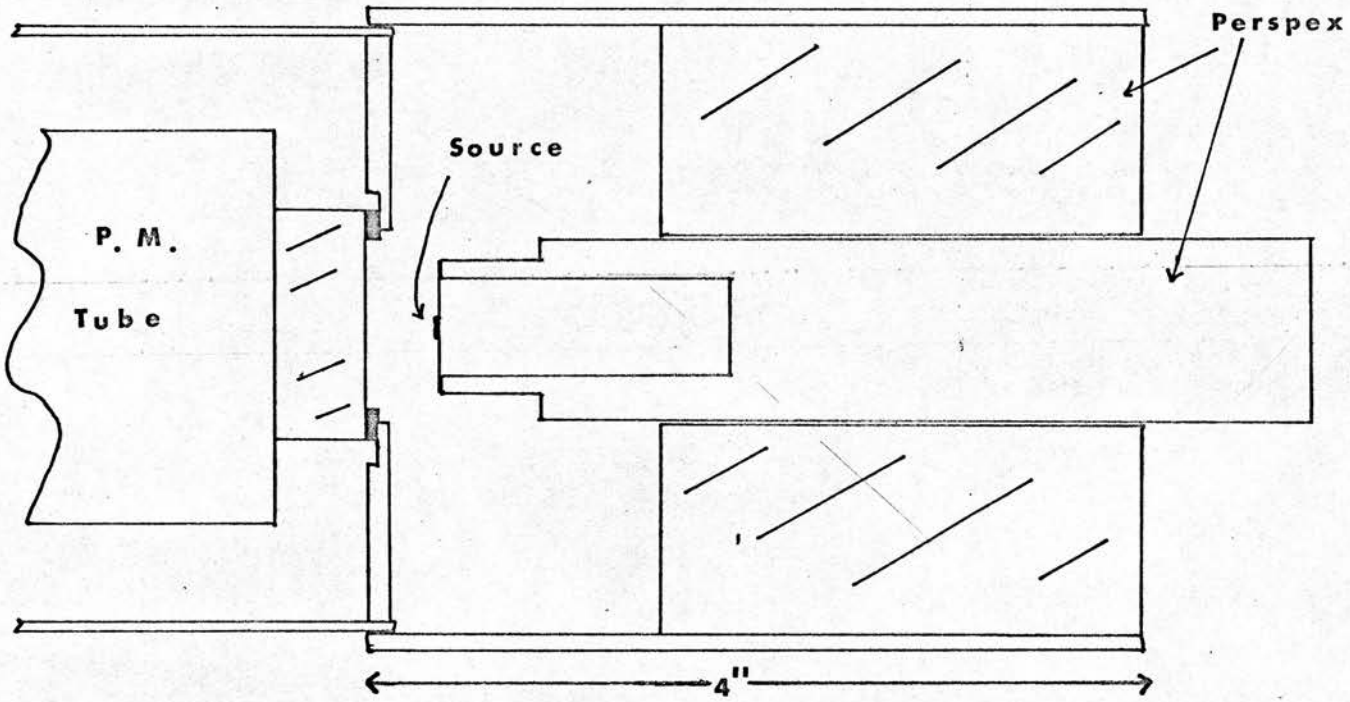

FIG 2.8

x/γ Versus ω

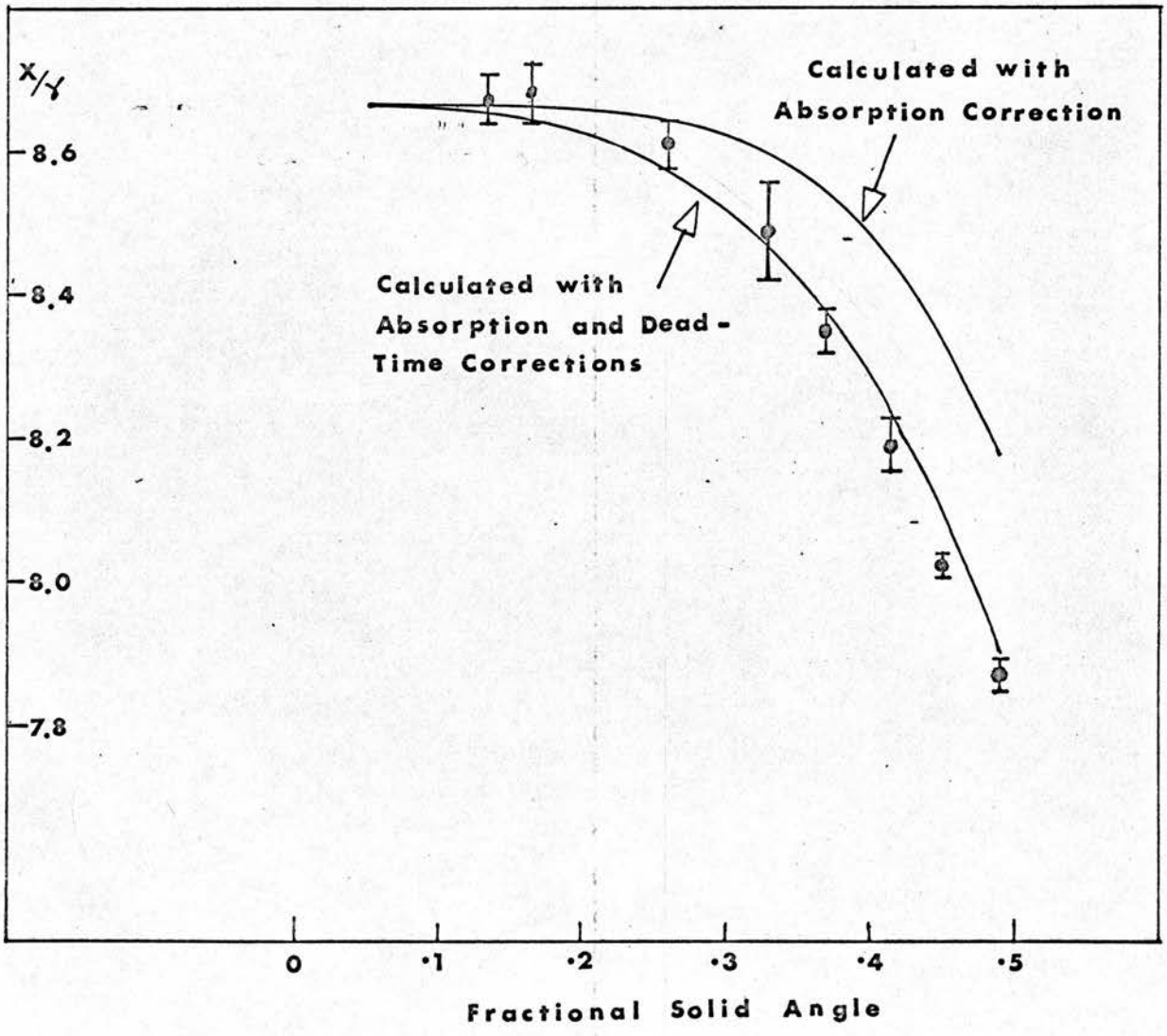

FIG 2.9

This may have been due to a systematic error which changed as the source intensity decreased, or a small percentage of some long lived contamination present in the source (emitting an X ray at about 10 keV). A careful search up to about 1 Mev revealed no peaks above 53.3 keV that did not appear in the background. A short lived contamination, emitting $\sim$54 keV γ's, is a possibility that can probably be ruled out, as the measurements were made about three years after the source was made. $^{X}/_{\gamma}$ as a function of time is shown in Fig. 2.7.

The conclusion that $^{X}/_{\gamma} \simeq 7.5$ [after correction for normal absorption] from this experiment suggested that a more accurate experiment might yield interesting results. To reduce the errors several requirements were clearly necessary:

1. Stronger source (that used above was < 0.1 μC)
2. Reduced background.
3. Improved resolution.

The first of these requirements was satisfied when a 10 μC source became available (supplied by the Radiochemical Centre, Amersham). One drop of this material produced a source about 50 times stronger than that used above. The other two factors were realised by use of a P.M. tube with improved cathode sensitivity and lower dark current and background noise (EMI Type 9635QB).

The strong source and improved counter yielded spectra like that shown in Chapter 5 Fig. 5.3a. The resolution was $\sim$ 13.5 % at 53.3 keV and $\sim$ 40% at 9.9 keV, and the tube noise was well below the 9.9 keV peak (see increased gain spectrum, Fig. 5.3a).

A somewhat different arrangement enabled the source position to be measured more accurately (d $\pm$ 0.1 mm). This consisted of a perspex source holder (hollowed to reduce scattering) which could

be screwed in and out of a perspex block fixed to the front of the counter (Fig. 2.8).

The experiment was repeated exactly as before except that the multi-channel analyser was used to set threshold and gate width values on single channel analysers (see Chapter 4). The results are given in Table 2.3 and $^{X}/_{\gamma}$ plotted as a function of solid angle in Fig. 2.9. Each value listed is an average of five runs and the error quoted is purely statistical. An estimate of the systematic error due to setting the analyser thresholds wrongly was found by experiment to be $\sim \pm 0.08$.

TABLE 2.3

Solid Angle	Mean $^{X}/_{\gamma}$
0.490	$7.87 \pm .02$
0.451	$8.02 \pm .01$
0.411	$8.19 \pm .04$
0.369	$8.35 \pm .03$
0.330	$8.50 \pm .07$
0.262	$8.61 \pm .03$
0.165	$8.68 \pm .04$
0.134	$8.67 \pm .02$

Result after extrapolation to zero solid angle and after normal absorption and dead time correction

$$^{X}/_{\gamma} = 8.95 \pm 0.2$$

No significant variation with time was found over a period of about two months.

Fig. 2.9 shows the variation with solid angle rather as

expected from the discussion of Sections 2 and 3 of this Chapter. Taking the asymptotic value of $^{X}/_{Y}$ to be 8.7 the calculation to take account of window absorption gives the upper curve shown.

The lower curve takes account of dead time as well.

The experimental points agree quite well with this last curve, implying that the true value of $^{X}/_{Y} = 8.95 \pm 0.2$. It is interesting that this is ~ 1.45 times the value obtained by Welker et al. (Cf. Section 4.)

It is difficult to understand the lower value (~ 7.5) obtained with the weak source, but it may be due to a systematic underestimation of the lower energy part of the X-ray peak due to P.M. tube noise.

CHAPTER 3

HALF-LIFE OF ARSENIC-73

As pointed out in Chapter 2 spectra were taken using the contaminated source for a period of about 30 days before the contamination was identified. These measurements were continued using this source for a further period of 250 days in an attempt to measure the As^{73} half-life reported as 76 or ~100 days (see Chapter 1) and to test a method for determining the contamination intensity. A fuller description of these measurements and the details of the ways in which the presence of the contamination was allowed for in calculating the half-life are presented in this chapter.

3.1. Counter Stability

The counter assembly was exactly as described in Chapter 2 (Section 2) throughout the period of measurement.

Since the background was found to change in intensity by up to 30°/o over a period of a few weeks it was considered best to take a noise spectrum just before or just after a source run. Thus a typical group of successive overnight readings was:

1. Background
2. Source
3. Source
4. Background.

This, of course, meant removing the source between readings to enable the background spectra to be taken. To ensure accurate

geometrical re-positioning the source was mounted on a paxolin ring which could be bolted to the front of the counter.

The gain stability of the counter was checked (before and after each spectrum was recorded) using a strong Eu^{152} source, giving peaks at 42 keV and 120 keV. The 120 keV peak drifted by less than $\pm$ 12 channels during the 250 day period of observation.

The number of counts under the 53.3 keV photopeak was taken as the measure of the activity. To enable the half life of the As^{73} activity to be calculated, it was necessary to discover how much of the 53.3 keV peak was in fact due to the 42 keV K X rays of the suspected Eu^{152} contamination. This was done in two ways:
1) by subtraction of a quantity $R_c e^{-\lambda ct}$ from the data before performing a linear least squares fit calculation on a log(acticity) versus time curve and adjusting R_c for best linearity. (Here $1/\lambda_c = \tau_c$ = the mean life of the Eu^{152} contamination). This will be described fully in Section 3.3.
2) by comparison with the spectrum of a pure Eu^{152} source (next section).

3.2 Estimation of Contamination by Comparison Method

Typical Eu^{152} (strong source) and contaminated As^{73} spectra are shown in Figs. 3.1a,b, the 42 keV contamination being apparent as a 'bulge' in the low energy side of the 53.3 keV photopeak. The 42 keV Eu K X ray overlaps with the 53.3 keV peak above channel number 28. The ratio

$$\eta = \frac{\text{No. of counts under the 42 keV peak above channel no. 28}}{\text{No. of counts under the 120 keV peak}}$$

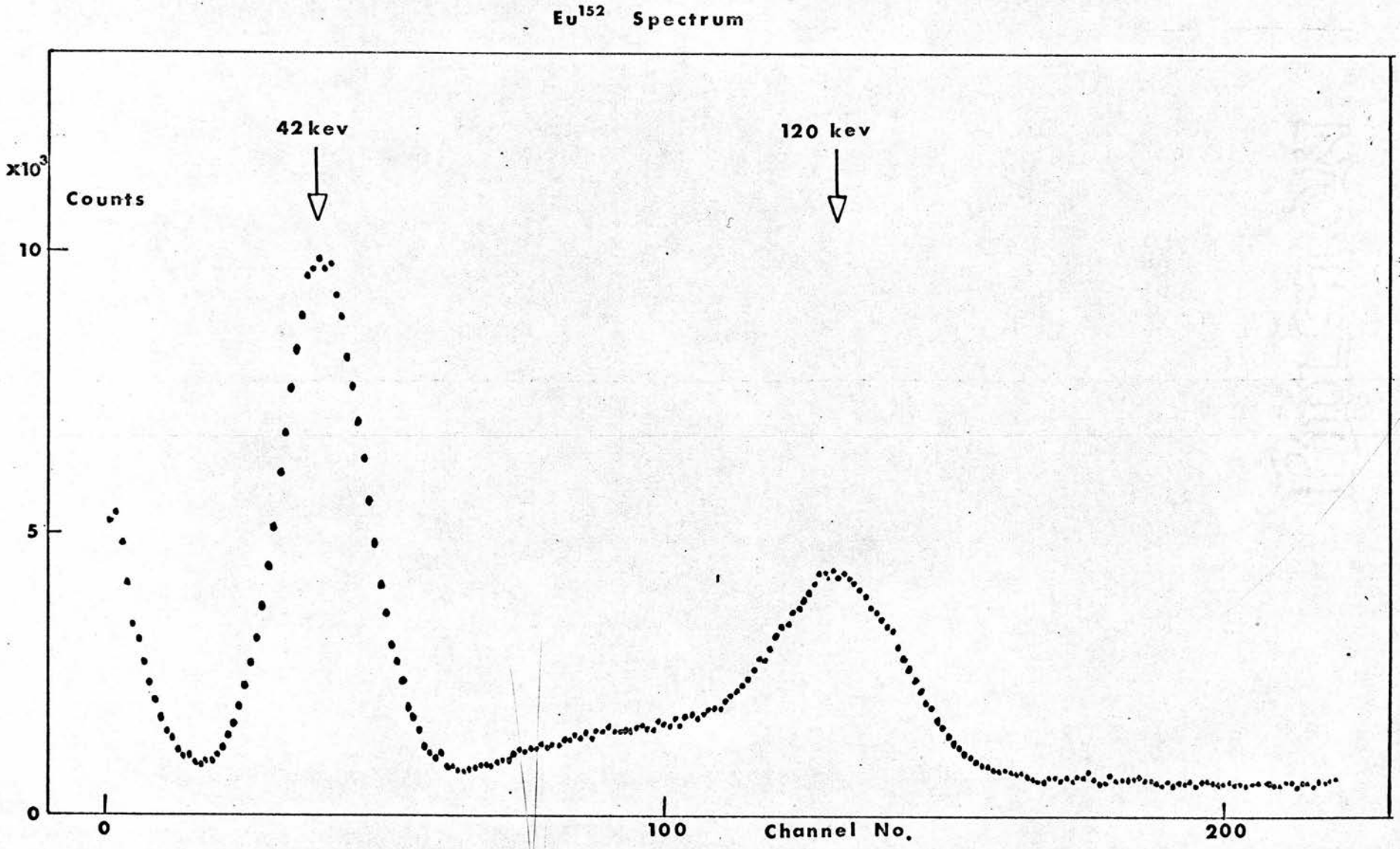
Eu152 Spectrum
42 kev
120 kev
x10³
Counts
10
5
0
0
100
Channel No.
200

FIG 3.1a

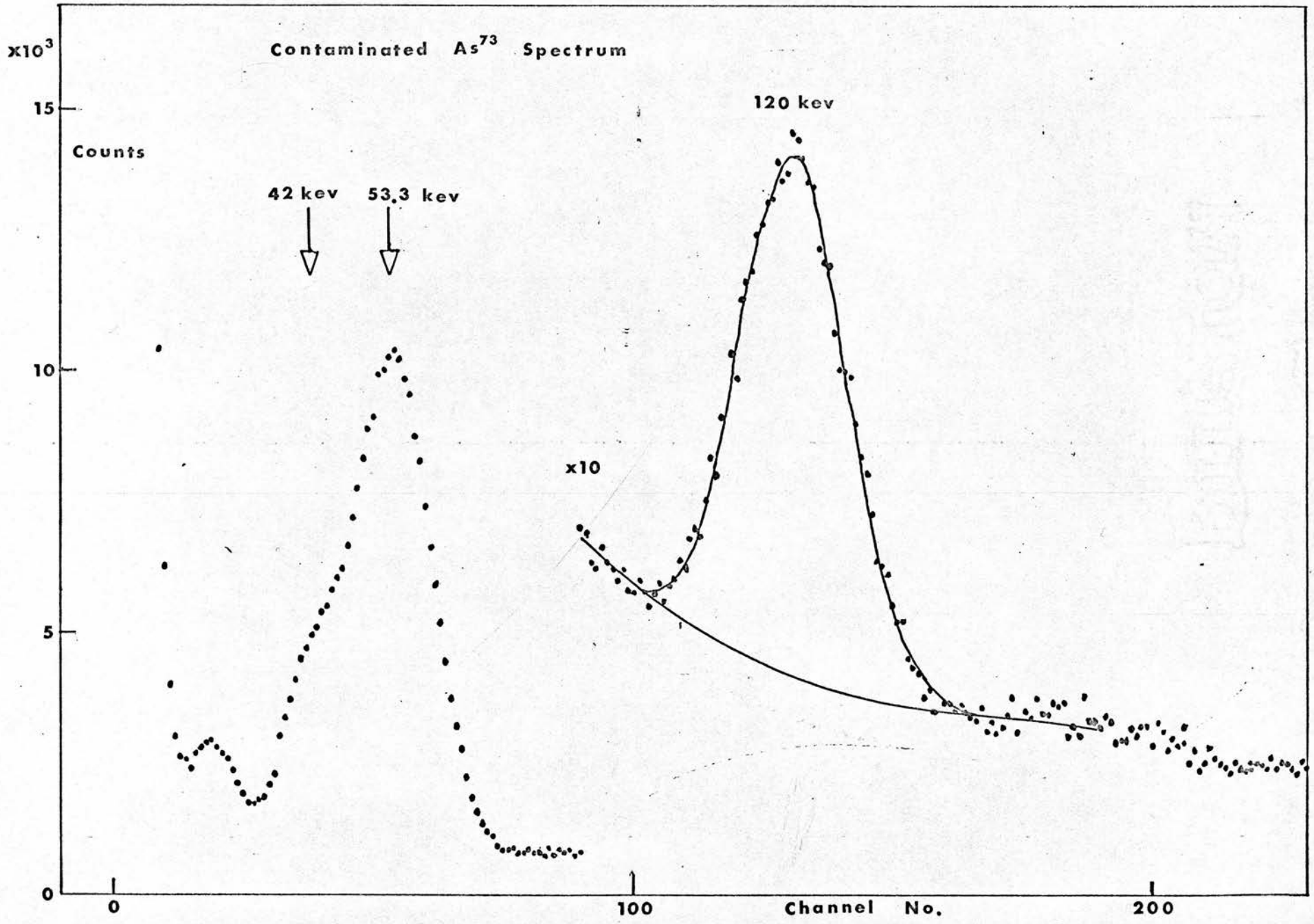
Contaminated As73 Spectrum
x10^3
15
Counts
10
5
0
42 kev
53.3 kev
120 kev
x10
0
100
Channel No.
200

FIG 3.1b

was evaluated for many of the calibration Eu^{152} spectra mentioned above. The average value was found to be $\bar{\eta} = 2.00 \pm 0.05$ where the error is the standard deviation $\sigma_{\bar{\eta}}$ of the mean calculated from the formula derived, for example, by Parrat[51]

$$\sigma_{\bar{\eta}} = \left[\frac{\sum_{i=1}^{n}(\eta_i - \bar{\eta})^2}{n(n-1)}\right]^{1/2}$$

where there are n measurements η_i and $\bar{\eta} = \sum \eta_i / n$.

Multiplication of the mean number of counts $\bar{R}$ under the 120 keV peak in the As^{73} case by $\bar{\eta}$ then gave the contribution of 42 keV Eu K X rays to the photopeak of the 53.3 keV As^{73} gamma.

Owing to the low intensity of the 120 keV line, the background was estimated graphically - the high and low energy ends of the peak being joined by a smooth curve shown typically in Fig. 3.1b. The required intensity was then calculated by finding the enclosed area under the peak. This procedure was adopted to remove the error outlined in Chapter 2 due to small changes in background intensity from run to run which are important for very weak lines. Using this method, however, it is more difficult to estimate where the high and low energy 'tails' of the peak merge with the background.

The average 120 keV peak intensity was found to be

$\bar{R} = 25{,}100 \pm 400$ the error being evaluated as before. Hence the 'contamination' counts in the 53.3 keV peak

$R_c = (50.2 \pm 1.6) \times 10^3$.

The error quoted is statistical only, it being recognized that the systematic error is likely to be larger (particularly

from the $\bar{R}$ contribution).

The above procedure assumes a constant contamination throughout the period of observation which is a reasonable approximation to the accuracy quoted (Eu^{152} half life ~ 13 years). Calculation of half-life from the gradient of the line $\log(R_{obs.} - R_C)$ versus t yielded the result $T_{1/2} = 87 \pm 1$ days.

3.3. Contamination by Linearity Method

Making the assumption that the probability for an excited nucleus to decay during the time between t and $t + \Delta t$ is proportional to Δt and the initial number of excited nucleons $N(t)$

i.e. $P = \lambda N(t) \Delta t$ where λ is a constant different for different nuclei, the decay rate or activity is given by

$$\frac{P}{\Delta t} = R(t) = \lambda N(t) = -\frac{dN}{dt}$$

$\therefore \quad \log N = -\lambda t + \log N_o$ where there are N_o excited atoms at $t = 0$

$\therefore \quad \log R = -\lambda t + \log R_o$

where R_o is the activity at time $t = 0$.

Thus for a pure source fixed relative to a counter of constant detection efficiency a plot of the log of the count rate as a function of time will yield a straight line with gradient $-\lambda$. It is easy to show that $\lambda = \frac{0.6931}{T_{1/2}}$ where $T_{1/2}$ is the half-life of the source. Note that $R \rightarrow 0$ as $t \rightarrow \infty$.

Addition of a long lived impurity will destroy the linearity of the above plot since the compound source activity will approach

the impurity rate rather than zero. In this case subtraction of the constant contamination is necessary before the log plot becomes linear. On the other hand, when the contamination is unknown it may be found by treating it as a parameter R_c to be adjusted for best linearity of the plot. The effect of varying R_c may be seen graphically in Fig. 3.2; if R_c is too small the plot remains curved upwards, if too large it is curved downwards and the plot is only linear when R_c is the decay rate of the contamination.

In practice owing to errors on the points only a 'best straight line' can be found and R_c must be adjusted to improve some 'criterion of linearity'. The criterion used here was the fractional standard deviation in the gradient.

The formulae for gradient b and intercept a derived for example by Parrat[60]

$$a = \left[\bar{y}\sum x_i^2 - \bar{x}\sum(x_i y_i)\right] / \sum(x_i - \bar{x})^2$$

$$b = \left[\sum(x_i - \bar{x})(y_i - \bar{y})\right] / \sum(x_i - \bar{x})^2$$

$$S_b = \left(\frac{n}{n\sum x_i - (\sum x_i)^2}\right)^{1/2} Sy$$

where $Sy = \left(\frac{\sum(y_i - a - bx_i)^2}{n}\right)^{1/2}$

(where $\bar{x} = \sum x_i/n$ and $\bar{y} = \sum y_i/n$, $x_i = t_i$ and $y_i = \log(R_i - R_c)$ for n values of R_i and t_i) were used in a computer program (written in Atlas Autocode) which performed the calculations for different R_c values provided in the data.

From the results a plot of S_b/b against R_c was drawn,

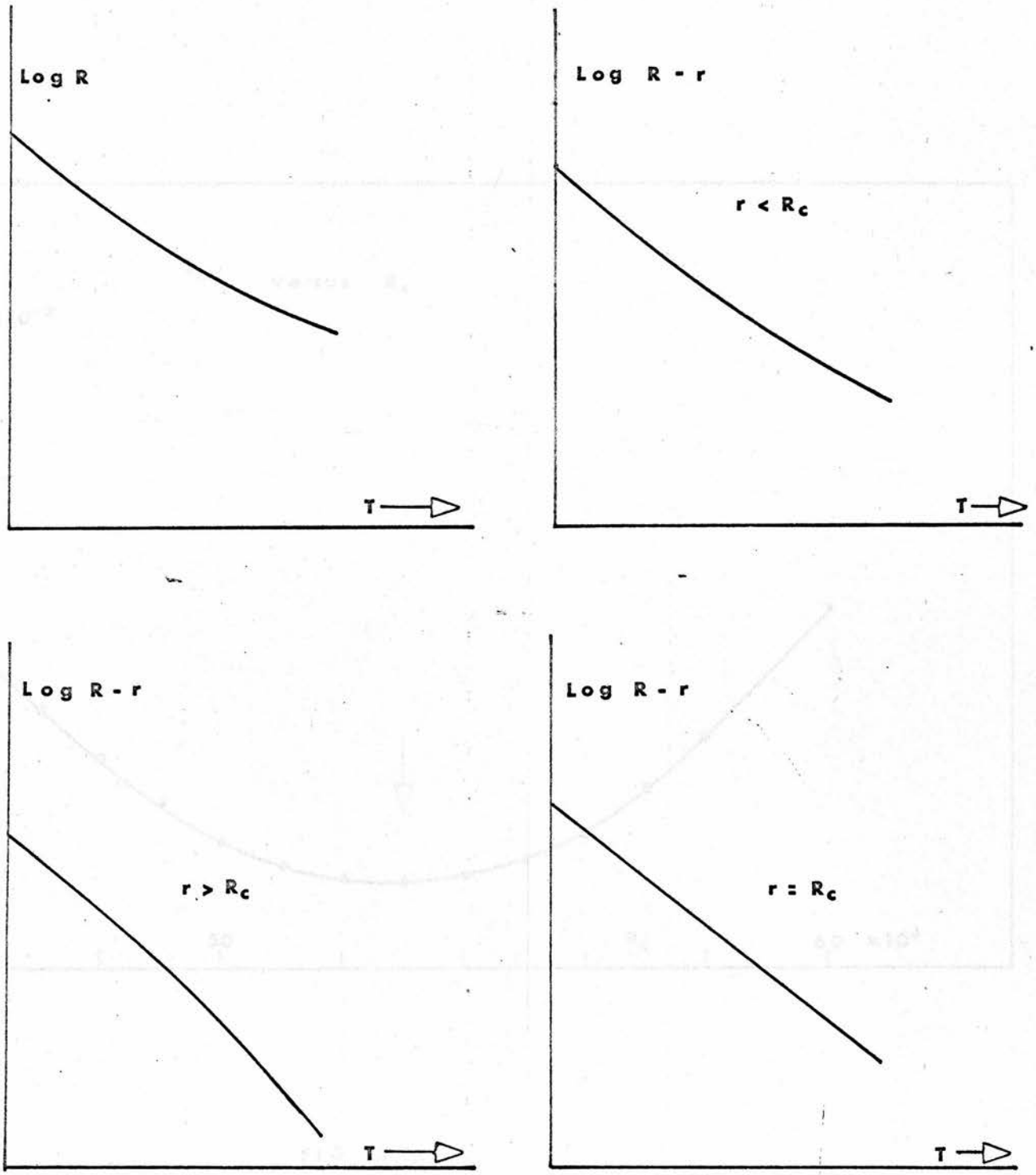

FIG 3.2

CHAPTER 4

LIFETIME OF THE 66.8 keV LEVEL

Probably the most commonly used technique for measuring the half-life of nuclear excited states is the delayed coincidence method. This has been fully described by Bell et al.[50] (1965) and is based on the correlation in time between the radiation (A) marking the 'birth' of the level and that (B) marking its 'death'. If (A) and (B) are counted in two separate detectors A' and B'

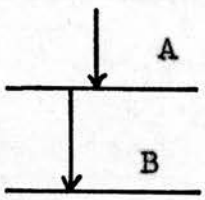

then the probability of a time delay 't' between pulses from the two detectors is of the form $e^{-\lambda t}$ where λ is the decay constant of the level ($\lambda = \frac{0.6931}{T_{1/2}}$ where $T_{1/2}$ is the half-life).

In the basic delayed coincidence method this time distribution is obtained from the observed coincidence count rate as a function of time delays introduced in the 'A' detector (e.g. De Bendetti and McGowan[54] (1948)).

This has recently been developed so that the delay time is changed automatically and the whole decay curve is obtained at once - the multichannel delayed coincidence method. The time delays in this case are measured by an analogue or digital method and the results stored in a multichannel pulse height analyser or computer. In the analogue system of measurement the first pulse starts the linear charging of a capacitor and the second pulse stops it. The amplitude of an output pulse taken from this

capacitor is a linear function of the time between the two input pulses.

In the digital system a high stability pulse generator is started by the first pulse and stopped by the second so that the number of output pulses is proportional to the time delay.

Multichannel digital time analysers have been used for many mean life measurements in the microsecond region, while analogue methods have enabled short ($< 10^{-7}$ sec.) mean lives to be measured.

In the present work an attempt has been made to measure the 66.8 keV level half-life (~ 0.5 sec.) using a time to amplitude converter and multichannel pulse height analyser. Consideration of the difficulties (particularly due to the large chance coincidence rate) involved (Section 4.1) leads to certain requirements for the converter design and calibration, which are discussed in Sections 4.2 and 4.3. The rest of this chapter is devoted to a description of the experimental arrangement and results.

4.1. Feasibility of the Delayed Coincidence Method for Long Half-lives

Chance Coincidences. If $\omega_A \varepsilon_A$ and $\omega_B \varepsilon_B$ respectively denote the probability that the 'birth' and 'death' of the level are detected, then the count rates in the two counters are given by $R_A = \omega_A \varepsilon_A R_o$ and $R_B = \omega_B \varepsilon_B R_o$, where R_o is the source strength, and background is neglected. Even if there is no correlation in time between the events occurring in the two counters there will still be a certain "chance" number of counts per unit time registered in each channel of time width dt, given by

$$R_{ch} = R_A R_B \, dt$$

provided that $t \ll \frac{1}{R_B}$, and $T_{\frac{1}{2}} \ll \frac{1}{R_A}$.

The true coincidence rate is given by

$$R_T = R_A \varepsilon_B \omega_B \lambda e^{-\lambda t} \, dt .$$

Hence the true/chance ratio is $R_T/R_{ch} = \lambda e^{-\lambda t}/R_o$ and for this to be large it is necessary that $R_o < \lambda$ i.e. $R_o < \frac{1}{\tau}$, where τ is the mean life of the level.

This requirement is easily satisfied when $\tau \leqslant 10^{-3}$ secs., but if $\tau \geqslant 1$ sec. it becomes necessary to use a source so weak that background is important. Also, the time required to collect the data becomes rather long.

To understand the even more stringent restriction $t \ll \frac{1}{R_B}$ it is helpful to consider the T.A.C. as a unit which, on being started by a type A pulse, sweeps through the time channels (each of width dt) until stopped by pulse B. A count is then registered in the channel reached and the 'sweep' returns to zero. The number of chance counts recorded in a channel is proportional to dt, R_B and the number of times the channel is opened. If the average time between type B pulses $\frac{1}{R_B}$ sec. is less than the total sweep time t_S (= n dt where n is the number of time channels) then it will often happen that the sweep will stop before it reaches the last few channels. In fact the number of times a particular channel is opened will decrease from first to last and the chance count rate will include an exponential time factor.

The above argument does not, of course, apply to a T.A.C. which is designed so that the sweep runs on to the maximum time t_S

(whether or not a pulse of type B occurs) before returning to zero. In this case each channel is opened for exactly the same number of times and the chance rate is constant for all channels of equal width.

A unit of this type is 'dead' to start (i.e. type A) pulses for a total time $N_S\ t_S$ (where N_S is the number of (complete) sweeps executed in the total counting time t".) i.e. it is 'live' for time $t'' - N_S\ t_S$, during which the counter A detects $N_A' = (t'' - N_S\ t_S)R_A$ events.

$$\therefore \quad R_S = (1 - R_S\ t_S)R_A$$

$$\text{i.e.} \quad R_S = R_A/(1 + R_A\ t_S) \ .$$

To sum up the above results it can be seen that good statistical accuracy (in a given counting time t") and freedom from background effects requires a strong source and a large number of sweeps (i.e. short sweep time), but this conflicts with the requirement of a large true/chance ratio and a long sweep time (so that the decay can be followed over several half-lives).

To find the optimum source strength and sweep time it is useful to introduce the following notation:

No = No. of source decays in time t" ; $R_o = {}^{No}/t''$

B_A = No. of background counts in time t" in counter A;

$$BR_A = \frac{B_A}{t''}$$

B_B = No. of background counts in time t" in counter B;

$$BR_B = \frac{B_B}{t''} \ .$$

$$N_A = No\ \omega_A\ \varepsilon_A + B_A \quad ; \quad R_A = {}^{N_A}/_{t''}$$
$$N_B = No\ \omega_B\ \varepsilon_B + B_B \quad ; \quad R_B = {}^{N_B}/_{t''} \qquad \text{(redefined)}$$

$N_T(t)$ = No. of true coincidences in a channel of width dt in time t'' ; $R_T(t) = \frac{N_T(t)}{t''}$.

N_C = No. of chance coincidences in a channel of width dt in time t'' ; $R_C = {}^{N_C}/_{t''}$.

$N_S = N_A/(1 + \frac{N_A t_S}{t''})$ as before ; $R_S = \frac{R_A}{1 + R_A\ t_S}$.

The number of genuine A pulses which start a sweep is now

$$N_S' = N_S(1 - \frac{B_A}{N_A})$$

$\therefore$ the number of true coincidences recorded in a channel is

$$N_T(t) = N_S'\ \omega_B\ \varepsilon_B\ \lambda e^{-\lambda t}\ dt \qquad . \qquad (4.1.1)$$

The number of chance coincidences per channel is now given by

$$N_C = N_S\ R_B\ dt = N_S\ \frac{N_B\ dt}{t''} \qquad (4.1.2)$$

In all channels the observed number of counts $N_{obs} = N_C + N_T$ and N_T is to be evaluated from this equation. Hence the standard deviation in N_T, σ_T say, will be such that $\sigma_T^2 = \sigma_{obs}^2 + \sigma_{N_C}^2$ in an obvious notation.

From equation (4.1.2)

$$\sigma_{N_C} = N_C \sqrt{(\frac{\sigma N_S}{N_S})^2 + (\frac{\sigma N_B}{N_B})^2}$$
$$= N_S\ \frac{N_B}{t''}\ dt \sqrt{\frac{1}{N_S} + \frac{1}{N_B}}$$

assuming no errors in dt and t''.

Also $\sigma_{obs} = \sqrt{N_{obs}} = \sqrt{N_C + N_T}$

$$\therefore \sigma_{T/N_T} = \sqrt{\frac{N_C}{N_T^2} + \frac{1}{N_T} + \left(\frac{N_S N_B \, dt}{t'' N_T}\right)^2 \left[\frac{1}{N_S} + \frac{1}{N_B}\right]}$$

$$= \sqrt{\frac{1}{t''}\left\{\frac{R_C}{R_T^2} + \frac{1}{R_T} + \left(\frac{R_S R_B \, dt}{R_T}\right)^2 \left[\frac{1}{R_S} + \frac{1}{R_B}\right]\right\}} \qquad (4.1.3)$$

Now the half-life value comes from the gradient m of the line $Y = mx + c$ where $y = \log_e N_T(t)$ and $x = t$.

$$\therefore \sigma_y \simeq \sqrt{\left(\frac{\partial Y}{\partial N_T}\right)^2 \sigma_{N_T}^2} = \frac{\sigma_{N_T}}{N_T} \quad .$$

If there are n time channels then there are n points $(x_i \; y_i)$ and the x values are $x_1 = 0$, $x_2 = dt$, $x_3 = 2\,dt$ ... $x_n = (n-1)\,dt$.

Making the assumption that the standard deviations in the y values are all equal to the value calculated using 4.1.3 with $t = \frac{1}{2}t_S$, then, (see for example Parrat[51])

$$\sigma_M = \left(\frac{n}{n\sum x_i^2 - (\sum x_i)^2}\right)^{\frac{1}{2}} \; Sy$$

where $Sy = \sqrt{\frac{\sum(\delta y_i)^2}{n-2}} = \sqrt{\frac{n\sigma_y^2}{n-2}} = \sigma_y \sqrt{\frac{n}{n-2}}$

$$\therefore \sigma_M = \sigma_y \sqrt{\frac{n^2}{(n-2)\left[n\sum x_i^2 - (\sum x_i)^2\right]}}$$

$x_i = (i-1)\,dt$ where the sums are over the range i = 1 to i = n .

The final expression for σ_M is

$$\sigma_M = \frac{\sigma_T}{N_T} \frac{n^2}{t_S} \sqrt{\frac{12}{(n-2)(n-1)\left[n^3 + 13n^2 - 24n + 12\right]}} \qquad (4.1.4)$$

using $t_S = n\,d\,t$.

where $\frac{\sigma_T}{N_T}$ is given by (4.1.3).

It is interesting to note that since σ_T/N_T contains a factor $\frac{1}{\sqrt{dt}}$ i.e. $\sqrt{\frac{n}{t_S}}$ the error in gradient is almost independent of n.

(n dependence of σ_m is $\sqrt{\frac{12n^5}{(n-2)(n-1)\left[n^3 + 13n^2 - 24n + 12\right]}} \rightarrow \sqrt{12}$ as $n \rightarrow \infty$.)

Equation (4.1.4) expresses σ_M as a function of R_o and t_S, and the optimum values of these variables are therefore those which give a minimum value of σ_M. Also evaluation of this expression gives the accuracy to be expected from the experiment if it is run for a counting time t", with a given background.

In the case of the 66.8 keV level of As^{73} the situation is slightly complicated by the fact that the only possible 'start' pulse comes from the detection of a 9.9 keV K X ray resulting from the K capture process. It is impossible to distinguish this K X ray from those that arise after conversion of the 53.3 keV or 13.5 keV gamma transitions which therefore contribute to the background B_A.

Some reduction of this contribution was afforded by arranging that the K X ray counter be 'switched off' for ~ 33 μsec. by a pulse due to a conversion electron from the 53.3 keV transition, which, (on this time scale) is coincident with these 'noise' K X rays.

The 53.3 keV conversion electrons were also chosen to provide the 'type B' pulse rather than the 53.3 keV γ rays. The 'figure of merit' here is the signal/noise ratio, and although the noise in the detector used (proportional counter) was about 3 times that of a good scintillator - PM tube assembly (for γ rays), the signal

was about 8 times greater ($\alpha_K \simeq 8$, see Chapter 1).

In the general results derived above it is only necessary to replace $\omega_B \varepsilon_B$ by $p_e \omega_e \varepsilon_e$, B_B by B_e, $\omega_A \varepsilon_A$ by $p_1 \omega_x \varepsilon_x$, and B_A by

$$\omega_x \varepsilon_x N_o\left[p_1'(1 - \omega_e \varepsilon_e) + p_1''(1 - p_e \omega_e \varepsilon_e)\right] + B_x$$

using the notation of Chapter 2 with $\omega_e \varepsilon_e$ the fractional solid angle and efficiency for 53.3 keV conversion electron detection and $B_{x/t''}$, $B_{e/t''}$ the actual background counting rates for K X ray and conversion electron counters respectively.

A computer program written in Atlas Autocode was employed to evaluate expression (4.1.4), taking the 'p' values listed in Table 2.1a and

$$\left.\begin{aligned} &\varepsilon_e \omega_e = 0.45, \quad \varepsilon_x \omega_x = 0.35, \\ &B_{x/t''} = 0.1 \text{ sec.}^{-1}, \quad B_{e/t''} = 0.33 \text{ sec.}^{-1} \end{aligned}\right\} \text{ (See Section 4.3)}$$

The results agreed with the general conclusions of Grant[52] and showed that the error in half-life measurement depended markedly on the value of t_S, optimum being about 1.8 secs. (i.e. $\sim$ 3 half-lives), and varied only slowly with R_o - optimum being $R_o = 2.50$ sec.$^{-1}$ (implying an X ray (gated) count rate of 1.7 sec.$^{-1}$ and a conversion electron rate of 0.9 sec.$^{-1}$). Calculation for $n = 40, 80, 120$ confirmed that the accuracy was (nearly) independent of n.

The results also showed that an error of about 5% might be expected for a total counting time of 10^6 secs., and that the

maximum true to chance ratio in the optimum case would be about 0.08. In view of the large chance contribution, it is obviously important that calculation of the chance rate be accurate. Since

$$R_{ch} \propto N_S \text{ and } dt$$ it is necessary that

provision be made for counting the number of sweeps, and that the dt be the same for all channels (i.e. the T.A.C. sweep must be accurately linear). The design of the present T.A.C. is discussed in the next section; calibration and a discussion of the way in which a small deviation from linearity was allowed for are presented in Section 4.3.

4.2. Time to Amplitude Converter

Basic Operation. The pulses to be 'converted' (type B) are applied to the input of the monostable circuit which provides an output pulse whose amplitude depends only on supply voltage. The supply voltage is usually constant but after detection of a type A pulse, it is made to decrease linearly with time by means of a ramp generator. The starting and stopping of the ramp are controlled by a bistable control circuit which is switched by the trigger (type A) pulse. The ramp starts and after one ramp sweep the control bistable is switched back again so that it holds the ramp 'off' until another trigger pulse arrives. Any trigger pulse arriving during the ramp sweep time t_S has no influence on the control bistable and is therefore lost.

Circuit Design. The complete circuit of the T.A.C. is given in Fig. 4.1. The heart of the unit is a 22μF capacitor C which is

Time to Amplitude Converter

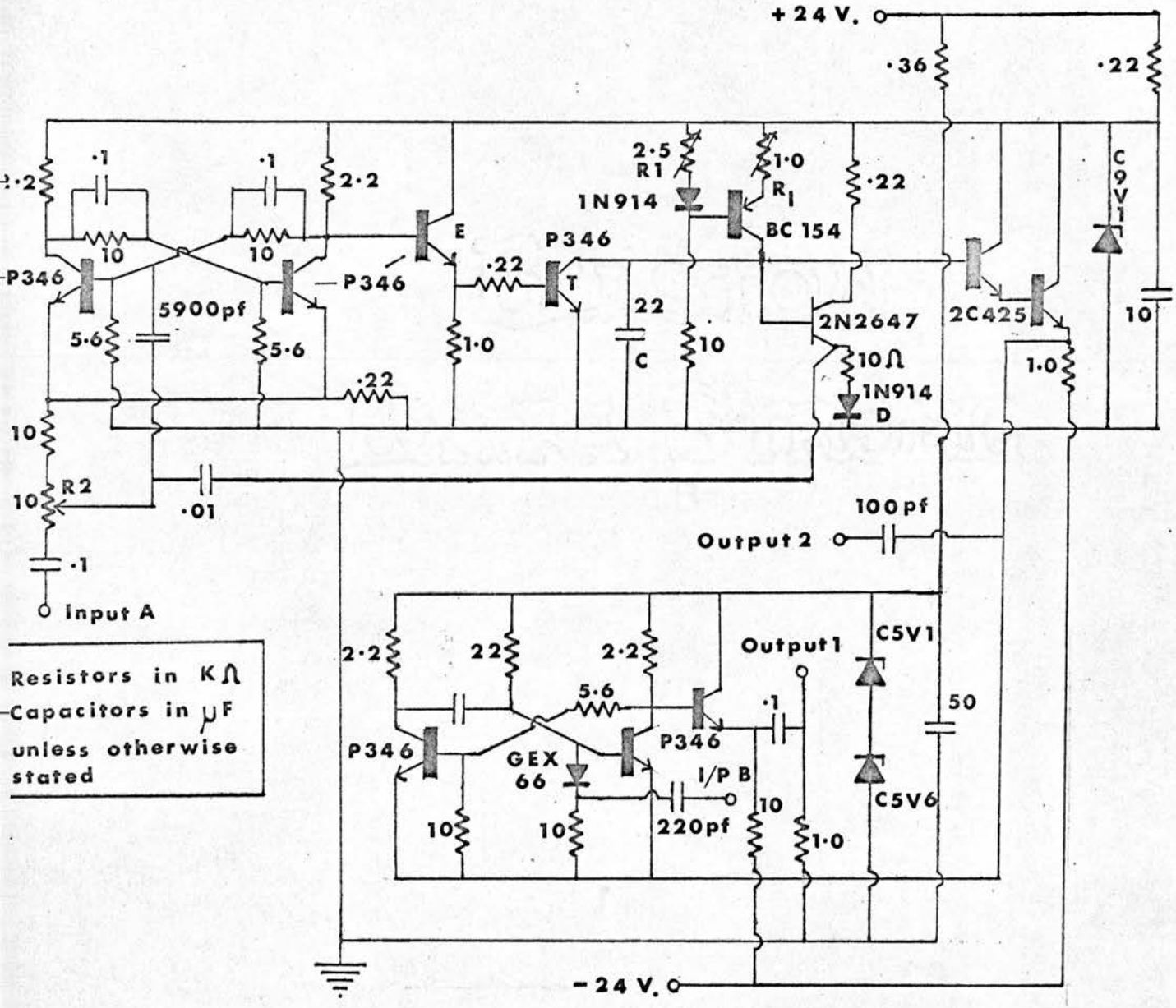

FIG 4.1

charged by a constant current generator - an emitter follower arrangement of transistor BC154. The base voltage of this transistor is set by the 2.5 kΩpot (R1) and the emitter follows this within the base-emitter voltage which is about 0.7 volts. The emitter and approximate collector current (i.e. current charging C) is then given by $(V_B - 0.7)/R_\ell$ where R_ℓ is the emitter load value. The silicon diode 1N914 is included to compensate for any thermal drifts in the base-emitter voltage.

When the voltage across the capacitor reaches the trigger voltage of the unijunction transistor 2N2647 (about half the supply voltage) the capacitor is rapidly discharged through the 10 Ω resistor and a pulse taken from this resistor marks the end of the sweep.

In order that the charging process be linear, it is important that the leakage current for capacitor discharge be kept to a minimum. For example a sweep time $t_s \simeq 1.8$ secs. requires a charging current of about 50 μA. Linearity to within 1% can be expected only if variations of the leakage current are <1 μA. The capacitor used was therefore of the low leakage tantallum type (Hunt's type TSR326, maximum leakage quoted at $< 2\mu A$). The maximum leakage of the unijunction type 2N 2647 is only 0.2 μA.

Since the output monostable requires a supply of about 2 ma a large ratio impedance transformer is clearly necessary to preserve linearity. This 'matching' is provided by the double emitter follower 2C 425, each half of which has a current gain of ≥ 100. The second emitter of this combination is taken to the -24v supply via a 1 kΩload. Hence the standing current in the load is ~ 24 ma which means that the first base draws $\leq 2.4\mu A$ from the

capacitor. The current drawn by the output monostable varies from ~ 1 - 2 ma (during the sweep), i.e. by about $\frac{1}{24}$th of the standing current. Hence the variation in base current is ~ 0.1 μA or about $\frac{1}{500}$th of the charging current.

The ramp voltage supply to the output circuit is shown in Fig. 4.2.

The output monostable consisted of two P346 transistors in a conventional arrangement.

A negative input pulse produced a positive pulse about 1 μS long, which was fed to the output via an emitter follower (another P346). Regular generator input pulses were used to obtain the series of output pulses shown in Fig. 4.3. It can be seen that the pulse length varies with amplitude from about 1.5 to 2.5 μS, but the rise time is almost constant (~ 200 nsec.). (A test of the Laben multichannel analyser showed that the channel into which a pulse was 'sorted' was independent of pulse length in the range 0.5 to 10 μS.)

Trigger and Control Circuit. In the absence of a start pulse the ramp voltage was kept at 'zero' by the transistor T (type P346) across the 22 μF capacitor. When this transistor is 'on' the capacitor is kept discharged. The ramp is triggered by switching this transistor 'off', leakage by this path then being < 1 μA.

The state of transistor T depends on the collector voltage of the right hand (R.H.) transistor of the control monostable which is either 0.4 volts (transistor 'on') or 7.5 volts (transistor 'off'). The emitter follower E supplies these voltages to the transistor T which is thus also either 'off' or 'on' respectively.

FIG 4.2 T.A.C. Ramp

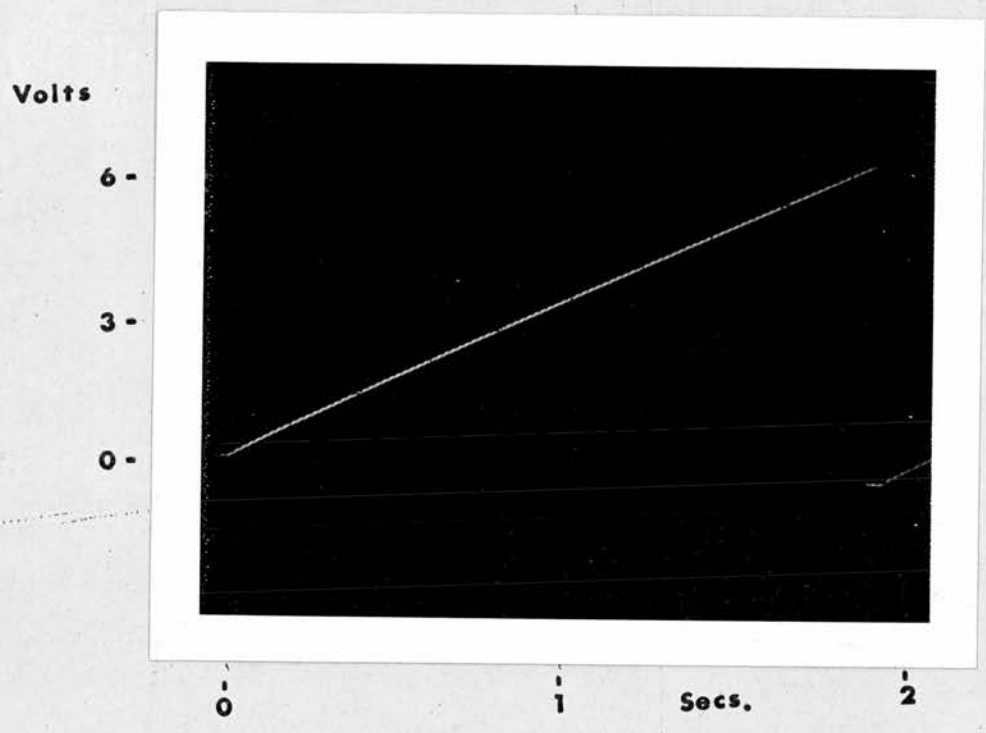

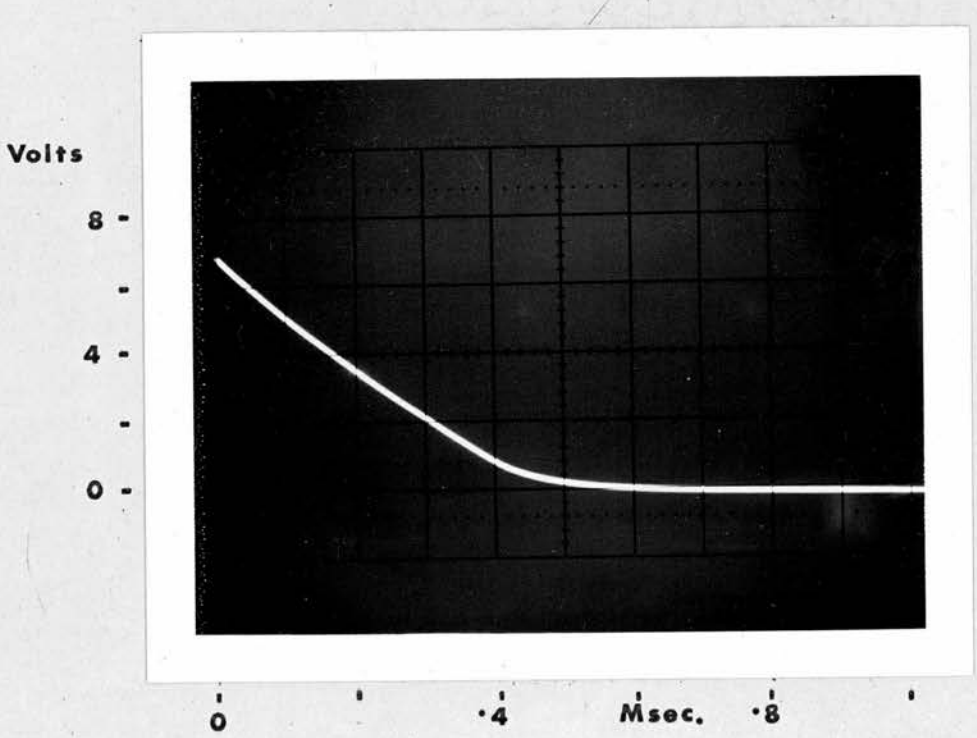

FIG 4.4 Ramp Flyback

T.A.C. Output Pulses

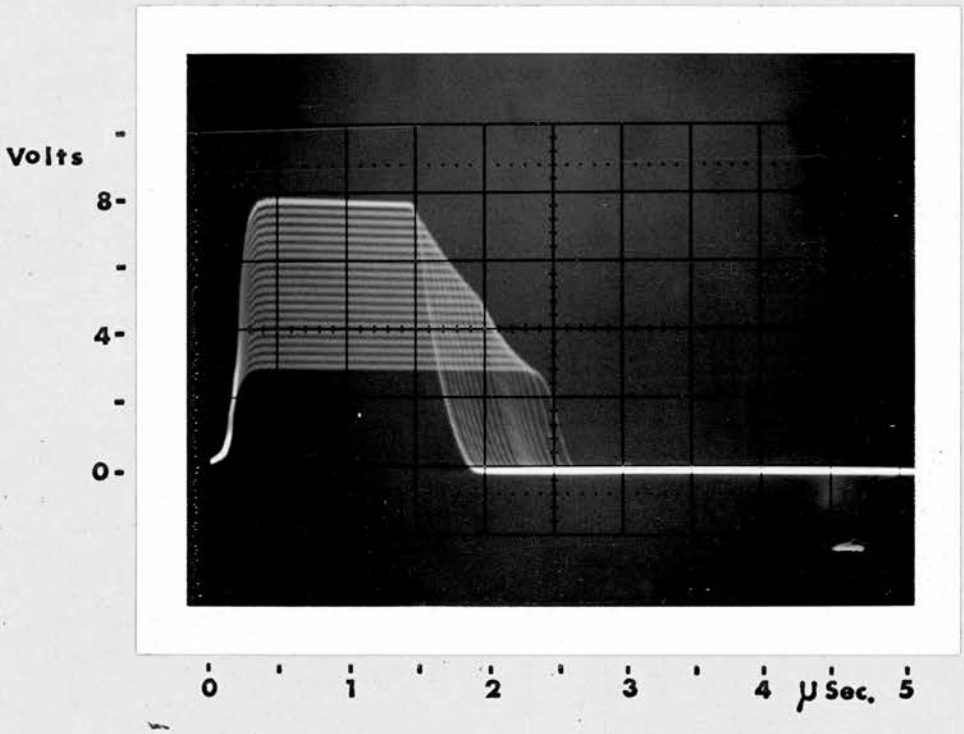

FIG 4.3

Consider the initial case when the L.H. transistor of the control monostable is 'off'. Any negative would-be trigger pulse applied to the base of this transistor cannot change its state, and is therefore lost. The R.H. transistor must be 'on', so that transistor T is 'off' and the 22 μF capacitor is allowed to charge up to the unijunction trigger voltage. When this point is reached the unijunction discharges C via the 10Ω resistor. A positive pulse appearing at the 10Ω is fed to the base of the L.H. transistor which is therefore switched 'on' and the R.H. one is switched 'off'. Transistor T is now turned hard 'on' and can assist the unijunction to discharge C. It will also prevent this capacitor from recharging.

This state persists until the bistable is switched by a (negative) trigger pulse, when the initial conditions described above are repeated and one complete sweep of the ramp is executed. The diode D prevents attenuation of the (negative) input pulse by the 10Ω resistor, and the minimum pulse amplitude necessary to trigger the ramp may be adjusted by the resistor R2.

A negative pulse was derived (output 2) from the sweep fly-back by means of the 100 pF capacitor. N_S was determined by counting these pulses with a scaler.

Preliminary Tests. Ramp linearity can be judged from Fig. 4.2. Leakage was tested by observing the voltage across C with a valve voltmeter, having disconnected the BC154. It took about one minute for this to discharge, implying a leakage current of about 2 μA.

As the output circuit is not dead during the period when the

ramp is returning to zero, it is important that this time be as short as possible. The ramp 'fly back' is shown in Fig. 4.4 from which it is apparent that the time taken is < 1 ms (see later).

4.3. T.A.C. Calibration

Since the multichannel analyser is a part of the system it is necessary to calibrate the complete T.A.C. - 'kick-sorter' combination. Ideally the channel no. into which a type B pulse is sorted should be a linear function of the time delay between pulses A and B, and all the channels should have the same width.

There are thus two basic measurements:

1) The overall time between the 'zero' and maximum time delay channels and the "integral" linearity in between. This measurement requires regular marker pulses with a spacing in time which is greater than the channel width.

2) The actual time width of each channel, i.e. differential linearity. For this measurement regular pulses with a spacing less than the channel width are preferable.

'Integral' Linearity. The marker pulses in this case were derived from the 100 c/s output of a crystal controlled generator, (Venner type TSA 3362), fed to a scaler (NE 5073) for suitable division. The type B pulses were supplied by the output from the first scale of ten giving a pulse every 100 msec.

The output pulse from the second scale of ten (one every second) was used to trigger the T.A.C. This was, of course, coincident with a pulse from the first scale of ten which goes into the 'zero' channel. The next pulse from the first scale comes exactly

100 msec. after the trigger pulse and therefore goes into the channel appropriate to a delay of 100 msec. Similarly the i^{th} pulse goes into the channel appropriate to a delay of (i) x 100 msec. provided (i) x 100 msec $< t_s$.

If, for example, t_s = 1.52 sec then after the 15th pulse was recorded in the channel appropriate to a delay of 1.50 sec. the sweep would reset and the next 5 pulses would be recorded in the zero channel. In the present case it was necessary to set t_s = 1.8 sec., i.e. the 18th pulse is recorded before the sweep resets and only 2 pulses per sweep are recorded in the zero channel, i.e. twice the number in the other channels. This provided a quick method for the initial setting and subsequent checking of t_s.

A schematic representation of this calibration system is shown in Fig. 4.5 and typical results illustrated by Fig. 4.6. A plot of delay time against channel number (Fig. 4.6) gives an indication of the linearity. The zero channel was found to be No. 80 (with bias subtraction on the analyser equal to 1.4 volts) and the T.A.C. was adjusted so that channel number 21 corresponded to 1.8 sec. delay, i.e. dt_{AV} = 30.5 $\pm$ 0.6 msec., where dt_{AV} is the average channel width.

Stability. After initial adjustment the zero channel was always found to be no. 80 and the 18th marker pulse in channel 21, a calibration of this type being done before and after every 'live' run.

By comparing the number of pulses counted on the 'division' scaler with the elapsed time measured (in seconds) on a stopwatch, a check on the accuracy and stability of the generator was obtained.

Arrangement for Integral Calibration FIG 4.5

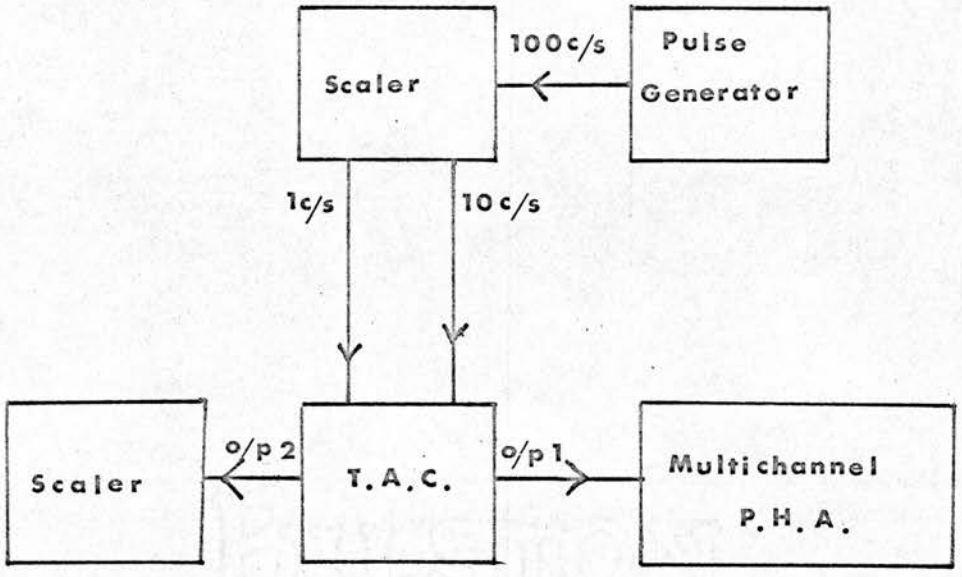

Arrangement for Delayed Coincidence Expt.

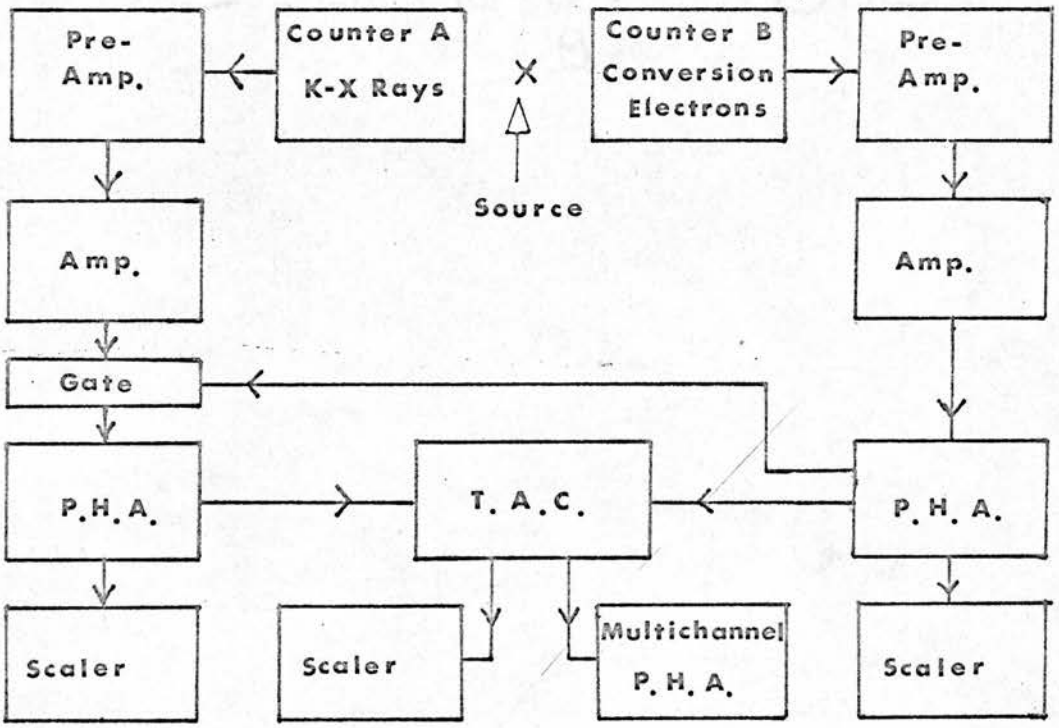

FIG 4.5a

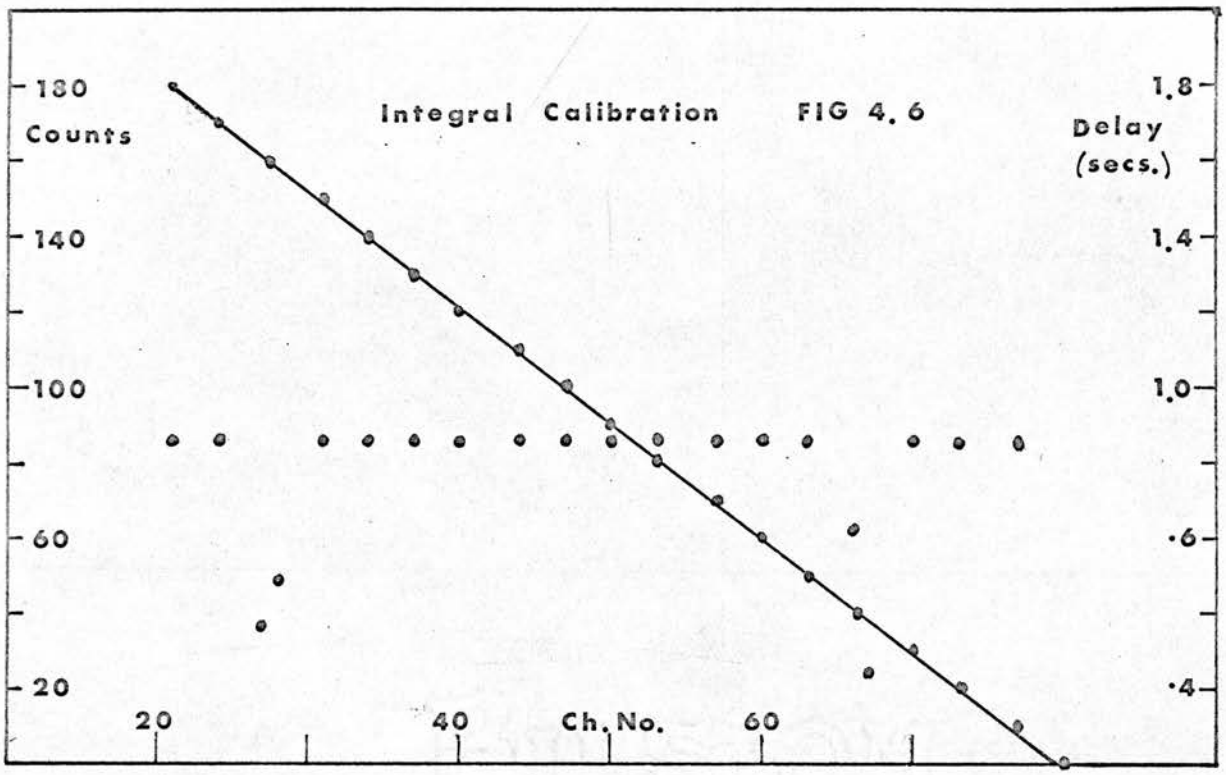
Integral Calibration FIG 4.6
180
Counts
140
100
60
20
1.8
Delay
(secs.)
1.4
1.0
.6
.4
20
40
Ch. No.
60

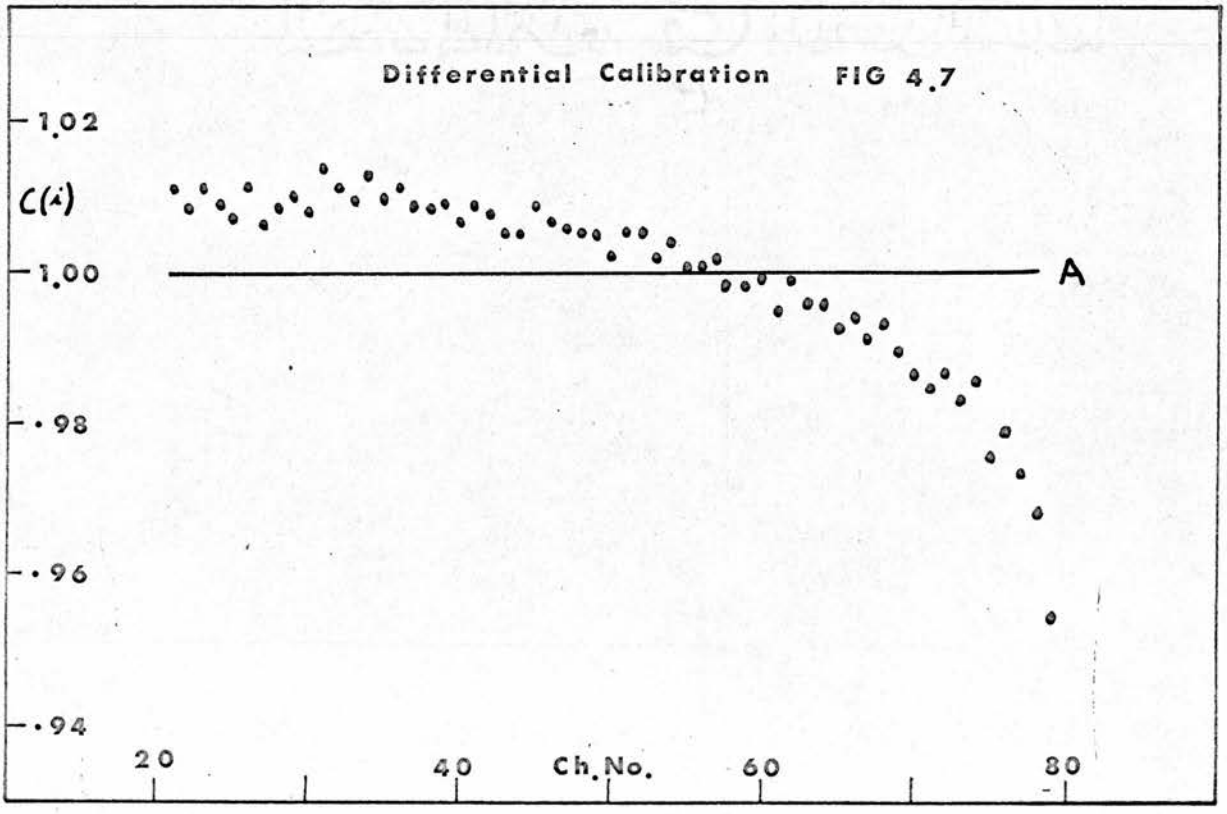
Differential Calibration FIG 4.7
1.02
C(λ)
1.00
.98
.96
.94
A
20
40
Ch. No.
60
80

No deviations were found outside the accuracy of the measurements (~ 1 in 10^4), supporting the makers' claim of 1 part in 10^6.

Differential Linearity

To measure the differential linearity of the T.A.C. it is necessary to use trigger pulses which are not correlated to those being 'converted'. The ways of providing such pulses will be discussed presently, but if in general there are N_S trigger pulses during a period when the average count rate of type B pulses is $\bar{R}_B$ then the number of counts $N(i)$ recorded in the i^{th} channel will be

$$N(i) = \bar{R}_B \, dt(i) \, N_S .$$

The width of the i^{th} channel is given by $dt(i) = \frac{N(i)}{R_B N_S}$, and the uncertainty in the measurement depends only on the statistical variations in R_B (in a time of the order of $dt(i)$) since N_S and $N(i)$ are known integers. The error therefore depends on the method of deriving the pulses for channel B.

The process may be thought of as one where the number of counts recorded in a channel during one sweep $N_1(i)$ gives a measurement of $dt(i)$ and this measurement is repeated N_S times. The average rate $\bar{R}_B$ is accurately known, but the true rates appropriate to the times for which a particular channel is open will show a distribution about $\bar{R}_B$, giving a distribution in $N_1(i)$ values of $\pm \Delta N_1(i)$ say.

Since the measurement is repeated N_S times, the fractional error in $N(i)$ and therefore in $dt(i)$ is

$$\frac{\Delta N_1(i)}{N_1(i) \sqrt{N_S}} \qquad (4.3.1)$$

when $N_S \gg 1$.

There are various ways of providing uncorrelated pulses:

a) The trigger pulses may be supplied from counter A exposed to source A, but shielded from source B, which is viewed only by counter B. This is the so-called independent source method of calibration.

In this case $\Delta N_1(i) = \sqrt{N_1(i)}$ and substitution in (4.3.1) gives $\Delta(dt)/dt = \frac{1}{\sqrt{N(i)}}$ where the approximation $N_1(t) = \overline{N_1(t)}$ has been introduced.

Thus as might be expected the error in $N(i)$ is $\sqrt{N(i)}$.

b) A single source may be used if it has no levels with lifetimes of the order of 0.5 secs., or is strong enough so that the number of true coincidences is negligible compared to the chance coincidences. In this case the independent nuclei are analogous to the independent sources of (a), and the error is as before.

c) The actual Arsenic source may be used with the roles of K X rays and conversion electrons reversed (i.e. conversion electrons act as trigger pulses and the K X rays are 'converted'). Since the conversion electron is emitted after the correlated K X ray the converted pulses can only arise from K X rays (uncorrelated in time) emitted by other independent nuclei of the source. The error in the measurement is again as in (a).

d) In this method the trigger pulses are supplied as in the experiment proper from the K X ray detector, but the converted pulses are supplied by a pulse generator. In this case (provided the generator is sufficiently stable and $\frac{1}{R_B} < dt(i)$, the number of pulses recorded in channel i during a particular sweep is

either the integer (p) below $R_B \times t(i)$ or the integer above this quantity depending on where the trigger pulse comes in relation to the generator pulse cycle.

In fact $dt(i) = zp + (1 - z)(p + 1)$ where z is the fraction of sweeps in which p counts are recorded in channel i.

The fractional error in a single measurement is $\lesssim \frac{1}{R_B\, dt(i)}$ so that the error in the final result is $\lesssim \frac{1}{R_B\, dt(i)\sqrt{N_S}}$, ie. the error in $N(i)$ is $\sqrt{N_S}$.

e) Each set of pulses may be supplied from independent generators, one of which, preferably that supplying the trigger pulses should not have stability better than 1 part in $n \times N_S$ (n is the number of channels). The error will then be the same as calculated in (d).

For given count rates R_B the accuracy of (d) and (e) is superior to that of (a), (b) or (c). This is because the time 'ruler' is the pulse generator in cases (d) and (e) and it has a constant 'scale division' - $\frac{1}{R_B}$. In methods (a), (b) and (c) the time 'ruler' is the radioactive source supplying the pulses in channel B and the scale divisions have a Poissonian distribution about the mean value $\frac{1}{R_B}$.

The present experimental arrangement (see Section 4.4) was unsuitable for method (a).

It was undesirable to use a high counting rate in the trigger channel for reasons to be given below. Method (b) would have required a strong source to yield accurate calibration curves rapidly, thus not satisfying this requirement.

Method (c) was used to show convincingly that there was a time correlation effect but 60 hours running was necessary to obtain an

accuracy of $\sim 3\%$ in each $dt(i)$ (Fig. 4.9).

Method (d) with the Venner generator supplying pulses at 1 kc/s (i.e. $\sim$ 30 pulses per channel per sweep) and triggered exactly as in the experimental situation gave an accuracy better than 0.15% in each $dt(i)$ after less than 30 minutes running. Twelve individual calibrations of this type (Fig. 4.7) were performed at intervals during the 300 hours for which the experiment was run. At this pulse rate in channel B the pulses are separated by 1 msec. - very much greater than the (fixed) 'kick-sorter' dead time of 4.7 μsec.

This pulse rate was, however, about 1000 times the actual experimental rate. Two calibrations done for 5 hours at R_B = 100 pulses per sec. yielded a (normalised) calibration with a R.M.S. deviation per channel of $\lesssim 0.1\%$ when compared to one of the twelve mentioned above (i.e. similar to the calculated error per channel). Also the shape of the calibration of method (c) fitted well with the others.

Derivation of the Necessary Correction from the Calibration

Only the shape of the calibration curve is of importance in determining the differential linearity, i.e. the comparative time widths of the channels. Let the average channel width for any range of n_1 channels be dt_{AV} and the corresponding average value of $N(i)$ be N_{AV}.

Then $dt_{AV} = \sum dt(i)/n_1 = \sum N(i)/R_B N_S n_1$, where

the sums are over the n_1 channels involved.

Hence $dt(i)/dt_{AV} = \frac{N(i)}{\sum N(i)} . n_1 = N(i)/N_{AV} = C(i)$ say.

It is therefore convenient to normalise the calibration spectra so that the average count per channel is unity.

A typical calibration curve normalised in this way is shown in Fig. 4.7, showing a fairly smooth variation (curve B) of C(i) from 1.015 to 0.955. This suggests a change in effective time width per channel along the sweep of about + 6%. The importance of calibration is emphasised by comparing this figure with the maximum expected true/chance ratio (Section 4.1) - ~8%. The straight line labelled A is to be expected for channels of exactly equal width.

If the number of counts observed in channel i of width dt(i) is $N'_o(i)$ then the number per channel of width dt_{AV} is given by

$$N_o(i) = N'_o(i)/C(i) \quad .$$

This correction formula applies whether the reason for a particular channel width being different from dt_{AV} is T.A.C. non-linearity or a discrepancy in the voltage width of a 'kick-sorter' channel. The latter is important as the quoted value of differential linearity for the 'kick-sorter' is 2%.

There are three possible reasons for the observed non-linearity:

1) Non-linearity of the T.A.C. itself: this could arise from a fall in the charging current as the voltage across C increases and that across transistor BC154 decreases (see Section 4.1)), or from a non-ohmic leakage which increases rapidly with voltage to start with and then becomes fairly constant.

2) Non-constancy of the 'kick-sorter' channel width - the quoted differential linearity of 2% is not alone large enough to account for the observed non-linearity but may contribute.

The method of correction outlined above is accurately valid for either or both the above causes. It is not, however, strictly correct for the third possible cause:

3) Accidental triggering during fly back. If this occurs it means that the sweep starts at a channel other than 'zero'. The chance of this happening is proportional to both the fly back time and the count rate in the trigger channel R_A, and the chance of the sweep starting in a particular non zero channel depends on the shape of the fly back curve. As can be seen from Fig. 4.4, this curve is fairly steep at the start of the fly back becoming less steep with a fairly long tail. This means that most of the "non-zero" sweeps will start in the first few channels. The 'swept' channels will register ~ 30 more counts (see page 85) every time this occurs, thus giving a calibration curve of the observed shape.

This may be described quantitatively by parameters $\alpha(i)$ - the average number of times a particular channel is opened per sweep. Clearly $0.92 < \alpha(i) < 1$. The number of counts per channel in a calibration is now given by $N(i) = N_S\, \alpha(i) R_B\, dt(i)$ since the i^{th} channel is now opened $\alpha(i)\, N_S$ times. For the chance coincidences the correction given above for non-linearity is still valid, $dt(i)$ being replaced by $\alpha(i)\, dt(i)$ in the discussion given previously.

This correction cannot be directly applied to the correlated (true coincidences) part of the observed counts. To see how this part is affected it is convenient to describe the effect of non-zero triggering in a slightly different way. Let $a(i)$ be the fractional number of sweeps starting in channel i. Then

$$\sum_{i=0}^{n-1} a(i) = 1 \quad \text{with} \quad a(0) \lesssim 1 \quad \text{and} \quad a(i \neq 0) \ll 1 \ .$$

Also $\alpha(i) = \sum_{j \leqslant i} a(j)$.

Thus instead of the form $N_o'(i) = N_S(R_C\, dt(i) + R_{OT}\, e^{-\lambda t_i}\, dt(i))$ where R_{OT} is the maximum true coincidence rate per unit channel width, the observed counts in channel i will be given by

$$N_o'(i) = N_S\, \alpha(i)\, R_C\, dt(i) + a(0)\, N_S\, R_{OT}\, e^{-\lambda t_i}\, dt(i) + a(1)\, N_S\, R_{OT}\, e^{-\lambda t_{i-1}}\, dt(i) + \ldots + a(j)\, N_S\, R_{OT}\, e^{-\lambda t_{i-j}}\, dt(i)$$

where $j \leqslant i$

$$= N_S\, \alpha(i)\, R_C\, dt(i) + N_S\, R_{OT} \left(\sum_{j \leqslant i} a(j) e^{-\lambda [t_i - t_j]} \right) dt(i) \ .$$

Correction by the method given above (i.e. division by $\alpha(i)dt(i)/dt_{AV}$ yields

$$N_o(i) = N_S\, R_C\, dt_{AV} + N_S\, R_{OT}\, dt_{AV} \cdot \frac{e^{-\lambda t_i}}{\alpha(i)} \sum_{j \leqslant i} (a(j)) e^{+\lambda t_j}$$

which is the proper correction for the chance part, but the correlated part is multiplied by a factor which is greater than unity for $i > 0$.

To find out how much this factor $f(i) = \sum_{j=0}^{i} a(j) e^{\lambda t_j} / \sum_{j=0}^{i} a(j)$ differs from unity it is necessary to make an estimate of the quantities $a(j)$. These may be found from the calibration since $a(i) = \alpha(i) - \alpha(i-1) \prec N(i) - N(i-1) \quad i > 0$.

The proportionality constant may be found if it is assumed that the overall effect is 6%, i.e. $\sum_{i=1}^{n} a(i) = 0.06$.

Since the differences $N(i) - N(i-1)$ are rather small (except for $i \lesssim 5$) the 'jitter' in the $N(i)$ makes it impossible to obtain every $a(i)$. However by collecting the channels into groups it is possible to estimate the average $a(i)$ for each group. These may be used to find an approximate value for $\sum a(j)e^{\lambda t_j}$.

The $a(i)$ calculated in the way described are plotted against channel number in Fig. 4.8. Since the shape of this curve is rather similar to the fly back curve, Fig. 4.4 (with the $a(i)$ axis corresponding to the time axis and the i axis corresponding to the voltage axis), it is possible that this effect is responsible for the apparent non-linearity.

The factor $f(i)$ has been estimated for the case where it most differs from unity, i.e. when $i = 60$. The result $f(60) = 1.17$ shows the importance of this effect if it accounts for all the apparent non-linearity.

To check whether this was the case several calibrations of the type (e) were performed using 1 kc/s in channel B as before but using a Dynatron type N117 signal generator to supply the trigger pulses at intervals of 2.5 secs. This gave at least 0.5 secs. for the sweep to return to 'zero', i.e. non-zero triggering was impossible. The calibration curve obtained was very similar to those of type (d) with an overall fall of 5.6%. The R.M.S. difference between the two curves was about 0.2% - comparable to that found for two calibration curves of type (d).

Thus non-zero triggering must occur for $< 1\%$ of the sweeps

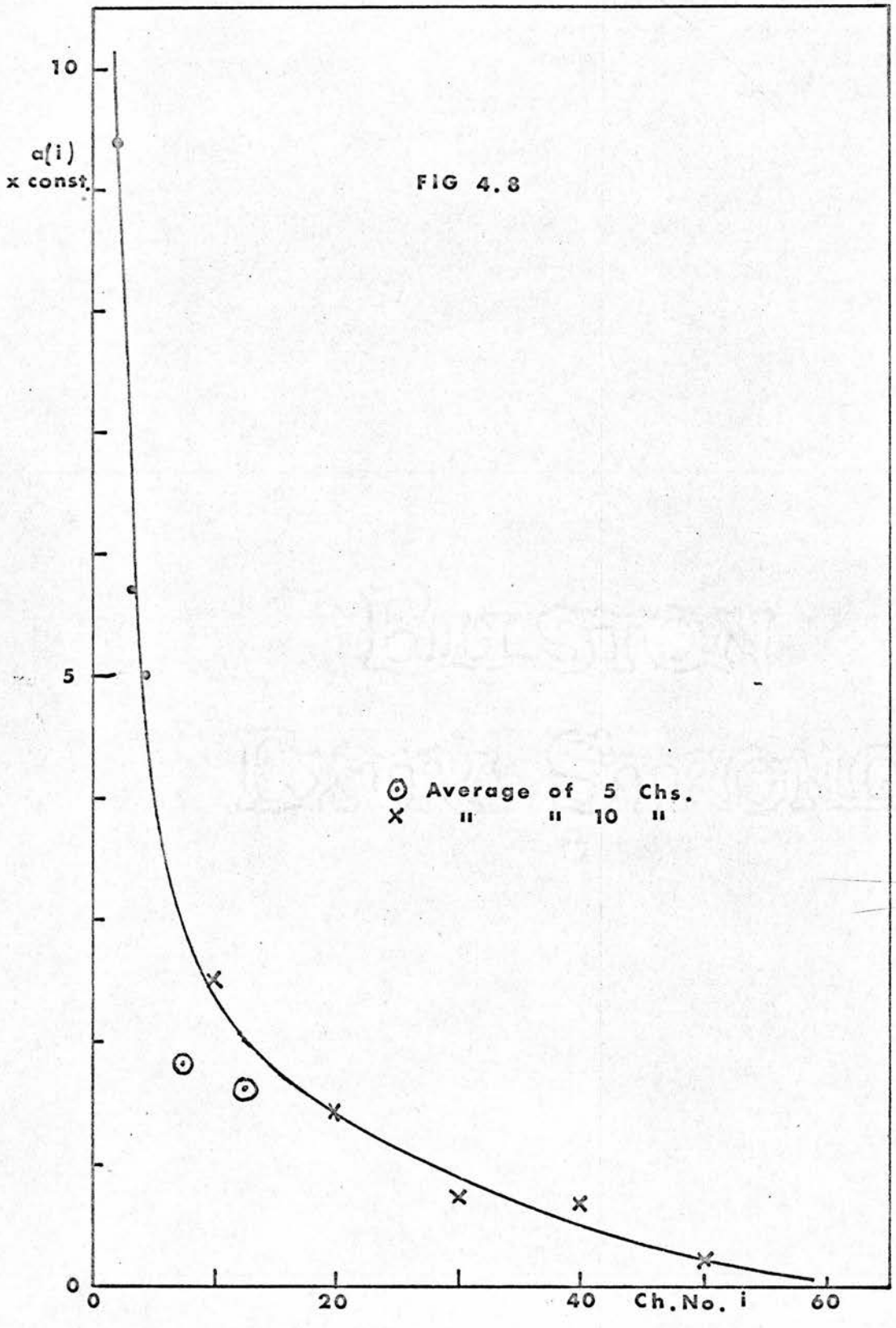

FIG 4.8

(at the count rates used) and the error involved because of this factor is then $< 2\%$ in the worst case.

During calibrations it is possible to see one or sometimes two counts being recorded on the 'kick-sorter' during fly back, implying that the total fly back time is ~ 2 ms. With a count rate of 1 sec.$^{-1}$ the chance of a trigger pulse occurring during this fly back time is $\sim 2 \times 10^{-3}$, i.e. $\sim 0.2\%$ of the sweeps do not start at zero.

Since the effect was small at the count rates used no attempt was made to remove it. This could easily be done by routing the trigger pulses through a gate which is closed during the sweep and re-opened by a pulse from the sweep control bistable delayed by ~ 10 msec.

4.4. Experimental Arrangement

A block diagram of the experimental set-up appears in Fig. 4.5a. K X rays detected in a scintillation counter provided the 'type A' pulses while the 'type B' pulses were taken from a gas proportional counter set to detect the conversion electrons of the 53.3 keV transition.

The Proportional Counter. This counter was designed and constructed by F. Shaikh[23] (of this department) and reference (23) gives a full description. The main features are outlined below.

The counter chamber, consisting of a brass cylinder 16" long and $5\frac{3}{4}$" in diameter, could be filled with a continuously purified mixture of Argon (90%) and Methane (10%) at 60 cms. Hg. pressure. A thin tungsten anode wire at earth potential held centrally in a cylindrical aluminium cathode (2" dia.) kept at

- 1640 volts, comprised the counter proper, which was held centrally in the counter chamber by insulating rings.

The entrance window was a ½" diameter hole in the centre of the cathode. A melinex film coated with a thin aluminium layer was employed as source holder and secured to the cathode with sellotape, the source being in the centre of the window, and on the inside.

At the gas pressure used the counter efficiency for 53.3 keV γ ray detection was $< 2\%$ while that for electrons of about 50 keV was almost 100%. The effective (fractional) solid angle was probably less than that calculated geometrically (0.38) because of source thickness effects (see Chapter 5).

Output pulses taken from the anode wire were fed to a charge sensitive preamplifier (Ortec type 101) followed by a voltage amplifier (Ecko type N567B). For calibration purposes the amplifier output was fed to the multichannel analyser. A typical As^{73} spectrum (displayed on 100 40 mv channels, Fig. 4.11) shows the K and L + M conversion electron peaks. The low energy peak is due to the K X rays (9.9 keV) for which the detection efficiency is about 32%.

In normal operation the amplifier output pulses were fed to an analyser (type NE 5102) for selection of a particular energy band of the spectrum. Analyser output pulses were fed to a scaler, input 2 of the T.A.C., and also to the gating input of the linear gate unit in the K X ray counter (see below).

The Scintillation Counter. In order to reduce the background counts a thin (0.08" thick) sodium iodide crystal 1" diameter was used to detect the K X rays. This thickness is sufficient to absorb

almost 100% of the 9.9 keV K X rays (and 99.6% of the 53.3 keV γ rays) at normal incidence. The reduction in background is achieved because a thin crystal is less efficient for higher energy background radiations (which give pulses at low energy due to Compton scattering) and because of slightly improved resolution. This crystal was also fitted with a 36 mgm/cm^2 thick Be window.

The contribution to the background from photomultiplier tube noise was also reduced by using a low noise P.M. tube (EMI type 9635BQ) with a photo cathode of high quantum efficiency. This tube gave a considerable improvement in resolution thus further reducing the background. It was supplied with a quartz window to reduce background counts due to K^{40}.

The scintillator was coupled to the P.M. tube using silicon optical grease and the complete assembly (base, P.M. tube and crystal) was mounted (by paxolin rings) in a 2.8" diameter brass tube. Light pressure applied by springs kept the assembly pressed firmly against the front of the tube which was recessed to take the crystal. The 1" diameter window was covered by a film of melinex cemented in position with 'Araldite'. The front part of the tube was a sliding fit in an entry in the proportional counter outer cylinder such that the detector was placed just behind the source (see Fig. 4.13). A flange fitted with an 'O'-ring 3.8" from the front of the tube enabled a gas tight seal to be made with the proportional counter.

To keep background effects to a minimum, it was necessary to count the source activity with as large a solid angle as possible, i.e. to have the detector as near as possible to the source.

Ideally the front of the tube should be in contact with the cathode

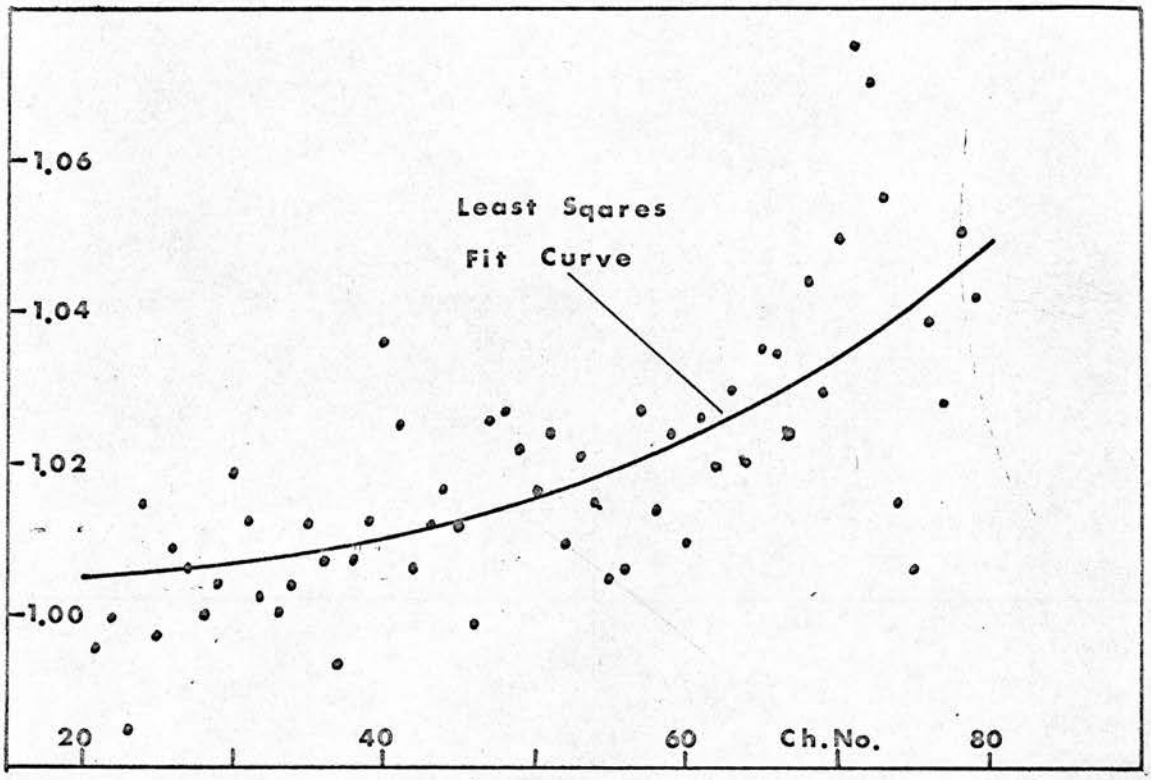

FIG 4.10 Normalised Delayed Coincidence Curve

FIG 4.9 Same with Counters Interchanged-

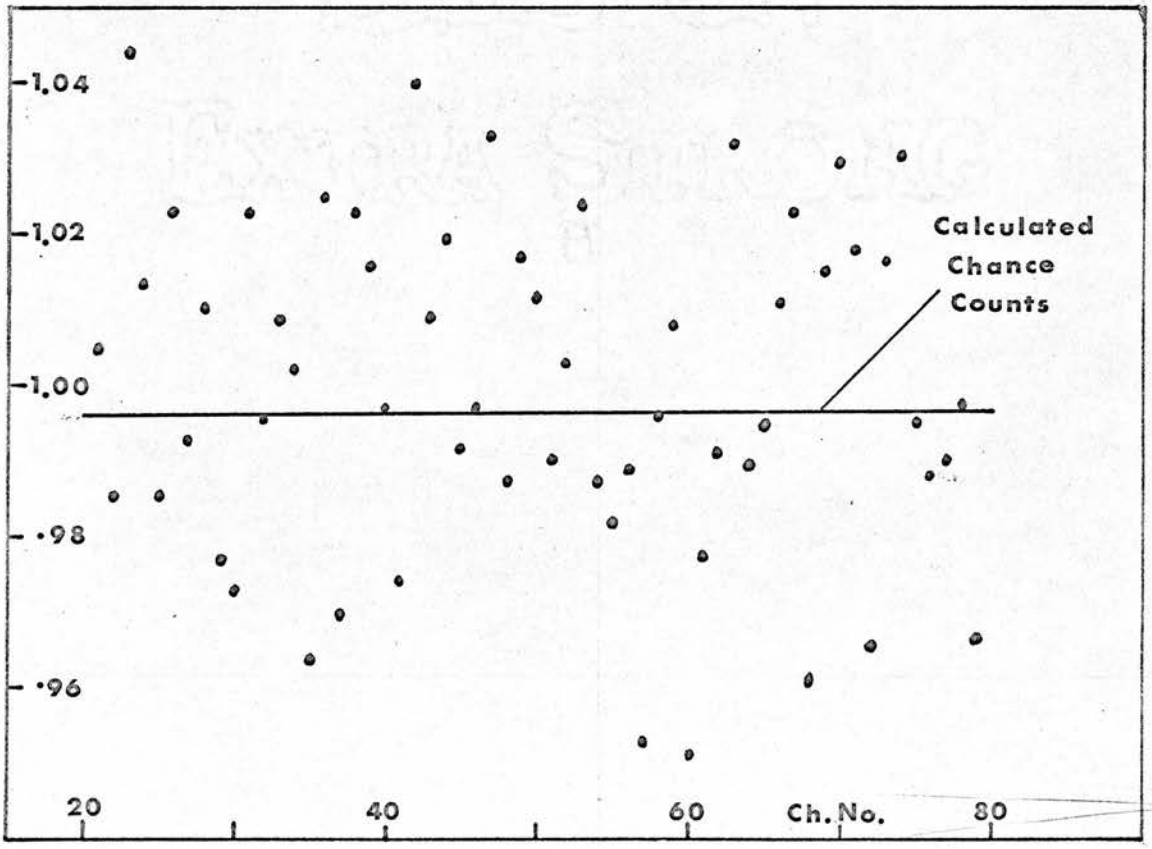

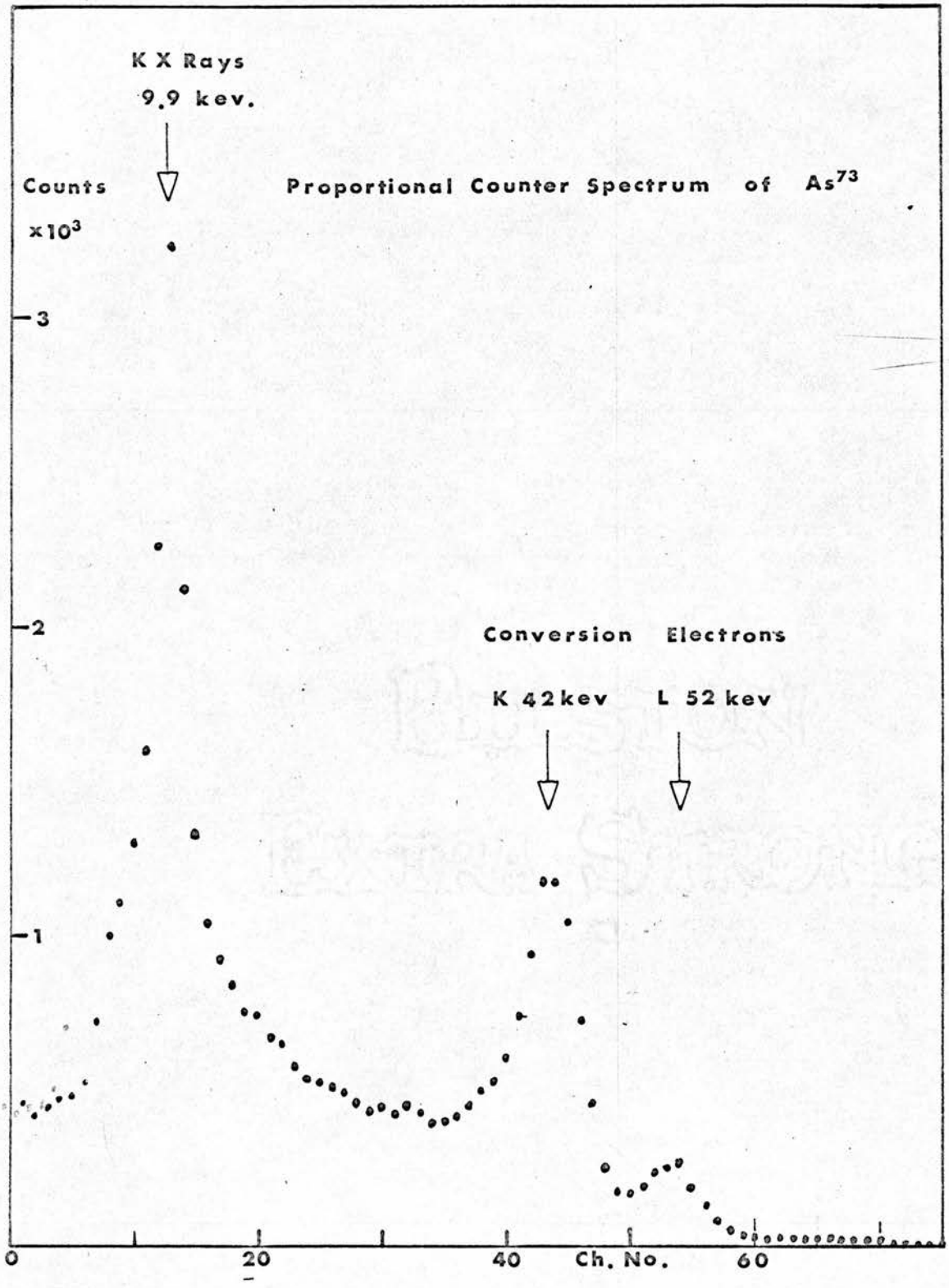
K X Rays
9.9 kev.
Counts
x10³
Proportional Counter Spectrum of As⁷³
3
2
1
Conversion Electrons
K 42kev
L 52 kev
0
20
40
Ch. No.
60

FIG 4.11

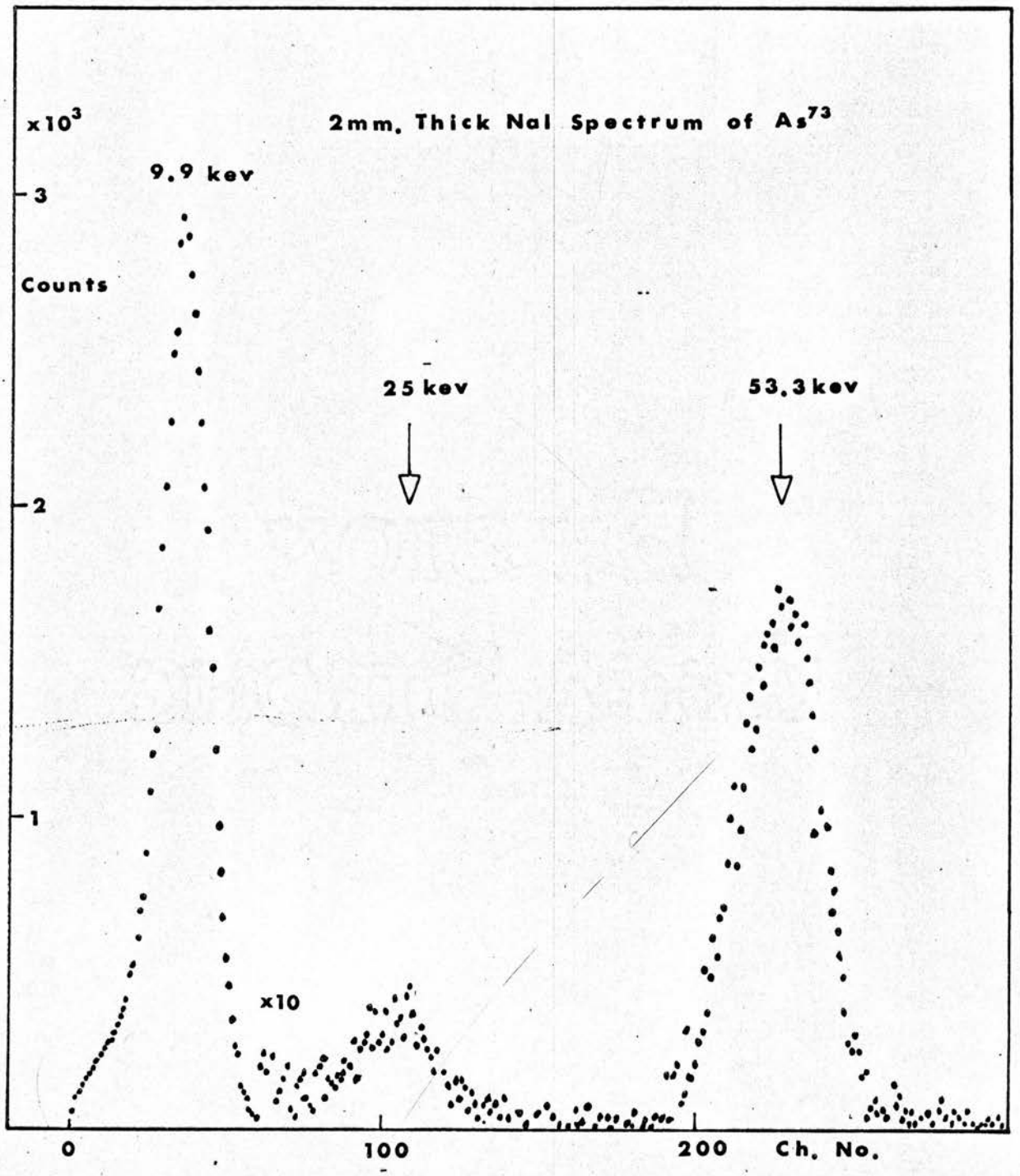
x10³
2mm. Thick NaI Spectrum of As⁷³
9.9 kev
3
Counts
25 kev
53.3 kev
2
1
x10
0
100
200
Ch. No.

FIG 4.12

Proportional and Scintillation Counter Assembley

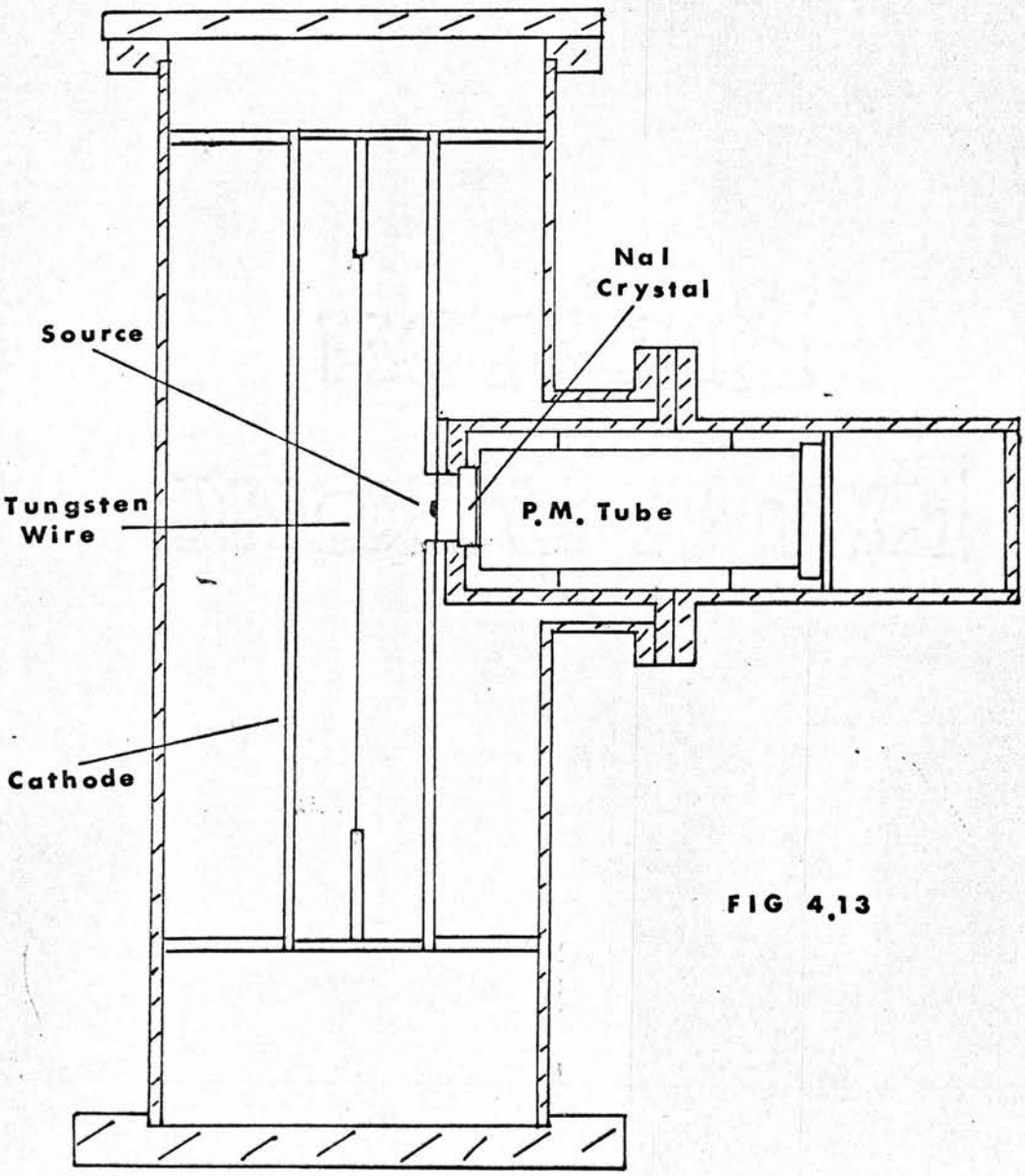

FIG 4.13

of the proportional counter, but as the latter was at - 1640 V it was necessary to fit the front of the tube with a PTFE insulator. This was 1 mm thick and the total source to crystal distance was ~ 4.5 mm, giving an effective fractional solid angle of ~ 0.24 for K X rays.

The P.M. tube was operated at an E.H.T. of 1 kV supplied by an Isotope Developments type 532A E.H.T. unit. Output pulses from the anode were fed to a type NE 5281 pre-amp. followed by an amplifier type NE 5259, operating in the R-C mode with integration and differentiation time constants both equal to 1 μsec. Pulses corresponding to 9.9 keV K X rays or 53.3 keV Y rays were selected by means of two analysers of type NE 5159. The 9.9 keV analyser output was fed through a gate unit type NE 5730 (modified slightly) so that the gate was turned off for ~33 μsec when a gating pulse (supplied by the proportional counter channel) was applied. The output pulse from the gate was used to trigger the T.A.C. (input 1) and was also fed to a scaler.

For calibration purposes an output from the amplifier was taken to the multichannel analyser. A typical Arsenic-73 spectrum (displayed on 300 40 mv channels) is shown in Fig. 4.12. The resolution is about 40% at 9.9 keV and 18.5% at 53.3 keV.

The complete counter system is shown in Fig. 4.13.

Setting-Up. The analysers in both channels were checked to ensure that the gate widths were correct, and then were calibrated against the 'kick-sorter'. For this purpose several Am^{241} and Eu^{152} spectra at different gain settings were taken, using count rates about 50 times the Arsenic case. Points on these calibration curves were also provided by the position of the 9.9 keV peak at various gains. This was done so that the analysers

could be set quickly on a desired peak from the 'kick sorter' spectrum.

The stability of the scintillator assembly was excellent and it was found unnecessary to change the analyser settings during the experiment ($\sim$3 weeks). Frequent checks showed that the 53.3 keV photopeak drifted by $\sim \pm 4$ channels in 226 during this time.

The proportional counter gain decreased with time fairly rapidly at first and then less rapidly (as described by Shaikh[23]). The analyser threshold was adjusted before each run of $\sim$15 hours and the 42 keV conversion electron peak fell by about 1 channel in 80 during this time. Since the threshold was set at the minimum of the broad trough between the K X ray and conversion electron peaks the effect on the observed count rate was small. Deterioration of the resolution made it necessary to refill the proportional counter twice during the experiment.

Back ground. Some reduction in background was afforded by surrounding the counter assembly by 2" thick lead blocks.

The measured background was 0.33 $sec.^{-1}$ for the proportional counter set to detect conversion electrons, and 0.08 $sec.^{-1}$ for the scintillator set to detect K X rays.

Source. The source was made by allowing several drops of the active solution to evaporate on the melinex film. The strength was such that the conversion electron count rate was 1.2 $sec.^{-1}$ - slightly higher than the optimum value (see Section 4.1).

Operation. The experiment was run for a total counting time of more than 300 hours taken in three 100 hour groups, each group

consisting of seven periods of continuous counting (about 15 hours each). In between these counting periods the analyser settings were checked by taking 'kick-sorter' spectra, and the T.A.C. was checked (roughly) by the integral method.

Several calibrations of type (d) (see Section 4.3) were performed at intervals during each 100 hour group. A further group of results with a total counting time of 60 hours was taken with the counters interchanged (i.e. T.A.C. triggered by conversion electrons).

4.5. Analysis of Results

The delayed coincidences per channel for a 100 hour group were calculated by addition of the counts recorded in that channel during each of the 15 hour periods.

An average of the calibrations done during the '100 hours' (normalised to unit channel width) was used to correct for non-linearity in the way described in Section 4.3.

The three groups were then added to give a total delayed coincidence curve due to 300 hours counting. About 15×10^3 counts were accumulated in each channel during this time.

The group taken with the counters interchanged was treated in exactly the same way and the (normalised) result is shown in Fig. 4.9.

Calculation of Chance Rate

The average number of chance coincidences per channel for each 15 hour period was calculated from $\bar{N}_C = N_S \bar{R}_B \, dt_{AV}$ where $\bar{R}_B$ is the average count rate ($^N B/t''$) in channel B.

The total number of chance coincidences was then obtained by addition.

The error ($\sigma_{\bar{N}_C}$) in $\bar{N}_C$ is given by

$$\frac{\sigma_{\bar{N}_C}}{\bar{N}_C} = \sqrt{\left[\frac{\sigma_{\bar{R}_B}}{\bar{R}_B}\right]^2 + \left[\frac{\sigma_{dt_{AV}}}{dt_{AV}}\right]^2}$$

since N_S is known exactly. $\sigma_{dt_{AV}}$ was taken to be the standard deviation in the mean given by the calibrations and it was found that $\sigma_{dt_{AV}/dt_{AV}} = 0.15\%$.

Strictly in the calculation of $\bar{N}_C$, $\bar{R}_B$ should be replaced by $\bar{R}'_B$ where $\bar{R}'_B$ is the average count rate in channel B during the time $N_S t_S$ for which the T.A.C. is sweeping. As this is a large (~ 70%) random sample of the total running time t", drift is not important, and the error in assuming $R'_1 = \bar{R}_B$ is purely statistical. This fractional error is

$$\frac{\sigma_{\bar{R}'_B}}{\bar{R}'_B} = \frac{\sqrt{\frac{N_S t_S}{t''} N_B}}{\frac{N_S t_S}{t''} N_B} .$$

Since $N_B \simeq 1.2 \times 10^6$ the error here is 0.108%

$$\therefore \quad \frac{\sigma_{\bar{N}_C}}{N_C} = 0.18\% \quad \text{and} \quad N_C = 14556 \pm 27.$$

The delayed coincidence curve normalised to N_C is shown in Fig. 4.10, and the small correlation can be seen by comparing this figure with Fig. 4.9 which was obtained with the counters interchanged.

Curve Fitting. Because of the large statistical error on each channel, subtraction of the chance counts in some cases gave a negative answer. It was therefore not possible to perform a linear least squares fit to a $\log(N(i) - \bar{N}_C)$ versus time plot.

Instead the points $(N(i), t_i)$ were fitted to a curve of the form

$$N(i) = Ae^{-\lambda t_i} + B \quad \text{with} \quad B = \bar{N}_c \ .$$

According to the principle of 'least squares', the 'best' values of A and λ are such that

$$\sum_i \left[N(i) - (Ae^{-\lambda t_i} + B)\right]^2 w_i = \text{minimum}$$

where w_i is the weight assigned to the point $(N(i), t_i)$.

To obtain the best values of A and λ it is necessary to start with trial values $\bar{A}$, $\bar{\lambda}$ say.

For any function $f_i(A\,\lambda) \simeq f_i(\bar{A}\,\bar{\lambda}) + \left(\frac{\partial f_i}{\partial \bar{A}}\right)_{\bar{A}\bar{\lambda}} a + \left(\frac{\partial f_i}{\partial \bar{\lambda}}\right)_{\bar{A}\bar{\lambda}} \ell$

where the correct values are given by $A = \bar{A} + a$, $\bar{\lambda} = \bar{\lambda} + \ell$.

In this case $f_i(A\lambda) = Ae^{-\lambda t} + B$ with $\left(\frac{\partial f_i}{\partial A}\right)_{\bar{A}\bar{\lambda}} = e^{-\bar{\lambda} t_i}$ and $\left(\frac{\partial f}{\partial \lambda}\right)_{\bar{A}\bar{\lambda}} = -\bar{A}\, t_i\, e^{-\bar{\lambda} t_i}$. The problem is now reduced to finding the best values of a and ℓ to satisfy the n condition equations

$$N(i) - f_i(\bar{A}\,\bar{\lambda}) = (e^{-\bar{\lambda} t_i})a - (\bar{A}\, t_i\, e^{-\bar{\lambda} t_i})\ell \ .$$

Since these equations are linear in a and ℓ the usual method may be applied to minimise the weighted sum of the squares of the derivations:

$$\sum_{i=1}^{n} d_i^2 w_i = \sum_{i=1}^{n} \left\{N(i) - f_i(\bar{A}\,\bar{\lambda}) - \left[(e^{-\lambda t_i})a - (\bar{A}\, t_i\, e^{-\lambda t_i})\ell\right]\right\}^2 w_i$$

with respect to a and ℓ (see for example Whittaker and Robinson[53])

This is done by solving the normal equations which may be conveniently written in matrix notation:

$$P\begin{pmatrix} a \\ \ell \end{pmatrix} = \begin{pmatrix} C_1 \\ C_2 \end{pmatrix} \quad \text{where } P \text{ is the matrix } p_{jk}$$

with $p_{11} = \sum e^{-2\bar{\lambda}t_i} w_i$, $\quad p_{12} = -\bar{A}\sum t_i e^{-2\bar{\lambda}t_i} w_i$

$$p_{21} = p_{12} \quad \text{and} \quad p_{22} = \bar{A}^2 \sum t_i^2 e^{-2\bar{\lambda}t_i} w_i ,$$

and $C_1 = \sum e^{-\bar{\lambda}t_i} (N(i) - f_i(\bar{A}\,\bar{\lambda}))\, w_i$

$$C_2 = -\bar{A}\sum t_i e^{-\bar{\lambda}t_i} (N(i) - f(\bar{A}\,\bar{\lambda}))\, w_i \quad .$$

The solution is $a = \begin{vmatrix} C_1 & p_{12} \\ C_2 & p_{22} \end{vmatrix} \Big/ |P|$

$$\ell = \begin{vmatrix} p_{11} & C_1 \\ p_{21} & C_2 \end{vmatrix} \Big/ |P|$$

and the error in a, ℓ is $\sigma_a = \sigma\sqrt{\frac{p_{22}}{|P|}}$

$$\sigma_\ell = \sigma\sqrt{\frac{p_{11}}{|P|}}$$

where $\sigma = \sqrt{\frac{\sum d_i^2 w_i}{n-2}}$.

The correct weight appropriate to the point $(N(i), t_i)$ is $\frac{1}{\sigma_{N(i)}} = \frac{1}{\sqrt{N(i)}}$. In this case (because of the large ~ constant chance rate) the $N(i)$ only decreased by ~8% from $i = 1$ to $i = n$ so the weights were taken to be equal.

A computer program was written to calculate a, ℓ, σ_a and σ_ℓ according to the above results, when supplied with starting values $\bar{A}$, $\bar{\lambda}$ and $B = \frac{N_C}{\bar{A}}$. The program was run several times, each time starting with $\bar{A}$, $\bar{\lambda}$ values indicated by the previous run. The

process was stopped when the recommended corrections a, ℓ were about 0.5%.

The result of fitting the total 300 hours running was

$$T_{\frac{1}{2}} = 0.57 \pm 0.09 \text{ secs.}$$

and the results for the three 100 hour groups are shown in Table 4.1. The error quoted is the statistical error derived from the least squares fit as explained above, and does not include error,

Table 4.1

Results for 53.3 keV Level Half-life

Group No.	$T_{\frac{1}{2}}$
1	0.62 ± 0.16
2	0.60 ± 0.14
3	0.49 ± 0.14
Total	0.57 ± 0.09

arising from the uncertainty in B. Changing the value of B by $\pm$ 27 was found to change the half-life value by $\pm$ 0.03 sec.

The result obtained is in good agreement with the value $0.53 \pm .03$ sec. obtained by Campbell and Nelson[22] (see Chapter 1).

CHAPTER 5

DELAYED COINCIDENCE EXPERIMENTS ON THE 13.5 KEV LEVEL

This chapter is devoted to a description of some experiments done using the stronger As^{73} source mentioned in Chapter 2. The half-life of the 13.5 keV level has been measured by the delayed coincidence technique using a time to amplitude convertor, and employing various different radiations to mark the 'birth' of the level.

The intensities of the 'prompt' and 'delayed' parts of the coincidence curves have been used to estimate the K/L+M ratio for 13.5 keV conversion electrons, the fluorescence yield for K X rays and the K capture fraction in As^{73} decay.

The strong source was also used in a direct measurement of the total conversion coefficient α of the 53.3 keV transition with special attention being given to the calculation of effective solid angle for conversion electrons.

5.1 Half-Life of the 13.5 keV Level

The conditions necessary for a successful half-life measurement by the delayed coincidence method discussed in Chapter 4 are easily met when $T_{1/2} \simeq 3$ μsec. Background counts were made almost negligible by using a source $\gtrsim 100$ times stronger than that of Chapter 4. Even with this source strength, and a T.A.C. sweep time t_s such that the decay could be followed over more than three half-lives, the true/chance ratio was always > 10 for

the 'worst' time channel.

Also, in the notation of Chapter 4, $\frac{1}{R_B} \simeq 10^{-2}$ sec. and $t_S \simeq 2 \times 10^{-5}$ sec. Hence the condition $\frac{1}{R_B} >> T_S$ is satisfied, and the chance rate per channel may be taken as a constant for every channel, even if the T.A.C. is of the type which stops the sweep on receiving the type B pulse.

One possible difficulty arises because of the lengths of the output pulses from the detectors. In fact is is only the 'rise' times that are important and these are controlled by the decay time of the scintillation phosphor and the charge migration velocity in the proportional counter. The former is almost negligible (~ 250 ns) but for the latter, due to the motion of the heavy positive ions, the duration of pulse formation may be many tens of μsecs. Fortunately half of the maximum pulse height is reached in a time (a/b) in terms of the total pulse length where 'a' and 'b' are the radii of the anode and cathode respectively. In the present counter $a/b \simeq 10^{-3}$ so that if the total output pulse is 50 volts of 100 μsecs. length then half of the pulse, i.e. 25 volts would be realized in 0.1 μsec. Differentiation of the counter output pulses (in the amplifier) can therefore be used to reduce the size of the pulse, and the delay, which is then $<$ 0.1 μsec. The sharp differentiation is only possible, however, if a high gain low noise and fast electronic system is used with the proportional counter.

Experimental Arrangement. The arrangement was similar to that used for the half-life measurement of the 66.8 keV level.

As it was unnecessary to gate the K X ray detector the gate unit was removed from the scintillation counter system.

The T.A.C. with 1.8 sec. sweep was replaced by one with a (maximum) sweep time of about 20 μsec. This unit was designed and constructed by the Electronic Workshop of this department and was of the type where the sweep is stopped by the pulse from counter 'B'.

Because time delays in the two counters were likely to be of a magnitude comparable to $T_{1/2}$ (~ 3 μsec.) it was necessary to introduce a delay into channel 'B'. The unit used was made by F. Shaikh (of this department) and enabled pulses to be delayed by a time variable from zero to ~ 10 μsec.

Source. The source was made by allowing one drop of the 10 μC source solution to evaporate on a melinex film coated with a thin aluminium layer. This was fixed by sellotape to the cathode of the proportional counter in the same way as before. The count rates were found to be about 120 times those of the weak source used in the ½ sec. half-life measurement.

T.A.C. Calibration. 'Integral' calibration was performed by means of pulse pairs derived from a double pulse generator (Flemming type 1147C). These were fed to the pre-amplifiers of the two counters, the 0 - 10 μsec. delay between pulses (available from the generator) being augmented by the delay unit in counter B so that the range 0 - 20 μsec. could be covered. The delay between pulses of type A and type B was measured at the inputs to the T.A.C. by a Hewlett Packard type 175A

oscilloscope. A typical calibration of this type is shown in Fig. 5.1. The channel corresponding to a particular time delay between pulse pairs was found to drift slowly by about 3 channels during the course of the experiment, but the average channel width dt_{AV} found from this calibration method was always $0.33 \pm .01$ μsec.

The differential calibrations (e.g. Fig. 5.2) were obtained by triggering the T.A.C. with counter 'A' pulses (as in the experiment proper) and using regular 1 kc/s pulses derived from the Venner (type TSA 3362) pulse generator for the 'B' input. (i.e., method 'd' of Chapter 4). The fractional error in the measurement of the time width dt(i) of the i^{th} channel is $\frac{\sqrt{N(i)}}{N(i)}$ (where N(i) is the number of counts recorded in that channel) in this case because the maximum number of counts recorded per sweep is unity. (Cf. Chapter 4). It was found necessary to calibrate for ~5 hours to obtain ~1000 counts in each channel, i.e. an accuracy of ~3°/o. From Fig. 5.2 it can be seen that the differential linearity is at least as good as this except for the first 10 channels of the sweep, which are slightly wider than the rest. The delay in counter B was always set greater than 3 μsec. so that the time 'zero' occurred above this region.

In the absence of a large chance coincidence contribution to the count rate, small deviations from linearity are not very important, so no correction for this was applied. The average channel width found by this method was found to increase slightly during the course of the experiments, the mean result of all such calibrations being $dt_{AV} = 0.326 \pm .002$ μ sec.

FIG 5.1

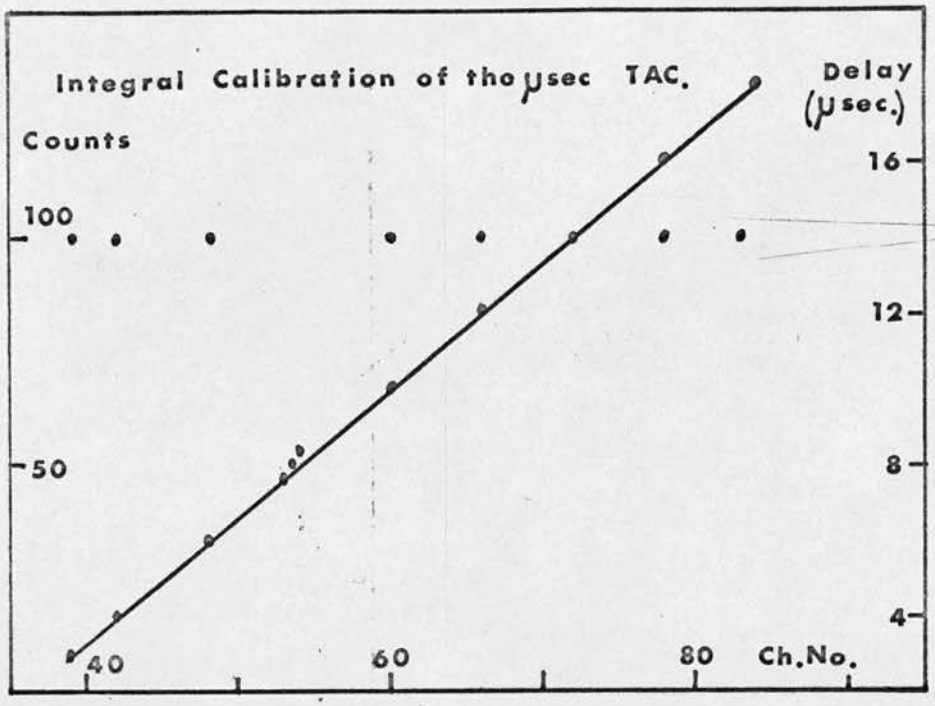

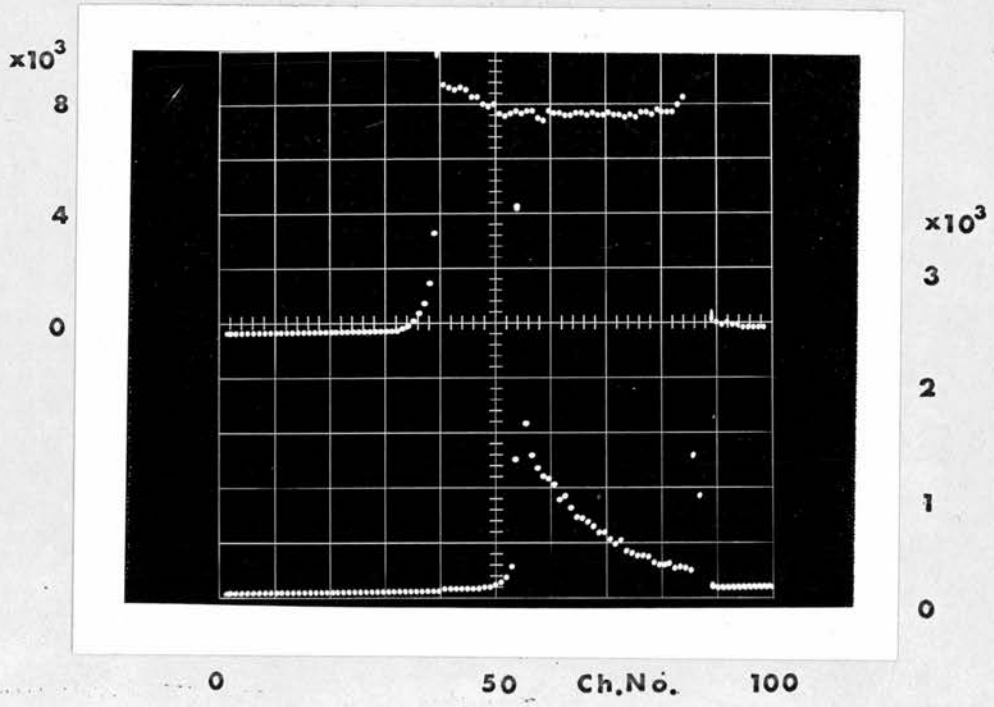

Upper : Differential Calibration L.H. Scale

Lower : Delayed Coincidence Curve R.H. Scale

FIG 5.2

FIG 5.3 NaI Spectrum of As^{73}

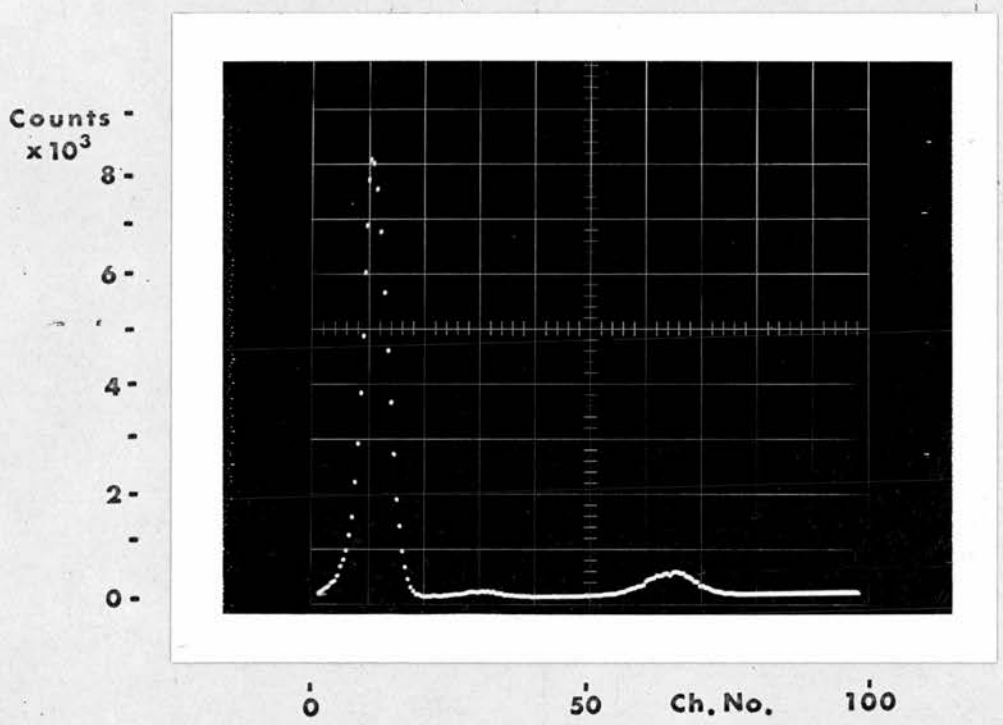

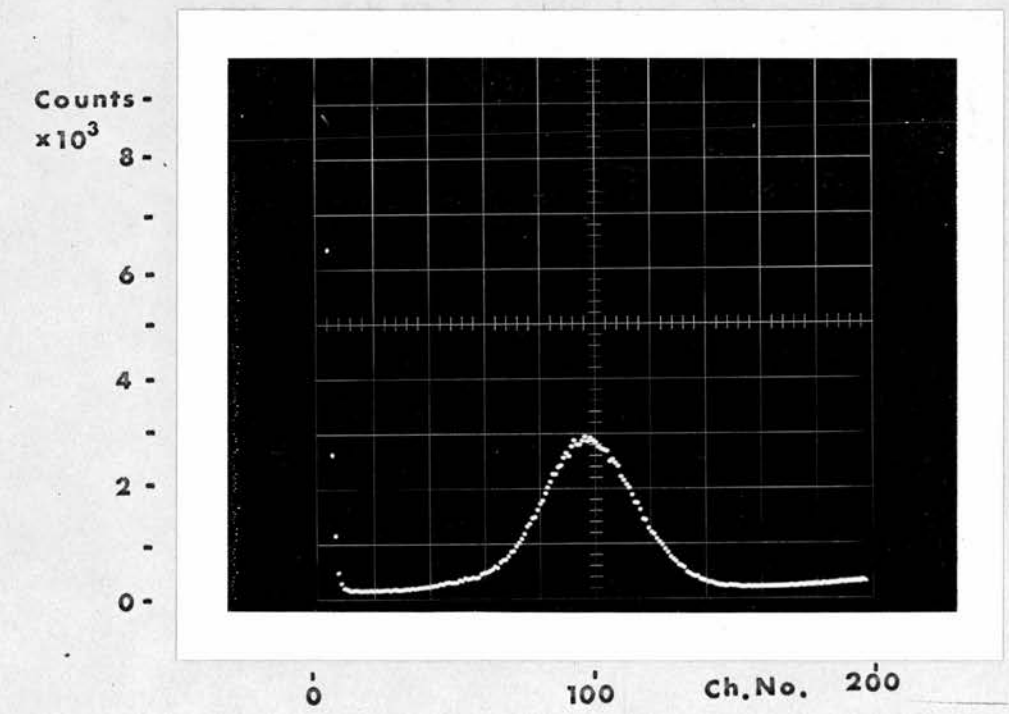

FIG 5.3a NaI Spectrum of As^{73} at High Gain Showing Tail of P.M. Tube Noise

Proportional Counter Spectrum of As^{73}

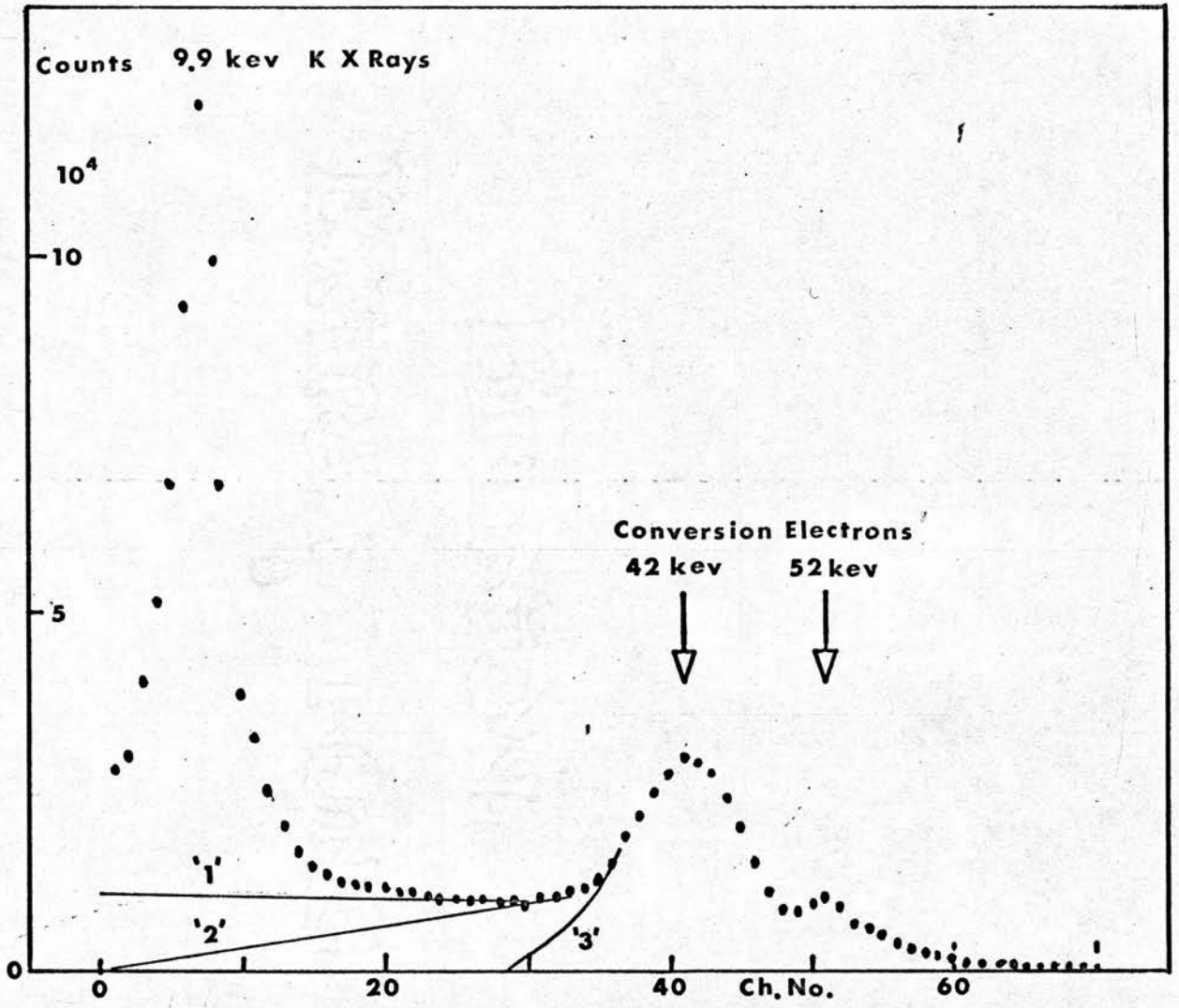

FIG 5.4

Counter Calibration. The single channel analysers were again set up from multichannel kick sorter spectra examples of which are shown in Figs. 5.3, 5.3a, 5.4. The 53.3 keV transition may give rise to a 53.3 keV γ ray, a K conversion electron (and therefore possibly a K X ray) or a conversion electron from an outer shell. It is therefore possible to detect the 'birth' of the 13.5 keV level by setting the counter A on one (or more) of these radiation types. There are therefore four possible experiments - each using a different radiation to supply the T.A.C. trigger pulse. These will now be discussed in turn.

K + L Conversion Electron - K X Ray Coincidences. Conversion electrons detected in the proportional counter (setting the analyser threshold in the trough between the K X ray and 42 keV peaks) provided the T.A.C. trigger pulses for the coincidence curve shown in Fig. 5.5. The large 'peak' in the curve is due to coincidences between the K conversion electrons and the K X rays that are emitted when the atomic vacancy formed by the K conversion electron fills. Since this takes place with an average time delay of $< 10^{-15}$ sec, it is to be expected that these 'prompt' coincidences should all be recorded in the 'zero' channel (since the channel width is $\sim$ 0.3 μsec.). However, due to the time "jitter" in counters the result is a 'peak', the width of which gives a measure of the time "jitter". In fact the width at half height was about 2 channels implying a time jitter of about $\pm$ 0.3 μsec. overall.

The 'delayed' part of the curve is due to coincidences between conversion electrons from the 53.3 keV transition and the

K X rays which arise when the atomic vacancies left by conversion of the 13.5 keV transition are filled. The half-life of the 13.5 keV level can be obtained by fitting this part to a curve of the form $N(i) = Ae^{-\lambda t} + B$ (where $\lambda = \frac{0.6931}{T_{1/2}}$ and B = the number of chance coincidences per channel) as discussed in Chapter 4. In this case the points were weighted by the quantities $\frac{1}{\sigma_{N(i)}^2} = \frac{1}{N(i)}$.

Because the 'prompt' peak is more "intense" than the delayed part of the curve, 'prompt' counts contribute appreciably to the delayed channels, particularly the first few. To overcome the effect of this the curve was fitted only for those channels corresponding to delays > 3 μsec. (e.g. in Fig. 5.5 the fit was done on channels 60 - 80).

The number of chance counts was calculated from

$N_C = N_S' R_B dt_{AV}$ where $N_S' = N_A - N_p - N_{AB}$

with $\begin{cases} N_p = \text{number of 'prompt' coincidences} \\ N_{AB} = \text{background counts in counter A.} \end{cases}$

The term $- N_p$ in the calculation of N_S' arises because the relevant number of sweeps in calculation of the chance rate for the 'delayed' part of the curve is the number which actually sweep asfar as the channels in question. Of the total number N_S ($\simeq N_A$ since $\frac{1}{R_A} >> t_S$ and dead time effects can therefore be neglected), N_p are stopped before reaching the 'delayed' channels - hence

$N_S' = N_A - N_p$. Because the chance counts $<<$ true counts this correction is not very important.

FIG 5.5

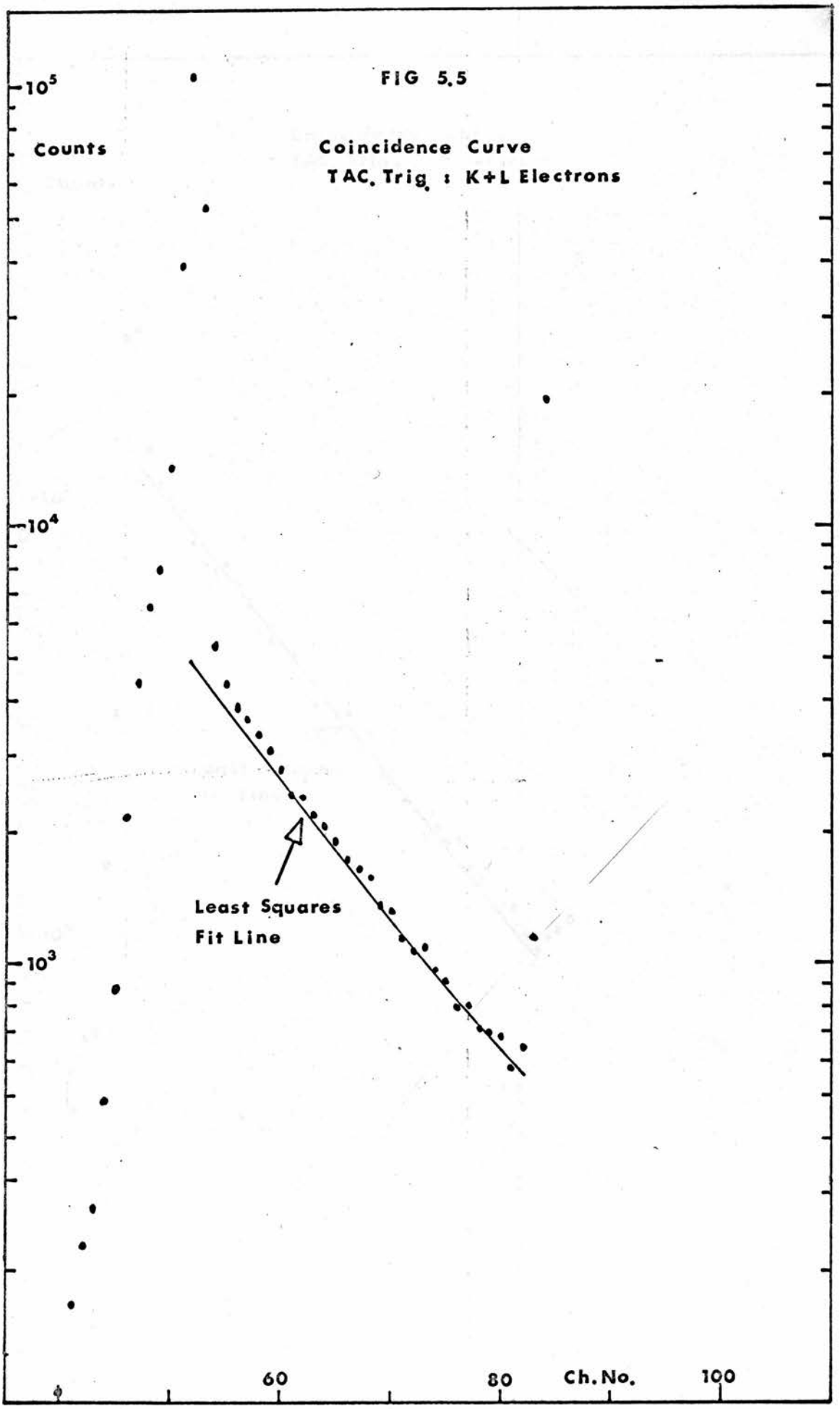
Counts
Coincidence Curve
TAC. Trig : K+L Electrons
10^5
10^4
10^3
Least Squares
Fit Line
60
80
Ch. No.
100

As well as the half-life the numbers of prompt N_p and delayed N_D coincidences are also of interest. The number of delayed counts in the region under the prompt peak was calculated by extrapolation of the fitted line, and thus number was subtracted from the number of counts under the prompt peak in the calculation of N_p.

L Conversion Electron - K X Ray Coincidences. By setting the proportional counter analyser threshold in the trough between K and L + M electron peaks an attempt was made to observe coincidences between L + M conversion electrons and K X rays. As may be seen from a typical result (Fig. 5.6 and the lower curve of Fig. 5.2) the prompt part of the curve is considerably reduced. It is not completely removed because of a contribution to the trigger pulses from the high energy tail of the K electron peak (which overlaps with the L + M peak slightly). The reduction in the prompt peak, however, allowed the curve to be fitted over a wider time range than in the previous case - only the first 3 channels being omitted.

K X Ray - K X Ray Coincidences. When the 53.3 keV and 13.5 keV transitions are both converted in the K shell it is possible that both result in the emission of a K X ray. Since there are no prompt pairs of K X rays the time correlation curve between K X ray pulse pairs should yield only a 'delayed' part.

By covering the source with an aluminium cap thick enough (7 mgm/cm.^{2}) to stop the conversion electrons, proportional

counter spectra like Fig. 5.7 were obtained, showing only the 9.9 keV K X ray peak (and its escape peak). The trigger pulses were provided by setting the proportional counter analyser threshold just above the escape peak and the type 'B' pulses were supplied by the scintillation counter set, as before, to detect K X rays.

The coincidence curve obtained is shown in Fig. 5.8. Absence of a 'prompt' peak has already been explained, and the symmetrical shape of the curve about the time 'zero' is due to the roles of the two counters being interchanged, giving delayed coincidence counts in the 'negative' time region.

53.3 keV Gamma - K X Ray Coincidences. With the scintillation counter set to detect 53.3 keV γ rays and the proportional counter detecting K X rays in the way described above, curves of the type shown in Fig. 5.9 were obtained. The roles of the two counters were interchanged in this experiment - i.e. the scintillator (53.3 keV γ rays) provided the trigger pulses and the proportional counter (K X rays) the "stop" pulses.

Ideally there should again be no prompt coincidences. The small prompt peak is probably due to scattering, since a 53.3 keV γ ray may deposit enough energy in the scintillator to be recorded in the 53.3 keV peak and then be detected in the proportional counter as a 9.9 keV X ray. The curve fitting was again done on the channels above the prompt peak.

5.2 Results

Six sets of readings were taken for each of the above

FIG 5.7 K X Rays in the Proportional Counter

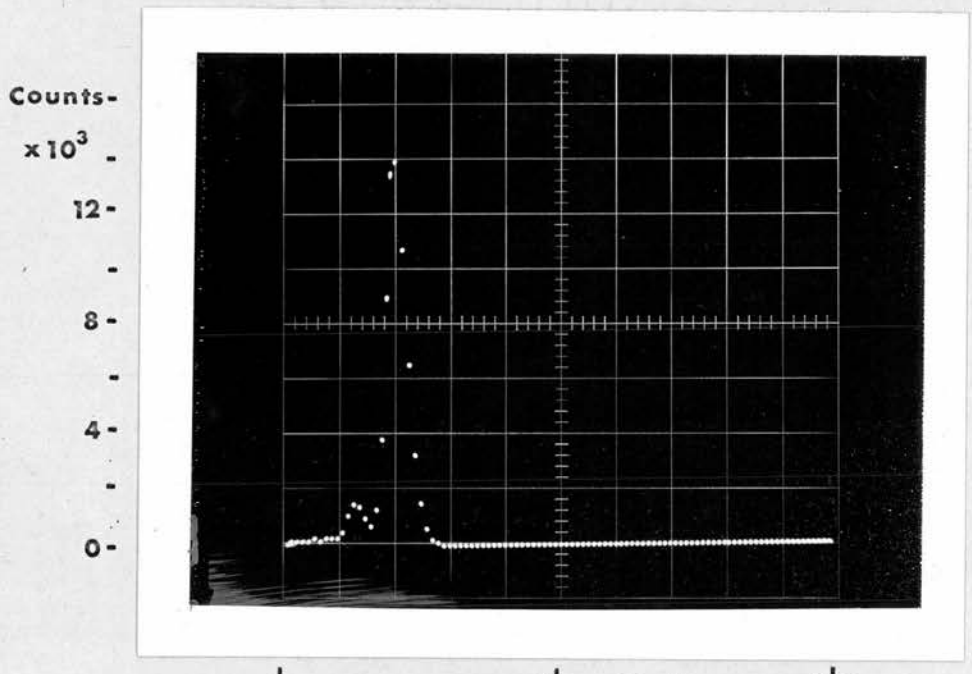

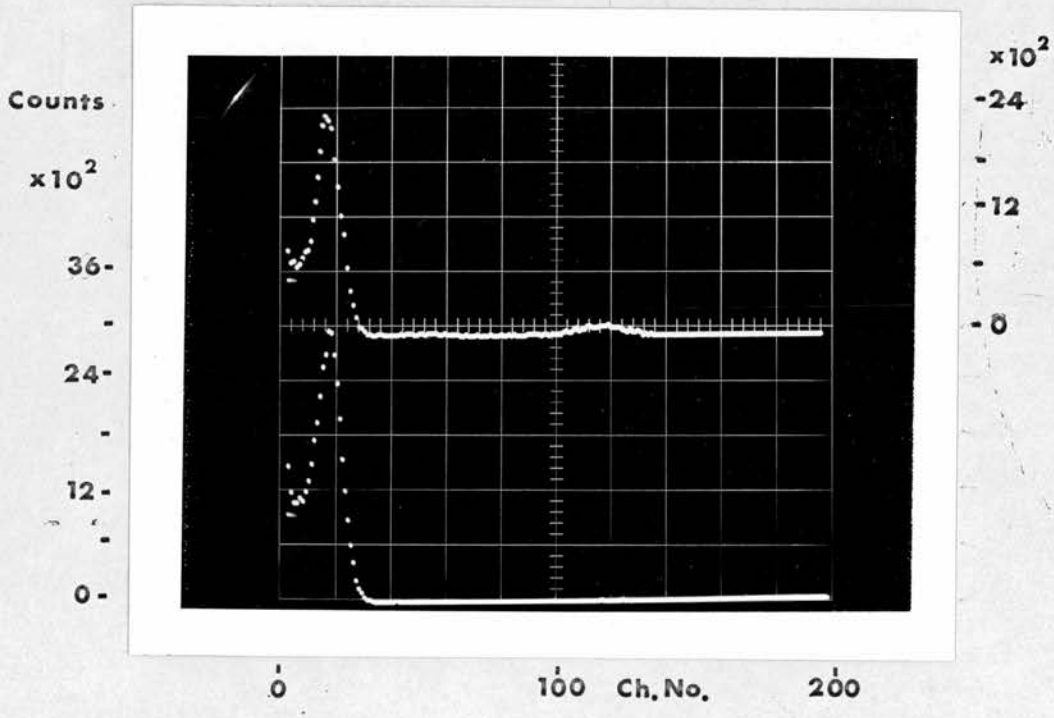

FIG 5.12 Gated NaI As^{73} Spectra

FIG 5.8

Coincidence Curve

TAC. Trig. : K X Rays

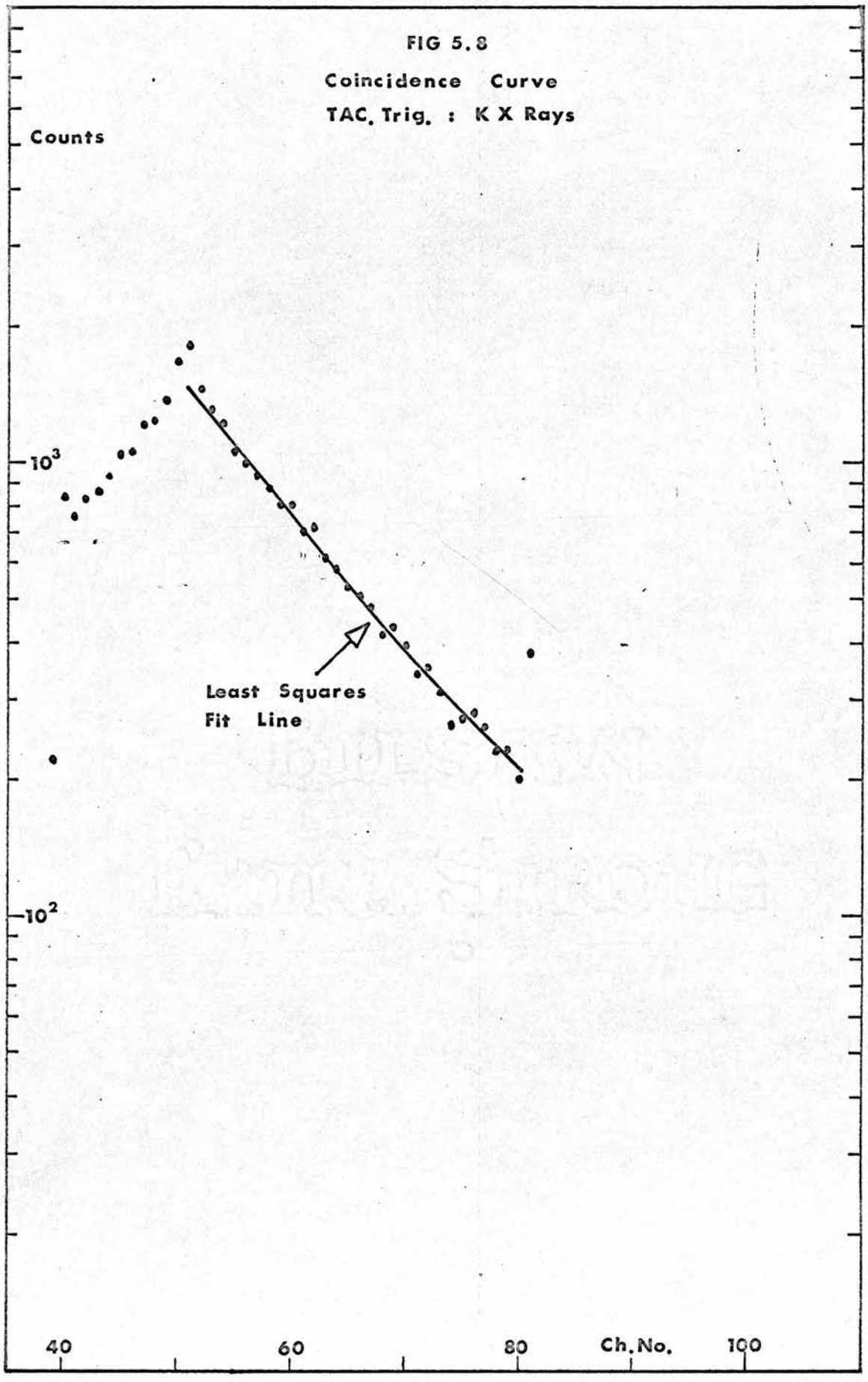

FIG 5.9

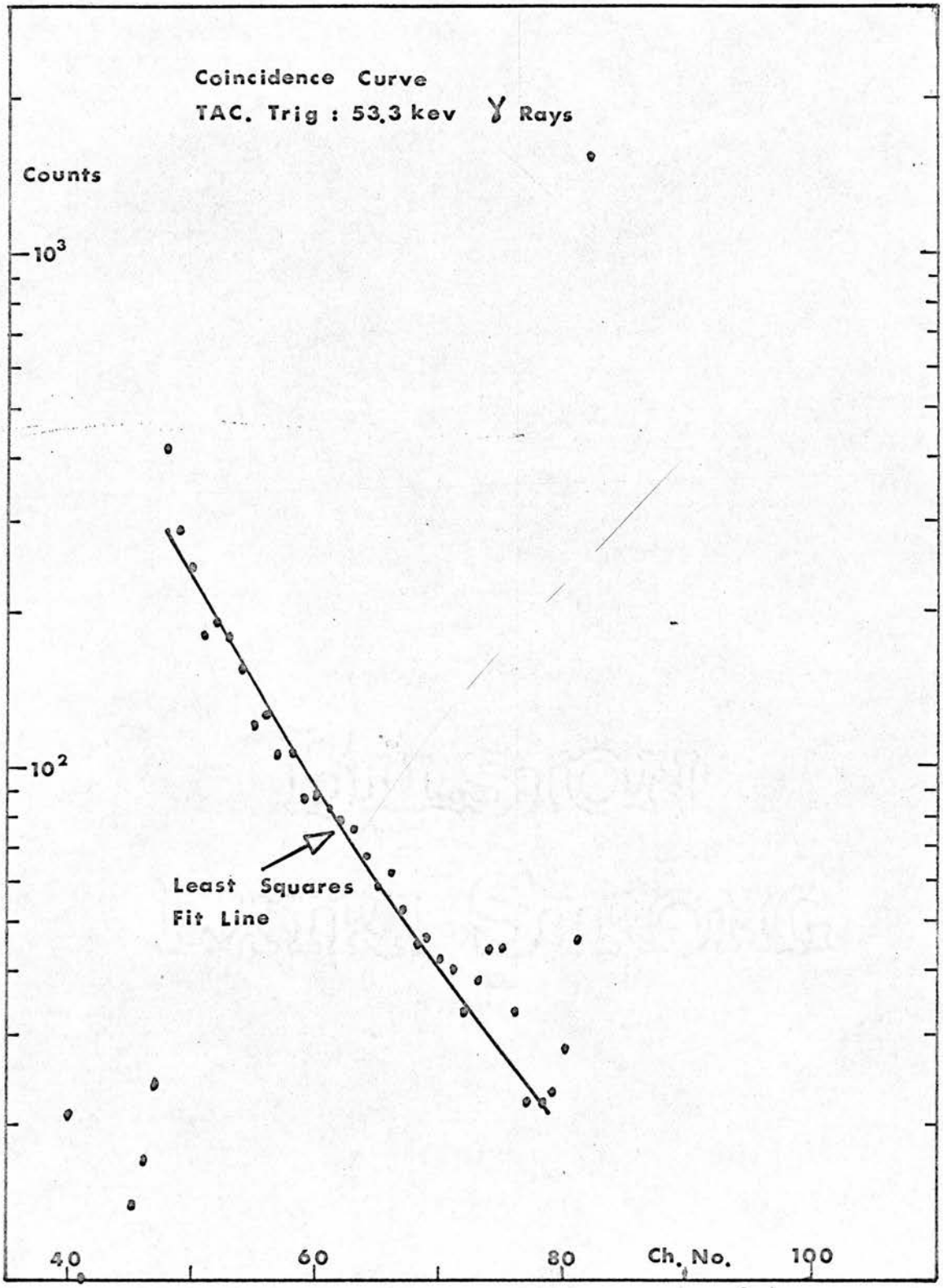
Coincidence Curve
TAC. Trig : 53.3 kev γ Rays
Counts
10³
10²
Least Squares
Fit Line
40
60
80
Ch. No.
100

arrangements and the (weighted) mean value of half-life for each is listed in Table 5.1. The errors quoted are the standard deviations of the (weighted) mean values combined with the error arising from the time calibration. The slight decrease in the $T_{1/2}$ value down the table is probably due to the increase in dt_{AV} value mentioned above (the results being taken in roughly the order stated) but could also be due to systematic differences in the time 'jitter' in the proportional counter. A large 'jitter' would enhance the 'long delay' channels, thus leading to a larger $T_{1/2}$ value. It is noticeable that where detection of conversion electrons is involved the $T_{1/2}$ value is slightly longer than in the K X ray cases.

Again, the K + L conversion electron case uses only those channels above the prompt peak, so that there could be a small systematic error in assuming the delay time and channel width is as given by the average of the calibrations which apply to all the channels above the first ten.

A weighted mean of all the observations gave

$$T_{1/2} = 2.94 \pm 0.03 \ \mu\text{sec.}$$

This is slightly lower than the value 3.04 ± 0.07 μsecs. quoted by F. Shaikh[23].

5.3. Prompt and Delayed Coincidences

In the notation of previous chapters, the number of prompt coincidences (i.e. the number of detected K X rays associated with a detected K conversion electron) is given by

$$N_p = N_{SK}\,\beta_K\,\varepsilon_X\,\omega_X = N_S''\left(\frac{1}{1+\left(\frac{L+M}{K}\right)_{53.3\ keV}}\right)\beta_K\,\varepsilon_X\,\omega_X \qquad (5.3.1)$$

where N_{SK} = number of sweeps due to the detection of a K electron.

N_S'' = " " " " " " any conversion electron.

$= N_A - N_{AB}$.

The fluorescence yield for K X rays is therefore given by

$$\beta_K = \left(N_p/N_S''\right)\left(1 + \left(\frac{L+M}{K}\right)_{53.3\ keV}\right)/\varepsilon_X\,\omega_X \quad .$$

The mean value of the quantity (N_p/N_S'') taken from the coincidence curves is listed in Table 5.1 and calculation from the source - detector geometry (with the absorption corrections allowed for as in Chapter 2) gave

$$\varepsilon_X\,\omega_X = 0.24 \pm .01 \quad .$$

Use of the result $(K/L+M)_{53.3\ keV} = 6.2 \pm .02$ quoted by Grigor'ev et al.[18] then gives

$$\beta_K = 0.46 \pm .02$$

where allowance has been made for absorption in air and melinex ($\sim 1\%$).

The fluorescence yield for Ge has not previously been measured experimentally, but this value is appreciably lower than the theoretical value quoted by Fink et al.[55] ($\beta = 0.51$ for $Z = 32$). Measurements of β_K for neighbouring elements Ga and As agree fairly well with theory and it is difficult to explain the low value in the present case, but it may be due

to overestimation of ε_X (= 1).

The number of delayed coincidence counts N_D is given by

$N_D = N_S' p_1'' \varepsilon_X \omega_X$ where $N_S' = N_A - N_p - N_{AB}$ as before.

$\therefore \quad N_D/N_S' = p_1'' \varepsilon_X \omega_X$ (5.3.2) and dividing this into equation (5.3.1),

$$\left[N_p/N_S''\right] / \left[N_D/N_S'\right] = \frac{\beta_K}{\left(1 + \left(\frac{L+M}{K}\right)_{53.3 \text{ keV}}\right) p_1''} = \frac{1 + \left(\frac{L+M}{K}\right)_{13.5 \text{ keV}}}{1 + \left(\frac{L+M}{K}\right)_{53.3 \text{ keV}}}$$

since $p_1'' = \beta_K \left(\frac{\alpha_{13}}{1 + \alpha_{13}}\right) / \left(1 + \left(\frac{L+M}{K}\right)_{13.5 \text{ keV}}\right)$

where the total internal conversion coefficient for the 13.5 keV transition $\alpha_{13} >> 1$.

Hence

$$\left(\frac{L+M}{K}\right)_{13.5 \text{ keV}} = \left(1 + \left(\frac{L+M}{K}\right)_{53.3 \text{ keV}}\right) \left[N_p/N_S''\right] / \left[N_p/N_S'\right] - 1 .$$

Taking the mean observed value of $\left[N_p/N_S''\right] / \left[N_D/N_S'\right] = 2.98 \pm .03$ and again using $\left(\frac{K}{L+M}\right)_{53.3 \text{ keV}} = 6.2 \pm .02$ gave the result $\left(\frac{L+M}{K}\right)_{13.5 \text{ keV}} = 2.46 \pm .04$.

This may be expressed as $\left(\frac{K}{L+M}\right)_{13.5 \text{ keV}} = 0.406 \pm .007$ or, (taking the result obtained by Johansson $\left(\frac{L}{M+M}\right)_{13.5 \text{ keV}} = 5.4 \pm .5$)

$$\left(K/L\right)_{13.5 \text{ keV}} = 0.47 \pm .01 .$$

Since the solid angle, efficiency, and fluorescence yield factors all cancel this result involves errors only in the decision between prompt and delayed coincidences which should be small. This view is strengthened by the fact that the average value of $N_D/N_S' = 0.0311 \pm .0004$ obtained from the (K + L) - K X curve agrees well with the value $0.0302 \pm .0005$ obtained from

the L - K X curve. The $(^{K}/_{L})$ value obtained agrees well with previous experimental results but is slightly larger than all the theoretical estimates of K/L ratio for an E2 transition of energy 13.5 keV. This may be due to the K conversion being near to the threshold.

Another result of interest is the number of delayed coincidences in the K X - K X case:

$$N_D^{KX} = \frac{p_1'}{p_1 + p_1' + p_1''} \times p_1'' \varepsilon_X \omega_X N_S^{KX} \qquad (5.3.3)$$

where $N_S^{KX} = N_A - N_{AB}$ for this case.

Division of equation (5.3.3) by equation (5.3.2) gives

$$r = \left[N_D^{KX}/N_S^{KX}\right] / \left[N_D/N_S'\right] = \frac{p_1'}{p_1 + p_1' + p_1''}$$

$$= \frac{K_{cap.\ frac.}}{K_{cap.frac.} + \frac{p_1'}{\beta_K} + \frac{p_1''}{\beta_K}}$$

where $K_{cap.\ frac.}$ is the ratio of K captures to total captures.

Now $p_1'/\beta_K = \frac{1}{1 + (\frac{L+M}{K})_{53.3}} (\frac{\alpha}{1+\alpha}) = 0.77 \pm 0.02$

with $(\frac{K}{L+M})_{53.3} = 6.2 \pm .2$ and $\alpha = 8 \pm 2$ (see later).

(Although the error in α is fairly large ($\sim 20\%$) the error in p_1'/β_K is much smaller because α only appears in the term $\frac{\alpha}{1+\alpha}$ which varies only slowly with α).

Also

$$\frac{p_1''}{\beta_K} = \frac{1}{1 + (\frac{L+M}{K})_{13.5\ keV}} \quad \text{assuming } \alpha_{13} \gg 1$$

$= 0.289 \pm .003$ using the value of $\left(\frac{L+M}{K}\right)_{13.5\ keV}$ derived above.

Hence $K_{cap.frac.} = \dfrac{(p_1' + p_1'')/\beta_K}{\frac{1}{r} - 1} = 0.82 \pm .03$

using the observed values $\dfrac{N_D^{KX}}{N_S^{KX}} = 0.0135 \pm .0002$

and $\dfrac{N_D}{N_S'} = 0.0311 \pm .0004$.

The theoretical L capture fraction is given as 0.11[5] (see Chapter I) and using the approximate result that capture fraction is proportional to $1/n^3$ (see Chapter 1) $M_{cap.\ frac.} = 0.032$ and $N_{cap.\ frac.} = .008$.

Hence the theoretical value of $K_{cap.\ frac.} \simeq 0.85$ $(= 1 - (L + M + N)_{cap.\ frac.})$, and agreement with experiment is reasonable.

The above results are summarised in Table 5.2.

5.4 Conversion Coefficient of the 53.3 keV Transition by Direct Measurement

An attempt has been made to measure the ratio α = conversion electrons/γ rays for the 53.3 keV transition directly, by counting conversion electrons in the proportional counter and γ rays in the scintillation counter. To calculate α it is necessary to estimate the solid angles and efficiencies of both detectors (i.e. $\varepsilon_e\ \omega_e$ and $\varepsilon_\gamma\ \omega_\gamma$). $\omega_\gamma = 0.25 \pm 0.01$ was calculated from the geometry - the small absorption correction (see Chapter 2) being neglected, and it was assumed that $\varepsilon_\gamma = 1$.

The overall efficiency of conversion electron detection is

TABLE 5.1 Results of 13.5 keV Level Half-Life Measurements

Trigger Pulses	Stop Pulses	Mean $T_{1/2}$ (μ sec.)	Prompt N''_S ($\times 10^{-3}$)	Delayed N'_S ($\times 10^{-3}$)
K+L Electrons	K X rays	$2.98 \pm .025$	$92.6 \pm .6$	$31.1 \pm .4$
L Electrons	"	$2.92 \pm .03$	-	$30.2 \pm .5$
K X Rays	"	$2.89 \pm .02$	-	$13.5 \pm .2$
53.3 keV γ Rays	"	$2.79 \pm .04$	-	-
Weighted mean :		$\overline{T_{1/2}} = 2.94 \pm .03$ μsec.		

TABLE 5.2 Results Derived from Delayed Coincidence Experiments Etc.

	Present Experiment	Theory	Previous Experiment
K-Fluorescence Yield β_K	$0.46 \pm .02$	0.51	-
K Capture Fraction $K_{cap.frac.}$	$0.82 \pm .03$	0.85	-
K to L+M Conversion $(\frac{K}{L+M})_{13.5}$	$0.406 \pm .007$	-	0.37 ± 0.06 [23]
Electron Ratio for the 13.5 keV transition			0.63 ± 0.22 [19]
Hence K to L Ratio $(K/L)_{13.5}$	$0.47 \pm .01$	0.38(E2) [8]	$0.44 \pm .08$ [23]

more difficult to estimate because of the effects of finite source thickness and backing foil. The first of these tends to reduce the energy of electrons emitted from atoms near the back of the source giving rise to a low energy 'tail' on the conversion electron peak. If such electrons lose enough energy, they give pulses below the analyser threshold (which must be set above the K X ray peak) and are lost, i.e. efficiency is effectively reduced. On the other hand, electrons back scattered from the backing foil without appreciable energy loss effectively increase the overall detection efficiency (i.e. the backing acts like a 'reflector'). If scattering is inelastic these electrons may contribute, instead, to the low energy tail mentioned above.

A typical proportional counter spectrum is shown in Fig. 5.4. It is only possible to extrapolate the low energy tail very roughly, probable limits being indicated by the curves '1' and '3' in Fig. 5.4. These extremes lead to an error in α of $\pm$ 20%.

The effective solid angle was found by measuring the count rate as a function of geometrical solid angle. The different solid angles were achieved by covering the source with various aluminium caps provided with windows of different diameters. The aluminium was thick enough (7 mgm/cm.^{2}) to stop the conversion electrons. The results are shown in Fig. 5.11 and imply a correction to the value calculated geometrically of $\sim$ - 10% giving an effective solid angle $\omega_e = 0.34 \pm 0.015$.

Using the mean of the observed ratios of conversion electrons/γ rays yielded the result $\alpha = 8 \pm 2$. This agrees with the previous direct measurement[21], but not with the values

FIG 5.10

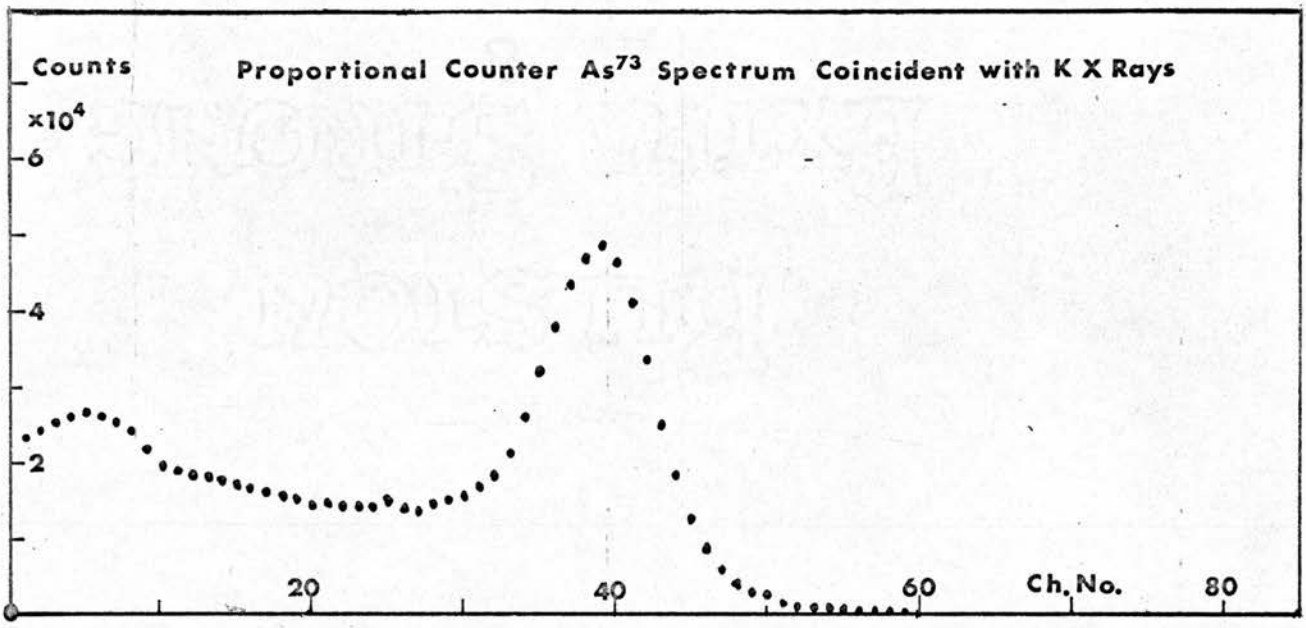

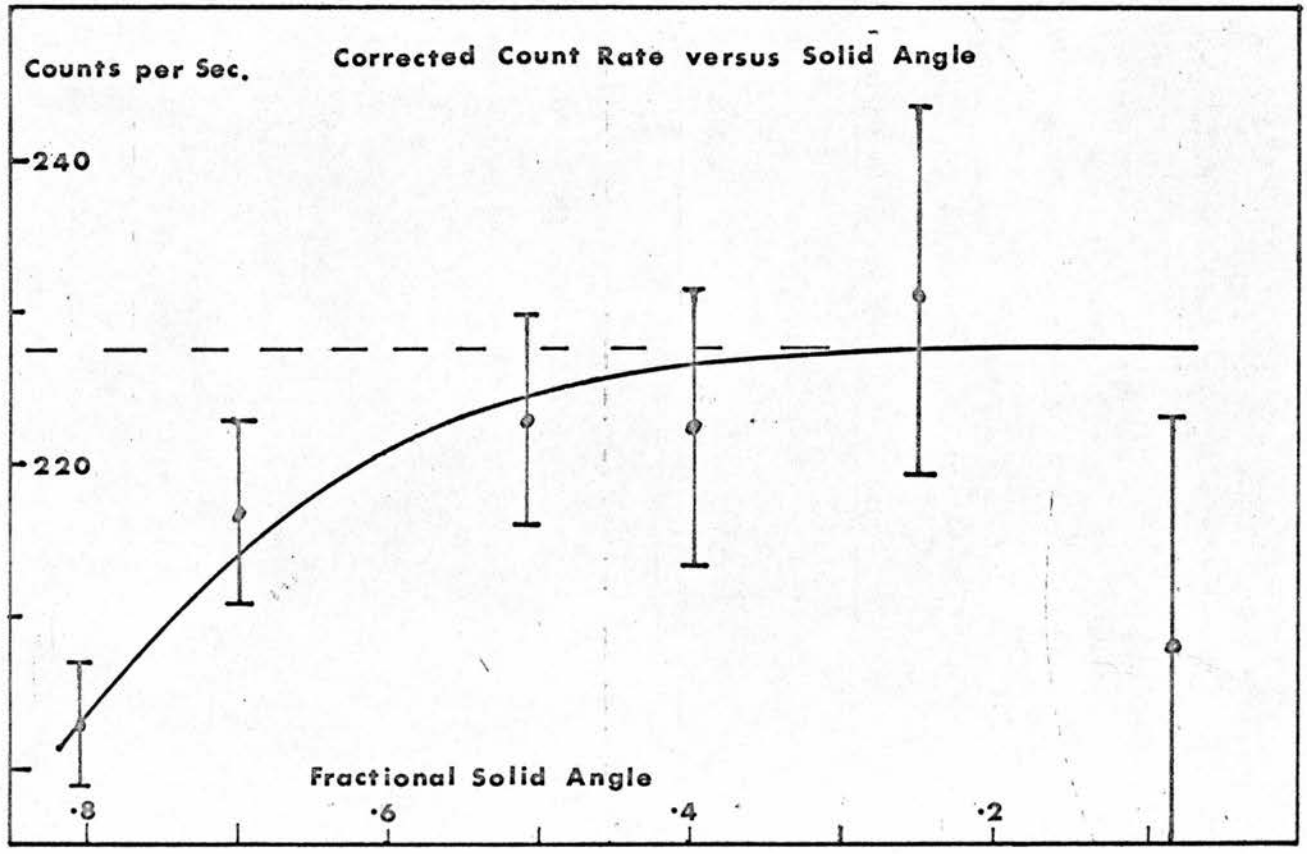

FIG 5.11

given by Welker et al.[19] and Shaikh[23]. However, both of these authors use the value of the ratio $^{X}/_{\gamma}$ in the calculation of α and both use the value $^{X}/_{\gamma} = 6.2$ (due to Welker) which, as shown in Chapter 2, is probably too low by a factor of ~ 1.4. In fact using the value of K electron/X rays = $0.77 \pm .15$ given in reference (23) and the value $^{X}/_{\gamma} = 8.95$ obtained in Chapter 2 leads to the result

$$\alpha = 8 \pm 2$$ - in good agreement with the present value.

For comparison with theory it is convenient to calculate the K conversion coefficient $\alpha_K = \alpha/(1 + (\frac{L+M}{K})_{53.3\ keV}) \simeq 7 \pm 2$ using $(\frac{K}{L+M})_{53.3\ keV} = 6.2$.[18]

This result agrees with the theoretical values quoted for an M2 transition within experimental error (see Table 1.3).

An attempt was made to discover the correct shape of the low energy tail of the conversion electron spectrum by using a linear gate type NE 5730. This unit acts as an amplifier of unit gain when switched 'on' by a gating pulse. In this case the gate was 'opened' for 1 μsec. by K X rays detected in the scintillator. The resulting spectrum, shown in Fig. 5.10, apparently indicates that the low energy 'tail' extends uniformly to very low energy and the extrapolation above underestimates the conversion electron intensity.

This, however, may be a little misleading as the spectra of Fig. 5.12 illustrate. Both are gated spectra taken from the scintillator, the upper one being switched 'on' by 10 kc/s generator pulses, and the lower one by conversion electrons

detected in the proportional counter. The second spectrum confirms that K X rays are coincident with some (K) conversion electrons while the 53.3 keV γ rays are not. A low energy 'tail' is, however, apparent in both cases - probably due to the gate unit.

Some caution is therefore necessary in the interpretation of Fig. 5.10 but it seems that the α value is more likely to be above 8 than below it.

5.5. Calculation of α from the Observed $^{X}/_{\gamma}$ Ratio

It is now possible to re-calculate the values of p_1 and p_1'' using the results listed in Table 5.2. p_1' may also be estimated if, in addition, the result due to Grigor'ev $(\frac{K}{L+M})_{53.3\ keV}$[18] = $6.2 \pm .2$ and the value $\alpha = 8 \pm 2$ taken from the last section are used. Only a rough value of α is required in the calculation since it appears only in the term $(\frac{\alpha}{1+\alpha})$. The revised p values appear in Table 5.3.

Now, the ratio $^{X}/_{\gamma}$ measured experimentally in Chapter 2 is given by $^{X}/_{\gamma} = \frac{p_1 + p_1' + p_1''}{p_2} = p_x/p_2$ where $p_2 = \frac{1}{1+\alpha}$.

Hence $\alpha = (^{X}/_{\gamma})/p_X = 1.$

Using the result of Chapter 2 $^{X}/_{\gamma} = 8.95 \pm .2$ then gives

$$\alpha = 9.5 \pm 0.6.$$

(A slightly more involved calculation inserting p_1' in terms of α gives the same result). Again using $(\frac{K}{L+M})_{53.3\ keV} = 6.2 \pm .2$[18] the K conversion coefficient α_K may be found. The result $\underline{\alpha_K = 8.2 \pm 0.5}$ is in excellent agreement with the most recent[8] theoretical estimate of α_K for an M2 transition ($\alpha_K = 8.2$) and is

significantly higher than the estimate for an E2 transition ($\alpha_K = 6.5$).

At first sight, it might be thought that a systematic error (see Section 5.3) in β_K could lead to a corresponding error in α (since the p's all involve β_K).

However, it is possible to write $({}^{X}/_{\gamma})/p_X = ({}^{X}/_{\gamma})_{obs} \cdot \left(\frac{\varepsilon_\gamma \omega_\gamma}{\varepsilon_X \omega_X}\right) / \frac{p_X}{\beta_K} \cdot \beta_K$

$$= \frac{({}^{X}/_{\gamma})_{obs}\ \varepsilon_\gamma\ \omega_\gamma}{\frac{p_X}{\beta_K} \cdot (\beta_K \varepsilon_X \omega_X)}$$

where, now, $\frac{p_X}{\beta_K}$ is independent of β_K and $\beta_K\ \varepsilon_X\ \omega_X$ is the quantity measured directly in the experiment for β_K, and is therefore independent of systematic error involved in assuming $\varepsilon_X = 1$.

5.6. Conclusions

The results derived in this and previous chapters have removed the apparent anomalies (see Chapter 1) in the ${}^{X}/_{\gamma}$ ratio and in the in the 53.3 keV conversion coefficient. Values for these and other quantities observed in the present work all tend to increase confidence in the accepted As^{73} decay scheme of Fig. 1.3.

The values of half-lives measured in the present work confirm the fact that the 13.5 keV and 53.3 keV transitions are enhanced and retarded, respectively, when compared to the single particle model. Possible reasons for this will be considered in the next chapter.

CHAPTER 6

THE LEVELS OF Ge^{73}

As pointed out at the end of the last chapter, all the available evidence tends to confirm the spin and parity assignments of the levels excited in As^{73} decay (Fig. 1.5). The enhancement and retardation of the 13.5 keV and 53.3 keV transitions are therefore almost certainly due to the nature of the 13.5 keV and 67.8 keV levels.

There are several ways in which excited nuclear states can arise. The simplest is described in the approximation of independent particle motion by the elevation of a single particle from one state to another. Levels of this type will be called "single particle" levels.

A slightly more complex excitation is where the ground state configuration remains unchanged but the nucleons change the relative orientation of their orbits. For example, the ground state and first excited state of $_{23}V^{51}_{28}$ are thought to be due to three protons in the $1f_{7/2}$ shell coupled differently to give spins $7/2^-$ and $5/2^-$ respectively. Levels which may be described in this way will be called "co-operative" levels.

Collective motion of many nucleons is well known, giving rise to excitations of the rotational or vibrational type in even-even nuclei. It has been suggested that a neighbouring odd A nucleus can be considered as an even-even 'core' plus a single odd particle, and that some excited levels should arise from excitation of the 'core' with the single particle remaining in its ground state.

Such levels will be degenerate since the angular momenta of core (j_c) and particle (j_p) can couple in several different ways to give a resultant in the range $-|j_c - j_p|$ to $(j_c + j_p)$. A weak particle - core interaction will remove the degeneracy so that a series of levels with spin values $J = -|j_c - j_p|, -|j_c - j_p| + 1. \ldots (j_c + j_p)$ should result - centred roughly about the corresponding excited level in the adjacent even-even nucleus. This idea first put forward by Lawson and Uretsky[56] has been applied to several nuclei by de Shalit[57]. A simple example is Tl^{203} the first few levels of which are shown in Fig. 6.1. In the average field of Hg^{202} the lowest allowed proton orbit is probably an $S_{1/2}$, giving the $\frac{1}{2}+$ ground state. The usual interpretation of the excited states is that the single proton is promoted to the $d_{3/2}$ and $d_{5/2}$ states. However $_{80}Hg^{202}_{122}$ has an excited (2+) level at 440 keV, which is very near to the "centre of gravity" of the excited levels of $_{81}Tl^{203}_{122}$. The alternative "core excited" interpretation of the levels is that the proton remains in the $S_{1/2}$ state and couples with the core excited to the 2+ level. By way of illustration of these 'core excited' levels the example of Au^{197} explained in this way by de Shalit is discussed in Section 6.2. Possible application in the Ge^{73} case is considered in Section 6.3.

First of all, however, the description of Ge^{73} levels as "co-operative" in the sense defined above, will be considered in the next section.

6.1. "Co-operative" Description of $_{32}Ge^{73}_{41}$ Levels

The forty-first neutron should be the first neutron in the

Levels of Hg^{202} and Tl^{203}

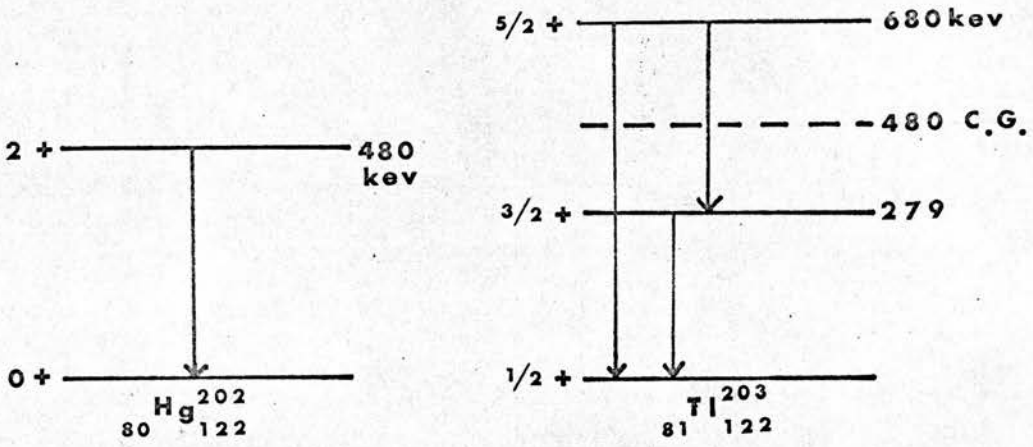

FIG 6.1

$g_{9/2}$ shell according to the single particle shell model. The ground state (9/2+) is therefore readily explained. Also a low lying excited level with spin ½- can be expected from the elevation of a neutron from the $p_{1/2}$ orbit (which lies just below the $g_{9/2}$ level) to pair with the one in the $g_{9/2}$ shell and leaving a 'hole' in the $p_{1/2}$ shell. There are, however, no low lying single particle states that could account for the 5/2+ level. Also the similarity in excitation energy of the ½- (66.8 keV) level and the 7/2+ (67.03 keV) level makes it unlikely that the latter is due to the single particle excited to the $g_{7/2}$ state.

A further difficulty is that single particle levels cannot account for the retardation and enhancements of the transitions.

Shaikh[23] (1968) has suggested that the ground state and the first excited state of Ge^{73} may be co-operative. He has assumed that because of a larger 'pairing' energy (due to the high value of ℓ) the $g_{9/2}$ level starts filling before the $p_{1/2}$ level, so that, in the present case there are three neutrons in the $g_{9/2}$ orbit, and the levels 9/2+ and 5/2+ are due to different couplings of the angular momenta, i.e. $(g_{9/2})^3_{9/2}$ and $(g_{9/2})^3_{5/2}$. On this assumption the enhancement of the 13.5 keV (E2) transition is explained since it arises merely from a re-coupling of three neutrons in the same $g_{9/2}$ shell, therefore showing collective properties.

The 66.8 keV level is still taken to be due to one of the three neutrons having transferred to the $p_{1/2}$ shell, leaving the other two paired to zero spin, i.e. $(g_{9/2})^2_0$ $p_{1/2}$. Thus the M2 transition at 53.3 keV should be retarded, because although the spin change is two the orbital angular momentum change

($p_{\frac{1}{2}} \rightarrow g_{9/2}$) is three. Therefore the M2 is an ℓ forbidden transition.

A 'co-operative' level with spin 7/2+ (with configuration $(g_{9/2})^3_{7/2}$) is predicted by this description and may be that at 67.03 keV excitation but it should decay to the ground state and 5/2+ level by enhanced M1 transitions (again because of re-coupling the spins of three neutrons in the same $g_{9/2}$ shell). However, the transition to the ground state is a retarded M1 and the 53.5 keV transition to the 5/2+ level has not been observed.

To go further it is necessary to consider the possible nucleon configurations in the various levels. The available single particle levels for neutrons or protons outside the closed shell at 28 are $p_{3/2}$, $f_{5/2}$, $p_{\frac{1}{2}}$ and $g_{9/2}$. Since the $_{33}As^{73}_{40}$ ground state spin is 3/2-, it is likely that there are either one or three protons in the $p_{3/2}$ shell with the remainder in the $f_{5/2}$ shell. The As^{73} ground state may therefore be

$$\underset{\text{(protons)}}{(f_{5/2})^2 \; p_{3/2}^3} \quad ; \quad \underset{\text{(neutrons)}}{(p_{3/2})^4 \; (f_{5/2})^6} \; (g_{9/2})^2$$

where it is assumed that, owing to the large 'pairing' energy the last two neutrons go into the $g_{9/2}$ shell.

The ground state configuration for Ge^{73} is probably

$$(f_{5/2})^2 \; (p_{3/2})^2 \quad ; \quad (p_{3/2})^4 \; (f_{5/2})^6 \; g_{9/2}^3$$

with the excited levels 5/2+ and 7/2+ due to re-coupling of the three neutrons in the $g_{9/2}$ shell.

The excited state at 67.8 keV ($\frac{1}{2}$-), as explained above, is

$$(f_{5/2})^2 \; (p_{3/2})^2 \quad ; \quad (p_{3/2})^4 \; (f_{5/2})^6 \; (g_{9/2})^2 \; p_{\frac{1}{2}} \; .$$

The K capture decay of As^{73} to the $\frac{1}{2}$- Ge^{73} level is now pictured as the decay of a proton in the $p_{3/2}$ shell which becomes a a neutron in a $p_{3/2}$ shell. The odd neutron is left in a p shell as required but must re-orientate to reach the $p_{\frac{1}{2}}$ orbit required by the As^{73} ($\frac{1}{2}$-) level.

Decay to the 5/2+ level would require the odd proton to change from a p shell to a g shell (i.e. an ℓ change of three), which explains the lack of a (first forbidden) feed to this level.

The Ga^{73} ground state configuration seems likely to be

$$(f_{5/2})^2 \ (p_{3/2})^1 \ ; \ (p_{3/2})^4 \ (f_{5/2})^6 \ (g_{9/2})^2 \ ,$$

but if so it is difficult to explain the absence of a β^- decay feed to the ½- As^{73} level. This (allowed) transition should occur by decay of a $p_{3/2}$ neutron which then 'pairs up' with the $p_{3/2}$ proton already in the $p_{3/2}$ shell, and leaves an odd neutron in the p shell - similar to the As^{73} capture case.

It might be expected that because of re-orientation of the $p_{3/2}$ neutron is necessary (to give the $p_{1/2}$ state), an enormous retardation of both transitions would arise. On the other hand, this may be the reason for the absence of the Ga^{73} β^- decay, the presence of the As^{73} capture decay being explained by a different ground state configuration of As^{73}, for example

$$(f_{5/2})^2 \ (p_{3/2})^2 \ g_{9/2} \ ; \quad p_{1/2} \ (f_{5/2})^6 \ (p_{3/2})^2 \ (g_{9/2})^3$$

where the odd $g_{9/2}$ proton couples with the four neutrons in $p_{1/2}$ and $g_{9/2}$ shells to give a resultant spin 3/2.

The capture decay is now explained as the decay of the $g_{9/2}$ proton which then pairs off with the 3 neutrons already in the $g_{9/2}$ shell giving the ½- Ge^{73} level with configuration

$$(f_{5/2})^2 \ (p_{3/2})^2 \ ; \quad p_{1/2} \ (f_{5/2})^6 \ (p_{3/2})^2 \ (g_{9/2})^4 \ .$$

Apart from the transfer of two neutrons from $p_{3/2}$ to $g_{9/2}$ this is the same configuration as given above. The 5/2+ and 7/2+ levels in Ge^{73} would now have 5 neutrons in the $g_{9/2}$ shell

rather than 3 as suggested above. This makes no difference to any of the above arguments but it is necessary to explain the 7/2+ [58] ground state spin of the next member of the A = 73 chain, namely $_{34}Se^{73}_{39}$. Its ground state and first excited state (½-) configurations may then be

$$(f_{5/2})^2 \ (p_{3/2})^2 \ (g_{9/2})^2 \ ; \ (f_{5/2})^6 \ (p_{3/2})^2 \ (g_{9/2})^3 \ 7/2$$

and $(f_{5/2})^2 \ (p_{3/2})^2 \ (g_{9/2})^2 \ ; \ (f_{5/2})^6 \ (p_{3/2})^2 \ (g_{9/2})^2 \ p_{1/2}$

respectively. The observed decay of the ½- Se^{73} level to the As^{73} ground state[58] is now explained as the decay of a $g_{9/2}$ proton. (Fig. 6.3).

Nothing, as yet, has been said about the allowed β^- decay of Ga^{73} to the 363 keV level of Ge^{73}. It is explained by the decay of one of the $p_{3/2}$ neutrons which 'pairs up' with the $p_{3/2}$ proton. Two of the remaining protons couple to zero spin, the odd one being responsible for the 3/2- spin of this state. (Alternatively, the 3 couple to give spin ½- : $(p_{3/2})^3_{1/2}$). The 363 keV level cannot be a coupling of $g_{9/2}$ nucleons because of its odd parity.

The higher energy levels have not yet been assigned spins and parities and no attempt has yet been made to explain their origin.

6.2. 'Core Excitation' Applied to Au^{197}

While the example quoted above and several other nuclei may be interpreted in an equally satisfactory way by assuming that

Decay of Se^{73}, As^{73} and Ga^{73}

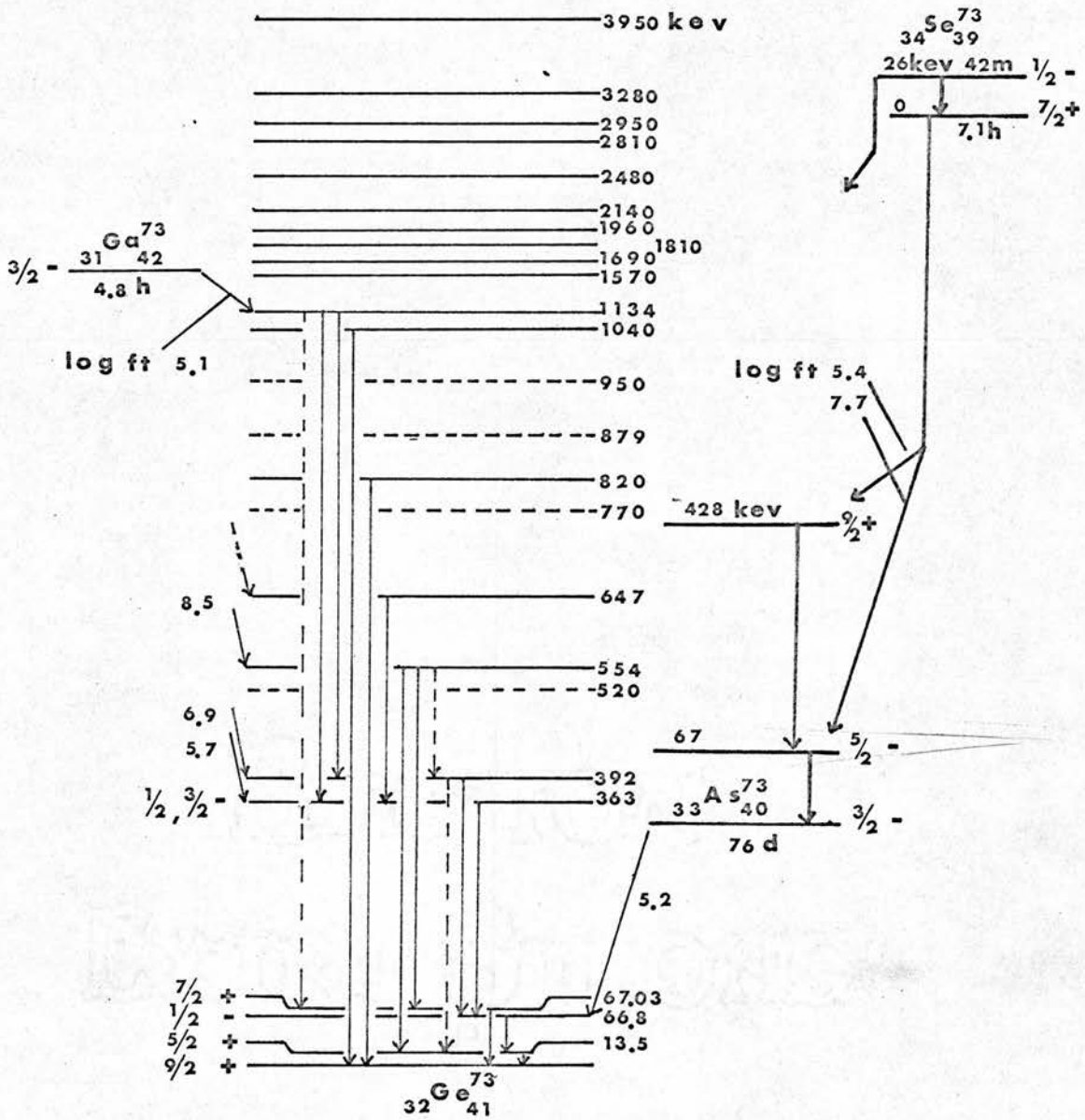

FIG 6.3

the excited states are either single particle or core excited, the situation is different for Au^{197}. The decay schemes of Pt^{197} and Hg^{197} are shown in Fig. 6.2. Also shown are some excited levels of $T\ell^{197}$. The odd proton in $_{79}Au^{197}$ probably moves in a $d_{3/2}$ orbit and that of $_{81}T\ell^{197}$ in an $s_{1/2}$ orbit. The 7/2+ and 3/2+ (excited) levels in Au^{197}, absent in $T\ell^{197}$, are difficult to interpret on the basis of single particle excitations. Also the magnetic moment of the 1/2+ level, 0.4 n.m., is very small compared to those of the 1/2+ ground states of $T\ell^{203}$ and $T\ell^{205}$ ($\mu \simeq 1.6$ n.m.).

'Core excitation' suggests a simple interpretation of these levels. The 79th proton is assumed to move in a $d_{3/2}$ orbit and the 81st in an $s_{1/2}$ orbit and the lowest excited states of positive parity are taken to result from the coupling of the odd proton to the 2+ core state. This gives the quadruplet 1/2+, 3/2+, 5/2+, 7/2+ for $_{79}Au^{197}$ and the doublet 3/2+, 5/2+ in the $_{81}T\ell^{197}$ case.

The model can be subjected to stringent quantitative tests since the reduced matrix elements for (E2) decay from the core excited levels to the ground state should all be the same and equal to that of the 2+ level in the 'core' nucleus. This is found to be true if allowance is made for 'impurity' of the states. For example, even a small admixture of a $d_{5/2}$ single particle state in the 5/2+ level affects the M1 transition to the ground state, and this level must therefore be described by

$$|5/2\rangle = A\,|2\ 3/2,\ 5/2\rangle + \sqrt{1 - A^2}\,|0\ 5/2,\ 5/2\rangle$$

where $|j_c\ j_p,\ j\rangle$ denotes the wave function for a core of spin j_c coupled to a single particle of spin j_p to give

Levels of Au^{197} and Tl^{197}

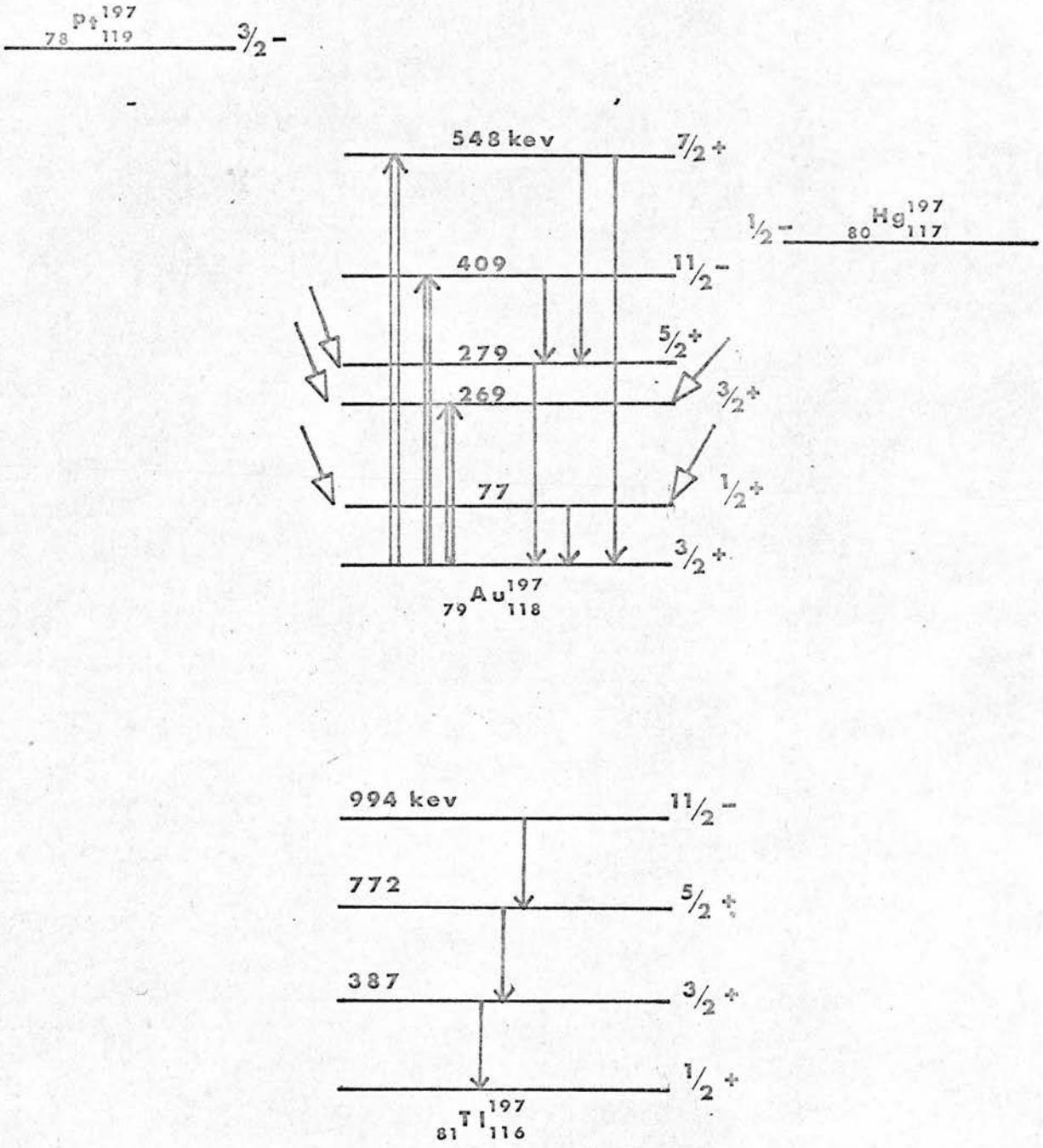

FIG 6.2

resultant total spin j.

An admixture of about 3°/o in this case and 4°/o in the case of the excited 3/2+ level is sufficient to explain the observed results.

The low magnetic moment of the ½+ level and at least part of the hindrance of the E3 transition ½- → 5/2+ are also explained by this model.

6.3. 'Core Excitation' in As^{73}

The possible 'cores' for As^{73} are Ge^{72} and Ge^{74} and both have 2+ levels at about 750 keV. With the 41st neutron in a $g_{9/2}$ single particle state 'core excitation' predicts a series of excited levels centred around ~ 750 keV with spins 5/2+, 7/2+, 9/2+, 11/2+, 13/2+.

The fact that such levels should be readily attained by Coulomb excitation from the 9/2+ ground state immediately suggests that the levels at 13.5, 67.03, 820 and 1040 keV might be of this type. This is strengthened by the assigned spins 5/2+, 7/2+ of the first two and the energy of the third, which should be close to the energy of the 2+ excited 'core' state (835 keV 2+ level in Ge^{72}).

The (E2) decay of the 13.5 keV level to the ground state now depends on properties of the core, and enhancement over the single particle estimate is to be expected. In fact the 2+ → 0+ transition in Ge^{72} is enhanced by a factor of ~23 which compares favourably with the enhancement (~ 18X) quoted in Chapter 1 for the 13.5 keV transition.

The retardation of the (M2) 53.3 keV transition is now explained by the assumption that it involves excitation of the 'core' and a single particle transition from an $S_{1/2}$ orbit to a $g_{9/2}$ orbit.

The retarded M1 67.03 keV transition 7/2+ $\longrightarrow$ 9/2+ is now explained since the magnetic dipole operator can now only act on the 'impurity' part of the state, i.e. the second term in

$$|7/2\rangle = A\,|2\ 9/2,\ 7/2\rangle + \sqrt{1 - A^2}\,|0,\ (g_{9/2})^3_{7/2},\ 7/2\rangle.$$

One apparent difficulty with this model is the lack of M1 transitions between successive members of the core excited multiplet. These might be expected to be enhanced as they involve only a re-coupling of 'core' and 'particle'. In fact the reduced matrix element involves the quantity $(g_c - g_p)^2$ (see ref. (57)), where g_c and g_p are the g factors of the core and the $g_{9/2}$ neutron respectively, and the absence of M1 transitions would be explained if these g factors are nearly equal.

6.3. The Absent β Decay Feeds in Au^{197} and Ge^{73}

The absence of the 'allowed' β^- decay from the Ga^{73}(3/2-) ground state to the ½- Ge^{73} level has already been pointed out (Section 6.1). It is interesting that in Au^{197} the excited 3/2+ level is fed by both β^+ and β^- decay but the ground state (also 3/2+) is not fed by either. De Shalit makes no mention of this point in his paper[57] but it is tempting to assume that the difference between the two 3/2+ levels is that one is a single particle state and the other is a core excited state. It may be significant that all the levels fed by β^+ or β^-

decay from the Pt^{197} and Hg^{197} ground states are those levels thought to be core excited, which possibly implies that the Hg^{197} and Pt^{197} ground states are themselves 'core excited'. This could happen if the splitting due to core-particle interaction was larger than the excitation energy of the 2+ core level. The 117th and 119th neutrons probably go into a $p_{\frac{1}{2}}$ shell so that on this picture there should be a triad of low lying levels with spins $3/2^-$, $\frac{1}{2}^-$, $5/2^-$ (not necessarily in that order) in both cases. Decay of the 'odd particle' now leaves the daughter in a core excited state rather than the ground state. (Alternatively, it could be that the decay process is such that the core becomes excited - if one of the 'core' nucleons is the one responsible for the decay then substantial re-organisation of the 'core' is necessary.)

This description of the β decay processes implies that both possible 'cores' be considered. For example Au^{197} may be thought of equally well as a $_{78}Pt^{196}_{118}$ core plus proton, or as a $_{80}Hg^{198}_{118}$ core plus a proton hole. States of Hg^{197}, Au^{197} and Pt^{197} must therefore be described in general by

$$\left|{}_{80}Hg^{197}_{117}\right\rangle = A\left|{}_{80}Hg^{196}_{116},\ n\right\rangle + B\left|{}_{80}Hg^{198}_{118}\ n^{-1}\right\rangle$$

$$\downarrow \ (\beta^+ \text{ decay}), \text{ Capture}$$

$$\left|{}_{79}Au^{197}_{118}\right\rangle = C\left|{}_{78}Pt^{196}_{118}, p\right\rangle + D\left|{}_{80}Hg^{198}_{118}, p^{-1}\right\rangle$$

$$\uparrow \quad \beta^- \text{ decay.}$$

$$\left|{}_{78}Pt^{197}_{119}\right\rangle = F\left|{}_{78}Pt^{196}_{118}, n\right\rangle + G\left|{}_{78}Pt^{198}_{120}, n^{-1}\right\rangle$$

where in the absence of 'impurities', $A^2 = 1 - B^2$

$$C^2 = 1 - D^2$$

$$F^2 = 1 - G^2$$

and different states may have different values of A, C and F.

The same description of As^{73}, Ge^{73}, Ga^{73} takes the form

$$\left|{}_{33}As^{73}_{42}\right\rangle = A\left|{}_{32}Ge^{72}_{40}, p\right\rangle + B\left|{}_{34}Se^{74}_{40}, p^{-1}\right\rangle$$

(β^+ decay), capture

$$\left|{}_{32}Ge^{73}_{41}\right\rangle = C\left|{}_{32}Ge^{72}_{40}, n\right\rangle + D\left|{}_{32}Ge^{74}_{42}, n^{-1}\right\rangle$$

β^- decay.

$$\left|{}_{31}Ga^{73}_{42}\right\rangle = F\left|{}_{30}Zn^{72}_{42}, p\right\rangle + G\left|{}_{32}Ge^{74}_{42}, p^{-1}\right\rangle .$$

The absence of β^- decay feeds to the $\frac{1}{2}^-$ and 5/2+ levels may now be taken to indicate that $D \simeq 0$ for these levels, i.e. they are almost pure 'Ge^{72} core plus neutron' levels. There is some support for this assumption for the 5/2+ level which is a member of the core excited multiplet centred on the 820 keV (7/2+) level. This excitation energy is very much nearer to that of the 2+ level in Ge^{72} (835 keV) than that of Ge^{74} (596 keV).

The absence of the electron capture (1st forbidden) to the 13.5 keV (5/2+) level is now explained by the necessity to excite the 'core' in the process.

The capture to the $\frac{1}{2}^-$ level is, of course, to be expected if the assumption $D \simeq 0$ (i.e. $C \simeq \sqrt{1 - D^2} \simeq 1$) is valid.

The allowed β^- decays to the levels at 363 keV and 1134 keV implies that these levels are both of odd parity. It is possible that the 363 keV level has spin 3/2, in which case it is tempting to suggest that the 1134 keV level is 5/2- and that together these two levels make up the doublet that might be expected from the coupling of a single particle in a $p_{1/2}$ (excited) level with the 2+ core

state of Ga^{72} or Ga^{74}. The fact that these levels are fed by β^- decay from Ga^{72} now implies that $D \neq 0$, i.e. that the Ge^{74} core is appreciably involved. The "centre of gravity" of the 'doublet' is at about 749 keV, which is very nearly half-way between the 2+ excitations of Ge^{72} and Ge^{74}, which suggests that $C^2 \simeq 1 - D^2$ in this case.

6.4. Conclusions

It seems that it is possible to explain the enhancement and retardation of the 13.5 keV and 53.3 keV transitions on either a 'core excitation' or a 'co-operative' interpretation of the levels. Provided certain assumptions are made a 'core excitation' interpretation (extended to include both possible 'cores') can be made to explain all the known features of the decay of Ga^{73} and As^{73}. It also predicts the spins and parities of levels that have not as yet been measured, and the magnetic moment of the 2+ level in Ge^{72}. Measurement of this moment and the spin of the 820 keV level in Ge^{73} would be crucial and spin and parity measurements on the 1040 keV and 1134 keV levels would also be interesting.

Some of this information might be obtained from further study of the Ga^{73} decay. For example, it might be possible to obtain the half-life ($\sim 10^{-11}$ sec.) of the 363 keV and 392 keV levels from γ-γ or β-γ delayed coincidence experiments. (Also, γ-γ and β-γ angular correlation experiments could yield some information about the spins and parities of the 363 keV, 392 keV, 554 keV, and 647 keV levels.)

Since the half-lives are expected to be so short, such information could probably be more easily derived from measurements of

the cross-sections for Coulomb excitation.

Although measurements of the internal conversion coefficients of the γ transitions at 284 keV and above would be difficult (because these coefficients are expected to be $<10^{-3}$), they are probably the most efficient way of obtaining information about the multipole types of these transitions. With a strong enough Ga^{73} source and a magnetic spectrometer of high resolution, it would probably be possible to measure the coefficients for the lower energy γ's and set upper limits for those of higher energy.

Appendix I

Computer Program to Calculate Effective Solid Angle

upper case delimiters

```
BEGIN

INTEGER i,j,k,l

REAL  t,u,c,h,teg,r,w,w1,w2,w3,w4


REAL ARRAY x(0:200)

REAL ARRAY integral(1:100) ; REAL ARRAY a,d(1:20)

read(r)


6:CYCLE k=1,1,10
read(d(k)); a(k)=d(k)/(sq rt((d(k))^2+r^2))
REPEAT

IF d(1)=0.02032 THEN t=0.036 ; IF d(1)=0.00254 THEN t=0.0069
IF d(1)=0.0254 THEN t=0.178

7:read(u) ; ->30 IF u=-100; ->31 IF u=-111; c=u*t

CAPTION $$$ Normal $ attenuation $ factor $ =
print fl(exp(-c),4)
CYCLE k=1,1,10
x(0) =a(k)
w=(1-a(k))/2

CAPTION $$ t$= ; print fl(t,4)
CAPTION $$$$ u$=; print fl(u,4)
CAPTION $a$= ; print fl(a(k),4)
CAPTION $$$ Fractional $ solid $ angle $ =
print fl(w,4)
CAPTION $$$$ Usual e1*w1 $= ; print fl(w*(exp(-c)),4)
CAPTION $ Approx, $ calcn, $ weff, $ =
```

```
w1= c*(log(a(k))/2) ;print fl(w1,3); CAPTION $$plus $$
w2=- c²*(1-1/a(k))/4 ; print fl(w2,3) ; CAPTION $ plus $
w3= c*3*(1-1/((a(k))²))/24 ; print fl(w3,3)
CAPTION $ equals $
print fl(w+w1+w2+w3,4)

CYCLE j=1,1,20
l=10*j;x(l)=1; h=(x(l)-x(0))/l ;teg=0

CYCLE i=0,1,l
x(i)=x(0)+i*h

IF c/x(i) >20 THEN -> 50 ; ->51
50: CAPTION $$ Point $ no. $ ; print(i,3,1)
CAPTION $ omitted ; ->20

51:->10 IF i=0 OR i=l
->11 IF frac pt(i/2)>0.1 ;->12

10:teg= 1/exp(c/x(i))+teg ; ->20
11: teg = teg +4/exp(c/x(i)) ; ->20
12: teg = teg +2/exp(c/x(i)); ->20

20:REPEAT

integral(j) = teg*h/6

CAPTION $ NO. $of $ steps $ = ; print(i,3,1)
CAPTION $$$$ Integral $ = ; print fl(integral(j),5)

REPEAT
CAPTION $ eff/frac solid angle $
print fl(integral(20)/w,4)
REPEAT

->7
30: ->6

CAPTION $$ Radius $ used $ = $ ; print fl(r,4)
newlines(2)

31: END OF PROGRAM



1.002

0.02032  0.1003  0.1083 0.2075  0.3030  0.5000
0.9836  1.1765  1.7614  2.3473
0.883  0.604  0.160  0.080  -100
```

```
0.00254  0.1003  0.1983  0.2975  0.3939
0.5000   0.9836  1.1765  1.7614  2.3473
0.338  0.237  26.5  26.2  -100

0.0254  0.1003  0.1983  0.2975  0.3939
0.5000  0.9836  1.1765  1.7614  2.3473
2.20  2.10  -111

***7
```

N.B. The first no. in the data is the crystal entrance window radius. The other nos. are in groups terminated by the no. -100. The first no. in each group is the absorber thickness, the next ten are source to crystal distances, and the rest are mss absorption coefficients.

APPENDIX II

MASS ABSORPTION COEFFICIENTS

The calculation of counter window attenuation factors described in Chapter 2 involved the absorption coefficients at 9.9 keV and 53.3 keV for Be and Aℓ, and for the calculation of the attenuation factors r in Section 2.6 the μ/ρ value for Zn at 53.3 keV was required. Three sources of this information were considered, namely, theoretical, semi-empirical and experimental.

Outline of Absorption Theory. At γ energies below 1.02 Mev a bsorption can occur by two processes:

a) Photo-electric effect.

b) Compton scattering.

a) Photo-electric effect. This is the process where a γ photon gives all its energy to a bound electron of the absorber which uses part to overcome its binding to the absorber atom and takes the rest a way as kinetic energy.

The total cross-section for ejection of a photoelectron in any direction from the K shell is :

$$\phi_K = 2 \int_{\text{all angles}} \frac{2\pi}{\hbar c} |H|^2 \rho_E \, d\Omega$$

where ρ_E is the density of final electron states.

H is the matrix element for the absorption of a single photon and the emission of an electron.

Exact evaluation of ϕ_K is difficult and tedious since

$H = \int \psi_b^* H_{int} \psi_a d\tau$ involves the solution to the Dirac relativistic equation for a bound electron.

(ψ_b is the wave function of the electron in the continuous spectrum.

ψ_a " " " " " " " " K shell.

H_{int} is the Hamiltonian for interaction between the γ and the electron).

Heitler[59] has obtained the result

$$\mu = \phi_K = \phi_o \frac{Z^5 e^8}{(\hbar c)^4} 4\sqrt{2} \left(\frac{mc^2}{E_\gamma}\right)^{3/2} \quad cm^2/atom$$

(where $\phi_o = 8\pi r_o^2/3$ the cross-section for Thomson scattering ($r_o = e^2/mc^2$)) by assuming:

1) Energy of photo electron >> binding energy of K shell, i.e. attraction of nucleons on the electron as it leaves the atom can be neglected. This means that the Born approximation $Ze^2/\hbar v \ll 1$ (where V = velocity of the ejected electron) is valid and plane waves can be used for ψ_b.

2) Photo electron energy $\ll mc^2$, i.e. non-relativistic case - can use

$$\psi_a = \frac{1}{\sqrt{[\pi a^3]}} e^{-r/a} \quad \text{where} \quad a = a_o/Z \quad \text{and} \quad a_o = \hbar^2/me^2 .$$

Calculations by Stobbe[60], using correct photo electric wave functions (but still making assumption (2)), give

$$\phi'_K = \phi_K \cdot 2\pi\left(\frac{E_B}{E_\gamma}\right)^{\frac{1}{2}} \frac{\exp(-4\xi \cot^{-1}\xi)}{(-\exp(2\pi\xi)}$$

where $\xi = Ze^2/\hbar v$.

A free electron cannot absorb a photon and become a photo electron since a third body (e.g. nucleus) is necessary to conserve momentum. It is to be expected (and theory shows) that provided

E_γ K shell binding energy $\phi_L, \phi_M \ll \phi_K$.

Non relativistic calculations have been done [61] for L_I, $L_{II} + L_{III}$ and M shells.

The theoretical results quoted above were used to obtain the values for $(\frac{\mu}{\rho})_{pe}$ given in "β and γ ray Spectroscopy"[50].

b) Compton Scattering where the photon is scattered by an electron of an absorber atom, the photon going off in a different direction with decreased energy, and the electron recoiling with the remaining energy

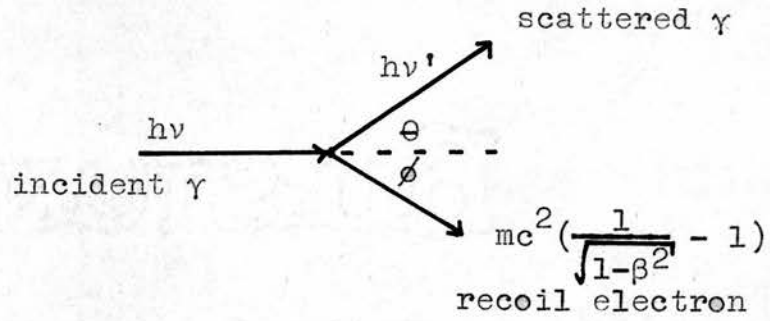

Using relativistic expressions the energy and momentum conservation laws give :

$$h\nu' = \frac{h\nu}{1 + \alpha(1-\cos\theta)} \quad .$$

Thus the maximum energy loss for a single Compton scatter occurs for $\theta = 180^\circ$ (backscatter) when the photon energy is reduced to

$$h\nu'_{min} = \frac{h\nu}{1 + 2\alpha} \qquad (7.1)$$

where $\alpha = h\nu / mc^2$.

Klein and Nishina[62], using the Dirac equation for the electron, have obtained for $d_e\mu$, the cross-section for the number of photons scattered into the solid angle $d\Omega$ in direction θ

$$\frac{d_e\mu}{d\Omega} = \frac{r_o}{2}\left\{\frac{1}{(1+\alpha(1-\cos\theta))^2}\left[1+\cos^2\theta+\frac{\alpha^2(1-\cos\theta)^2}{1+\alpha(1-\cos\theta)}\right]\right\} \tag{7.2}$$

with $r_o = e^2/mc^2$. This reduces for low energies ($\alpha<1$) to the classical Thomson equation

$$d_e\mu/d\Omega = (r_o^2/2)(1+\cos^2\theta).$$

The total Compton cross-section can be obtained by integrating this expression with respect to θ between 0 and 2π and with respect to ϕ between 0 and 2π giving

$$e^\mu = 2\pi r_o^2\left[\frac{1+\alpha}{\alpha^2}\left[\frac{2(1+\alpha)}{1+2\alpha}-\frac{1}{\alpha}\log_e(1+2\alpha)\right]+\frac{1}{2\alpha}\log(1+2\alpha)-\frac{1+3\alpha}{(1+2\alpha)^2}\right]$$

cm^2/electron.

The above applies to scattering by free electrons and in the more general case the effect of the binding of the electrons to the atom and their motions and distribution within the atom must be considered. The total scattering can be separated into coherent and incoherent scattering. In the coherent case the energy of the scattered radiation is the same as that of the incident radiation and there is a relation in phase of scattering from different electrons. In the incoherent part the scattered radiation gives up some energy to the electron and there is no phase relation between radiation

scattered from different electrons.

The differential cross-section can be written:

$$d\mu = d\mu_{coh.} + d\mu_{incoh.}$$

$$= Z d\mu_{KN} S + d\mu_{Thomson} \left(\sum_1^Z f_n\right)^2$$

where Z is atomic number of atom.

$d\mu_{KN}$ is the differential cross-section given by the Klein-Nishina equation (7.2), S is the incoherent scattering function which may be expressed as the square of a generalized atomic form factor summed over all excited states of the atom, integrated over the continuous spectrum and divided by 2. f_n is the electronic structure factor - the amplitude of the radiation scattered coherently by the n^{th} electron in terms of that scattered coherently by a free electron.

The above has been used to obtain the values for $(\frac{\mu}{\rho})_{ce}$ listed in "β and γ Ray Spectroscopy"(50).

The total absorption coefficient is then given by

$\mu = \mu_{pe} + \mu_{ce}$.

A similar method of calculation was used by McGinnies and Grodstein to obtain the values listed by Stainer(63).

<u>Semi-Empirical</u> - Values given by Victoreen in ref. (63) are calculated from

$$\mu/\rho = C\lambda^3 - D\lambda^4 + \mu_e N_o Z/A \quad \text{with } \lambda \text{ in } \mathring{A}$$

where C, D are constants depending on Z, N_o is Avagadro's number, A atomic weight and μ_e is the Klein-Nishina scattering cross-section per electron.

Values obtained in this way agree well, in general, with experimental values.

Experimental Values. Those due to Allen and Werde are quoted by Stainer[63]. The values given in the Phillips table compiled by Cauchois have also been considered.

Total $\frac{\mu}{\rho}$ values for 9.9 keV ($\lambda = 1.253$ Å) and 53.3 keV (0.230 Å) were obtained from the above sources by extrapolation of the given values on a graph of $\frac{\mu}{\rho}$ against λ.

Agreement was good for the $\frac{\mu}{\rho}$ values obtained from all the sources at 53.3 keV although Werde's experimental results were slightly smaller than the others.

The experimental value of Cauchois $\frac{\mu}{\rho} \simeq 0.83$ shows good agreement with the semi-empirical value of Victoreen and reasonable agreement with the experimental value of Allen, but is considerably larger than the theoretical result given by Siegbahn and that calculated by Grodstein which agree well with each other.

The Cauchois $\frac{\mu}{\rho}$ values were used for total $\frac{\mu}{\rho}$ in all cases.

However the μ value involved in the calculations of sections 2.4 and 2.6 is not quite the same as the total μ taken from the above. The latter refers to the case of a narrow beam where any scattering removes a photon from the beam. Clearly in the calculations of sections 2.4 and 2.6 a photon scattered in the forward direction has a good chance of reaching the detector, particularly if absorption is small.

The minimum energy of a photon scattered in a single Compton process is, from equation (7.1),

$$h\nu_{min} = h\nu / 1+2\alpha = 9.6 \text{ keV for } h\nu = 10 \text{ keV}.$$

In the detector with energy resolution $\sim$ 50% at 10 keV and 20% at 53 keV, these photons will not be resolved from unscattered full energy photons and will therefore be counted.

From the polar diagram of different Compton cross-section as a function of θ (see, for example, "β and γ Ray Spectroscopy"[50]) the probability of scattering in the forward is about equal to that in the backward direction. Thus about half the photons which are Compton scattered will reach the detector (assuming the absorber is close to the detector, which is true for the Al or Be window calculations. (In the Zn case the Compton contribution to the absorption is very small.))

Thus the μ value appropriate to the calculations of sections 2.4 and 2.6 is

$$\mu' = \mu_{pe} + \tfrac{1}{2}\mu_C = \mu - \tfrac{1}{2}\mu_C = \mu(1 - \tfrac{1}{2}r) \qquad (7.3)$$

where $r = \mu_c/\mu$.

The value of r was taken from the theoretical results for μ_c and μ and this was then used in equation (7.3) with the Cauchois value of μ. The effect of this is greatest in the low Z (Be) case where absorption is in any case small.

This fairly rough calculation is adequate since it is a "correction to a correction".

Cauchois' experimental values of $\frac{\mu}{\rho}$ for Na, H, As, O were again used to estimate the effects of source self-absorption. For this purpose the source was assumed to be made up of sodium arsenate ($Na_2 HASO_4$). The $\frac{\mu}{\rho}$ value for the compound was calculated according to the formula

$$\frac{\mu}{\rho} = \left(\frac{\mu}{\rho}\right)_1 a_1 + \left(\frac{\mu}{\rho}\right)_2 a_2 + \left(\frac{\mu}{\rho}\right)_3 a_3 + \cdots\cdots$$

where $\left(\frac{\mu}{\rho}\right)_i$ is the absorption coefficient in $cm^2/gm.$ and a_i is the fractional amount by weight of the i^{th} element in the compound.

The calculation yields $\frac{\mu}{\rho} = 23.8\ cm^2/gm.$ at 9.9 keV

and $\frac{\mu}{\rho} = 1.18\ cm^2/gm.$ in 53.3 keV.

By weighing the melinex backing before and after depositing the source the latter was found to weigh $\lesssim$ 0.1 mgm. The source area was roughly circular with diameter ~ 1.2 cm., i.e. area 1.1 cm^2.

Hence the 'ρx' for the source $\lesssim {}^{0.1}/_{1.1} \simeq 0.089\ mgm/cm^2$. The order of magnitude of the intensity reduction at 9.9 keV can be calculated from ${}^{I}/_{I_o} = \exp(-\frac{\mu}{\rho} \cdot \rho x) \simeq \exp(-1.18 \times 0.089 \times 10^{-3})$ $= .9999$, i.e. absorption is less than $0.01^{o}/o$.

Source self-absorption effects were therefore neglected.

Similarly for transmission through x cm of air

$\frac{I}{I_o} = \exp \mu x \simeq 0.995$ for $x = 1$ cm. using the Seigbahn[50] value for $\mu\ (= 52 \times 10^{-4}\ cm^{-1})$, so air absorption was neglected. Assuming the same absorption coefficient for the melinex used to cover the source yielded a similar result for this case.

ACKNOWLEDGEMENTS

I wish to express my thanks to Professor N. Feather, F.R.S., for making available the facilities of the department. I am very grateful to my supervisor Mr. J. Kyles, M.A., O.B.E., F.R.S.E., for his keen interest and helpful guidance throughout the course of this work.

I should also like to thank Dr. F. Shaikh for many helpful discussions on the decay scheme of As^{73} and on proportional counter operation; Mr. R.D.L. Mackie, who designed the 2-second sweep T.A.C. prototype; Dr. G. Bradford and Mr. C. McAnna who built the μsec. sweep T.A.C. and maintained the other electronic equipment; Mr. A. Headridge formerly Chief Technician, his successor Mr. H.J. Stevens, and the workshop staff.

Finally, I should like to express my gratitude to Mrs. R.W. Chester, who painstakingly typed the manuscript, and also to those members of the department, too numerous to mention, who have given useful advice and cooperated when necessary in the sharing of equipment.

REFERENCES

1. Konopinski, E.J. (1943) Rev. Mod. Phys. 15, 209.
2. Wu et al. (1957) Phys. Rev. 105, 1413.
3. Konopinski, E.J. (1959) Ann. Rev. Nucl. Sci. 9, 99.
4. Konopinski & Uhlenbeck (1941) Phys. Rev. 60, 308.
5. Rose & Jackson (1949) Phys. Rev. 76, 1540.
6. Blatt, J.M. & Weisskopf, V.F. "Theoretical Nuclear Physics".
7. Moszkowski, S.A. α, β and γ-Ray Spectroscopy, Ch. XV, Vol. I (1965). Ed. K. Siegbahn.
8. Hager, R.S. & Seltzer, E.C. (1968). Nuclear Data A Vol. 4, Nos. 1 and 2.
9. Band, I.M. & Sliv, L.A. (1965) Tables of Internal Conversion Coefficients, α, β and γ-Ray Spectroscopy, Vol. 2, 1639. Ed. K. Siegbahn.
10. Sagane, R., Kodjina, S., Miyamoto, G. and Ikana, M. (1139) Proc. Phys. Mat. Soc. (Japan) 21, 600 (quoted by Grigor'ev 1963).
11. Elliot, L.G. and Deutsch, M. (1943) Phys. Rev. 63, 459.
12. McCowan, D.A., Woodward, L.L. & Pool, M.L. (1948) Phys. Rev. 74, 1315.
13. Trail, C.C. & Johnsson, C.H. (1953) Phys. Rev. 91, 474.
14a. Fuller, G.H. & Cohen, V.W. (1965) Appendix I to Nuclear Data Sheet. Vol. 6. No. 5.
14b. Aksenov, S.I. & Vladimirski, K.V. (1954) Doklady Akad Nauk SSSR 96, 37; NSA 8-5343.
14c. Townes, C.H., Mays, J.M. & Dailey, B.P. (1949) Phys. Rev. 76, 700.
14d. Childs, W.J. & Goodman, L.S. (1966) Phys. Rev. 141, 15.
15. Johansson, S. (1952) Arkiv. Fysik 4, 273.
16. Goldhaber, M. & Sunyar, A.W. (1951) Phys. Rev. 83, 906.
17. Stoker, P.H. & Hok, O.P. (1953) Physica 19, 279.
18. Grigor'ev, E.P. Dzhelepov, B.S., Zolotavin, A.V. and Mishin, V.I. (1958) Izv. Akad. Nauk, SSSR, ser. fiz. 22, 927.

REFERENCES (Contd.)

19. Welker, J.P., Schardt, A.N., Friedlander, G. and Howland, J.J. (1953). Phys. Rev. 92 (2), 401.

20. Barloutand, R., Sartori, M. (1953) Compt. Rend. 236, 1872.

21. Barloutand, R., Ballini, R. & Sartori (1953) Compt. Rend. 237, 886.

22. Campbell, E.C. & Nelson, F. (1957) Phys. Rev. 107, 502.

23. Shaikh, F. (1968), Ph.D. Thesis.

24. Grigor'ev, Y.P. (1963) "Isobaric Nuclei with the Mass No. A = 73" (Pergamon Press).

25. Seigel, J.M. & Glendenin, L.E. (1946) Journal Am. Chem. Soc. 68, 2411. (Quoted in Ythier et al., 1958).

26. Perlman, M.L. (1949) Phys. Rev. 75, 988 (1949).

22. Marquez, L., Cybulska, E.W., Costa, N.L., Almeida, I.G., & Goldemburg, J. (1959) Nucl. Phys. 10, 28.

23. Holtzman, P.B., Sugarman, N. (1952) Phys. Rev. 87, 633.

24. Sharma, H.D. Thesis, Univ. Calif. Rad. Lab., UCRL (1951) 1265 (q uoted by Grigor'ev, 1963).

30. Ythier, C., Girgis, R.K., Rissi, R.A., van Lieshout, R. (1958/9) Nucl. Phys. 9, 108.

31. Goeckermann, R.H., Perlman, M.L. (1949) Phys. Rev. 76, 628.

32. Rudstam, G. (1956) Thesis, University of Uppsala.

33. Levkovskii, V.N. (1958) Atomic Energy 4, 79 (1958).

34. Schweizer, F., Eakins, G.W. & Van Klinker, J. (1966) Bull. Am. Phys. Soc. 11 No. 4, 458, BC7.

35. Temmer, G.M. & Heidenburgh, N.P. (1956) Phys. Rev. 104, 967.

36. Du Mond, J.W.M. (1958) Annual Rev. Nucl. Sci. 8, 163.

37. Holland, R.E. & Lynch, F.J. (1961) Phys. Rev. 121, 1464.

38. Alkhazov, D.G., Andreyev, D.S., Greenberg, A.P. & Lemberg, I.H. (1956) Nuclear Phys. 2, 65.

39. Retter, R.C., Stelson, P.H., McGowan, F.K., Robinson, R.L. (1962) Phys. Rev. 128, 2320.

REFERENCES (Contd.)

40. Vasilev, V.D., Erokhina, J.I., Lemberg, I.K. (1962) Columbia Tech. Transl. 26, 1000.

41. Silva, R.J., Eichler, E. (1962). Bull. Am. Phys. Soc. 7, 41, 315 MB5.

42. Bochin, V.P., Gridnev, K.A., Zhenebtsova, K.I., Kransov, L.V. Komarov, V.A., Lakomkin, Y.A., Litvin, V.F., Nemilov, Y.A. Orlova, T.V., Romanov, V.S. (1968) 16th All-Union Conf. Nuclear Spectroscopy & Structure of Atomic Nuclei, Moscow, p. 84 (listed in Nuclear Data).

43. Nuclear Data (1966) Section B 1 No. 6. B1-6-48.

44. Rose, M.E. (1958) "Internal Conversion Coefficients".

45. Gove, N.B. (1966) "Nuclear Spin-Parity Assignments (Academic Press)

46. Way, K., Kundu, D.N., McGuiness, C.L. and Lieshout, R.V. (1956) Ann. Rev. Nucl. Sciences 6, 129.

47. Spinard, B.I. (1955) Phys. Rev. 98, 1302.

48. Hebb, M.A. & Nelson, E. (1940) Phys. Rev. 58, 486.

49. Broyles, Thomas & Haynes (1953) Phys. Rev. 89, 715.

50. β and γ Ray Spectroscopy (1955). Ed. K. Siegbahn.

51. Parrat, L.G. (1961). 'Probability and Experimental Errors in Science', Wiley & Sons, Inc.

52. Grant, I.S. (1965) Nucl. Instr. & Meth. 36, 289.

52a. Hanson, R.J. & Marker, D. (1963) Il Nuovo Cimento 32, 793.

53. Whittaker, E.T. & Robinson, G. 'The Calculus of Observations' (1924).

54. Benedetti, S. de and McGowan, F.K. (1948) Phys. Rev. 74, 728.

55. Fink, R.W. et al. (1966) Rev. Mod. Phys. 38, 315.

56. Lawson, R.D., Uretsky, J.L. (1957) Phys. Rev. 108, 1300.

57. De Shalit, A. (1962) Physics Letters, 1, 264.

58. Murray, G. Private Communication.

59. Heitler, W. 'The Quantum Theory of Radiation'.

60. Stobbe, M. (1930), An. Physik 7, 661.

REFERENCES (Contd.)

61. Hall, H (1936) Rev. Mod. Phys. 8, 358.

62. Klein, O. & Nishina, Y. (1929) Z. Physik 52, 853.

63. Stainer, H.M. 'X-Ray Mass Absorption Coefficients'. I.C. Bureau of Mines Information Circular 8166.